EXPERIMENTAL AND FINITE ELEMENT INVESTIGATION OF TENSION-LOADED ASTM A325 BOLTS UNDER SIMULATED FIRE LOADING

by

Ali Shrih

A Dissertation Submitted in

Partial Fulfillment of the

Requirements of the Degree of

Doctor of Philosophy

in Engineering

at

The University of Wisconsin-Milwaukee

August 2013

ABSTRACT

EXPERIMENTAL AND FINITE ELEMENT INVESTIGATION OF TENSION-LOADED ASTM A325 BOLTS UNDER SIMULATED FIRE LOADING

by

Ali Shrih

The University of Wisconsin-Milwaukee, 2013
Under the Supervision of Dr. Adeeb Rahman

Nuts and bolts have been used in a wide range of steel structures for many years. However, these structures remain susceptible to fire damage. Conducting fire experiments on steel structures is costly and requires specialized equipment. The main objective of this research is to test, analyze and predict the behavior of ASTM A325 bolts in tension under simulated fire conditions and develop a reliable finite element model that can predict the response of similar bolts without the need for repeated testing.

The experimental work was conducted at the University of Wisconsin-Milwaukee; a furnace was custom-built to test a bolted specimen under tension loading. The tests were divided into two groups, the first one was used to calibrate the equipment and choose a final testing arrangement; the second group, consisting of four identical tests, was used to validate the finite element model. The temperature-displacement and load-displacement response was recorded.

The tested bolts exhibited a ductile fracture in which a cup-and-cone shaped failure surface forms in the threaded section, at the root of the nut.

A parametric three dimensional finite element model simulating the tested specimen and attachments was constructed in the ANSYS Workbench environment. The model included the intricate details of the bolt and nut threads, as well as all the other components of the tested specimen. A pretension load, a tension force and a heat profile were applied to the model and a nonlinear analysis was performed to simulate the experiments. The results of the FE model were in good agreement with the experimental results, deviations of results between experimental and FE results were within acceptable range.

TABLE OF CONTENTS

LIST OF FIGURES

LIST OF TABLES

ACKNOWLEDGMENTS

I wish to express my deepest appreciation to Dr. Adeeb Rahman, my advisor, for his support and guidance through the years. I also would like to thank Mr. Rahim Reshadi and Dr. Ben Church; without whom I would not have been able to finish my experimental work. My gratitude also to all the esteemed professors who accepted to serve on my committee: Habibollah Tabatabai, Rani El-Hajjar, Mustafa Mahamid, and Konstantin Sobolev.

Thanks to my family for their unwavering support and help. Many thanks to all my friends around the world and especially to those who helped me keep my sanity throughout graduate school: Andrew Dressel, Cem Gogtas and Mohammad Al-Momani.

CHAPTER 1

INTRODUCTION

1.1 Effect of Fire on Structural Steel

Steel has been used as a construction material for decades, and it proved to be a very effective construction material due to its high tensile and compressive strengths, ductility, and ability to be formed in almost any aesthetic shape. Nevertheless, steel structures are vulnerable to fatigue, corrosion and fire failures.

Fire-induced degradation of steel structures can be unpredictable and hard to account for during the design process. The common procedure is to use fireproofing materials, such as spray-on insulative, intumescent paint, or concrete filling and encasement, these measures are intended to delay the overheating of steel long enough for the occupants of the structure to evacuate safely and the firefighters to arrive.

Steel mechanical and thermal properties will change when subjected to a considerable change in temperature; this change can be determined using lab experiments for a specimen of a certain grade of steel. Normally, under elevated temperatures, steel will lose a substantial amount of its strengths and, depending on the steel member shape and location, it may undergo excessive deformations.

The performance of steel structures will be dramatically affected by the interaction between all structural members; this interaction may increase the fire resistance of steel members as compared to a lab specimen of the same steel. Hence, the following study of steel bolts under

elevated temperatures provides crucial answers for the actual behavior of a single component of a steel structure under fire conditions, predicts the failure mechanism of bolts and paves the way for more in-depth investigation of bigger and more sophisticated systems.

In order to start this study, a fundamental explanation of enclosure fire dynamics and the properties of the tested ASTM A325 bolts are presented in the following sections

1.2 STANDARD FIRES

Different nominal or standard fire curves have been developed for use during the design process of structures subject to fire conditions. The choice of using a certain fire curve over the other is largely dependent on the nature of the structural element being considered and the type of the structure itself (office building, offshore structure, tunnels or an industrial building.) There is, however, a widely used nominal fire curve that is often referred to as the "standard" fire curve which is published in several international codes such as the BS476 (British Standards for fire resistance of building materials), JIS A 1304 (Japanese Industrial Standard) or ISO834 (International Organization for Standardization) [1]. The standard fire curve is based on monitoring the temperature change of a fire in a special compartment where wood, paper or fabric is used as fuel [31], and it is described by the following equation:

$$T = T_o + 345 \times log_{10}(8t + 1) \qquad 1.1$$

Where, T: the temperature in fire compartment (ºC)

T_0: the ambient temperature (ºC)

t: time in minutes

This relationship can be used to control the temperature regime inside a furnace, although using such equations cannot be an exact prediction of a real fire, but it simplifies the design process and makes it more practical.

Different design codes provide slightly different fire curves, and Figure 1-1 shows a comparison between three standard fire curves:

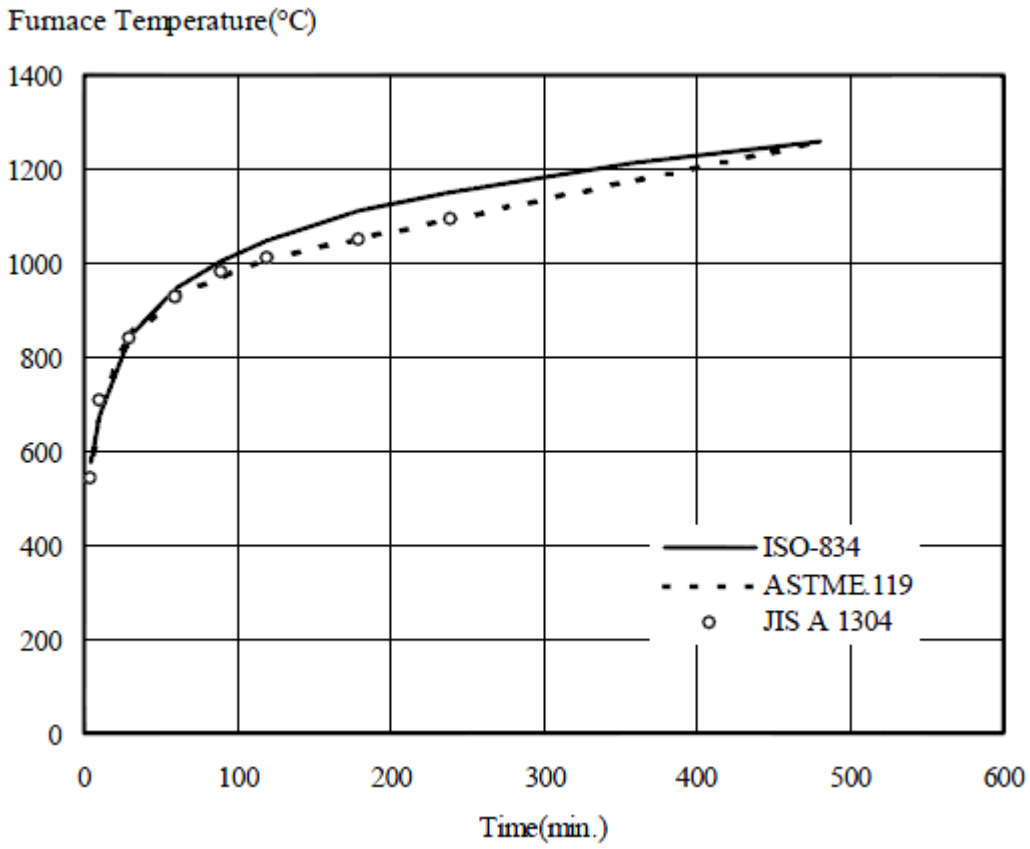

Figure 1-1 Standard fire curves (Al-Jabri K.S.)

1.3 Fire in Small Compartments

The space in a building is usually divided into smaller "compartments" which, depending on the function of the building, may serve as bedrooms, kitchens or offices. If a fire breaks out, these compartments, with proper insulation, can also be used to prevent the spread of fire between the different compartments of the building. This type of fire is called a "compartment

fire" [33], which (in fire safety design) is easier to handle than unrestricted fires in large open spaces. Older structures with smaller divisions provide a perfect example of the compartment fire behavior where a uniform distribution of design fires can be used in structural design. However, that is not the case in many of the new building-designs, where large open spaces are commonplace and the behavior of fire would not be restricted to a small compartment.

In a small compartment fire, a fire starting in a corner of a room would spread rapidly in what is known as "flashover" provided that an adequate supply of air and fuel (any combustibles in the room) is available. During a flashover, the fire would spread away from its origin when the upper level of hot gases trapped in the room under the ceiling builds up enough heat to convey downward through radiation and convection to any fuel on the lower levels of the room. When the combustible material reaches its ignition temperature it will ignite and fire will engulf the whole room.

1.4 Heavy Hex Structural Bolts Types

ASTM A325 and ASTM A490 are two national standards for structural bolts in the United States. Common Grade 5 or Grade 8 bolts, which are not approved for structural use in buildings, have similar strength charts to A325 and A490 bolts, respectively. However, A325 and A490 bolts are produced with a heavy hex head, which provides a wider bearing surface for better load distribution. In addition, the shank length (non-threaded portion) on the A325 and A490 bolts is longer than that of other bolts; which decreases the chances of having the threaded section in shear planes. Finally, there are also differences in thread-dimensions that add to the strength of the threaded part. [32]

Tables 1-1 and 1-2 present the types and main differences between A325 and A490 bolts as defined by the American Society for Testing and Materials (ASTM)

Head marking	Grade	Nominal size range [in]	Proof strength [ksi]	Yield strength (min) [ksi]	Tensile strength (min) [ksi]	Core hardness [Rockwell]
 or 	Type 1	½–1	85	92	120	C24–35
		1–1-½	74	81	105	C19–31
	Type 2	½–1	85	92	120	C24–35
	Type 3	½–1	85	92	120	C24–35
		1–1-½	74	81	105	C19–31

Table 1-1 Types and properties of A325 bolts (ASTM A325).

Head marking	Grade	Nominal size range [in]	Proof strength [ksi]	Yield strength (min) [ksi]	Tensile strength (min) [ksi]	Core hardness [Rockwell]
	Type 1	½–1-½	120	130	150 minimum 173 maximum	C33–38
	Type 2	½–1				
	Type 3	½–1-½				

Table 1-2 Types and properties of A490 bolts (ASTM A490).

The "core hardness" shown in the tables is a material property that is measured by an indentation test. The Rockwell test is usually used to determine the hardness by measuring the indentation depth caused by applying a large force to an indenter.

These tables show that A490 bolts have a higher strength but are less ductile. A490 bolts are not as commonly used as A325 in steel connections. This is why A325 bolts were selected for use in this study.

Furthermore, out of the three types of A325 bolts only bolts from Type-1, which are medium carbon steel, were tested. Type-2 has been withdrawn from ASTM in 1991 and Type-3 is used for the special case of weathering steel.

1.5 Dimensions of A325 Bolts

1.5.1 General Bolt Dimensions

Table 1-3 shows the general dimensions of available ASTM A325 bolts. Where,

D: is the nominal thread size.

TPI: is the number of threads per inch.

L.T.: is the length of the threaded part.

UNC: refers to bolts of type "Unified National Coarse" or (UNC). According to the Unified Thread Standard (UTS), which is commonly used in the United States and Canada, there are four different types of bolt threads. Unified coarse (UNC), unified fine (UNF), unified extra fine (UNEF) and unified special (UNS).

Dimensions F, G, h and B are shown in Figure 1-2

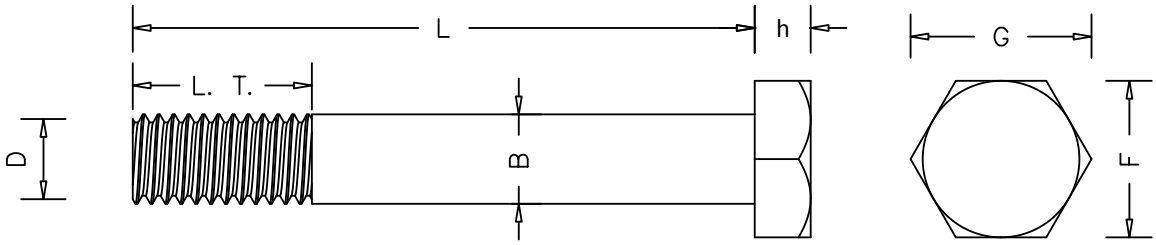

Figure 1-2 A325 bolt dimensions

D	TPI UNC	F Max.	G Max.	B Max.	h Nom.	LT	Length Range
1/2"	13	0.875"	1.010"	0.515"	5/16"	1.00"	1-1/2"-4"
5/8"	11	1.062"	1.227"	0.642"	25/64"	1.25"	1-1/2"-8"
3/4"	10	1.250"	1.443"	0.768"	15/32"	1.38"	1/2"-8"
7/8"	9	1.438"	1.660"	0.895"	35/64"	1.50"	1-1/2"-8"
1"	8	1.625"	1.876"	1.022"	39/64"	1.75"	1-1/2"-8"
1-1/8"	8UN	1.812"	2.093"	1.149"	11/16"	2.00"	2"-8"
1-1/4"	8UN	2.000"	2.309"	1.276"	25/32"	2.00"	2"-8"
1-3/8"	8UN	2.188"	2.526"	1.404"	27/32"	2.25"	2-1/2"-8"
1-1/2"	8UN	2.375"	2.742"	1.522"	15/16"	2.25"	2-1/2"-8"

Table 1-3 Dimensions of commercially available A325 bolts (ASME B18.2.6 2003).

1.5.2 Thread Dimensions

The Unified Thread Standard (UTS) defines thread dimensions for structural bolts in U.S. customary units, while the ISO (International Organization for Standardization) defines them in metric units. The threads form a symmetric V-section with a total height of H and a pitch of P. The relationship between the two can be deduced from Figure 1-3. Where,

D_{maj}: Major diameter

D_{min}: Minor diameter

D_p: Effective pitch diameter

$H = \cos(30^o) \times P \approx 0.866P$

$P = 1 / (\text{TPI} - 1)$

For example, in case of a ½"-diameter bolt where the number of threads per inch is 13:

$P = 1 / (13 - 1) = 0.0833$" and,

$H = 0.866 \times 0.0833 = 0.0722$"

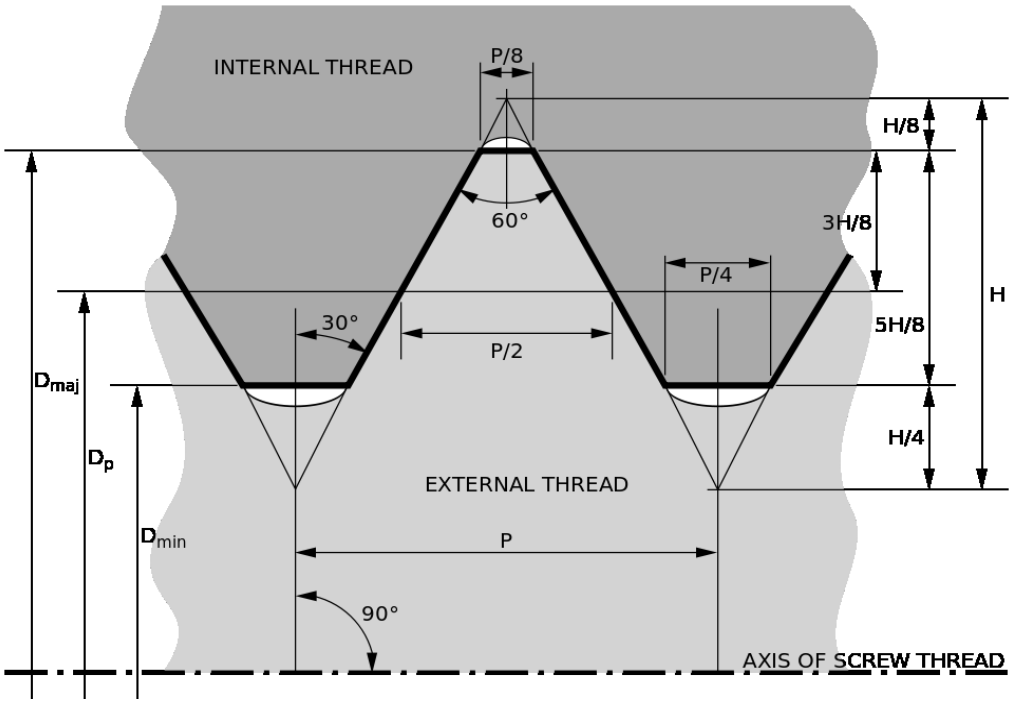

Figure 1-3 Thread dimensions (from Wikipedia Commons, based on the American National Standards Institute ANSI B1.1)

1.6 LITERATURE REVIEW

In recent years, a number of powerful finite element software packages such as ABAQUS, LUSAS, ANSYS, and LAGAMINE have become commercially available. They have the capability to solve a wide range of engineering problems in an efficient and accurate manner.

The basis to the finite element method as we know it today was first presented by Richard Courant in a lecture he gave to the American Association for the Advancement of Science in 1941[38]. However, the finite element method and its full development and implementation lagged behind until the early 1970's. That is when big industries started using FEA to

streamline their products. Nowadays, and with the advent of cheap supercomputing devices; FEA has become an integral tool in the engineering design process. Many engineers have tried to investigate the effects of elevated temperatures on steel connections with mixed results and through different analyses approaches.

Bose et al. made the first attempt to investigate the connection response making use of finite element analysis to study the behavior of welded beam-to-column connections by considering strain hardening, buckling and material plasticity in the analysis. The obtained results compared closely with the available experimental data [5].

Another early attempt to study the steel moment-connections behavior came in 1984, when Patel and Chen analyzed welded connections where the beam was either fully welded to the column or partially welded at the flange, and treated the connection as a two-dimensional problem [6]. This simplified the problem greatly since there were no bolts and the whole analysis was done in two dimensions. A general purpose program NONSAP developed by Bathe et al. based on plane stress isoparametric elements was used for this analysis and obtained satisfactory correlations with experimental results.

In 1988, a three-dimensional finite element analysis was conducted by Atamiaz Sibai and Frey [7] on un-stiffened welded connections using shell elements, and showed good agreement between the experimental and numerical results. These positive findings indicate the efficiency and reliability of the finite element method in accurately predicting the behavior of welded beam-to-column connections.

Krishnamurthy et al. [8] studied the behavior of bolted end-plate connections and developed a finite element methodology for the analysis of splice-plate connections. A moment–rotation

relationship was established based on the analysis of a large number of geometric configurations of connections.

Lipson and Hague [9] developed a finite element model with the primary aim of improving the understanding of single angle connections welded to the column flange and bolted to the beam web. Richard et al. [10] conducted finite element analyses on single web plate connections to simulate the full connection arrangements as well as part of the beam. An inelastic finite element model was developed to account for the bolt response based on a statistical evaluation of tests on single bolts. In addition, Richard et al. developed a finite element model to predict the response of double web cleat connections, and obtained a good agreement between the simulation results and experimental data.

Krishnamurthy developed a sophisticated finite element model that takes into account the bolt preloading and considers the support of the end-plate as rigid. The close correlation between the numerical results and experimental data demonstrated the importance of including the bolt heads and welds in the numerical models in order to accurately define the connection response [11]. Based on the work conducted by Krishnamurthy et al., Murray and Kukreti [12] studied the behavior of flush end-plate connection and eight types of extended end-plate arrangements. K.S. Al-Jabri et al. [13] developed a 3D finite element model using ABAQUS, in which he studied the behavior of a group of flush-end plate connections under elevated temperatures with good agreement to some experimental results of the same connections he conducted as part of his Ph.D. dissertation. The experimental work developed extensive data about the moment-temperature-rotation response of bare steel flush-end plate connections.

Recently, a detailed 3D nonlinear FE model was developed by Rahman and Mahamid et al. [14] [15] to study shear tab steel connections. This study was published by the American Institute of Steel Construction.

Han et al. [16] developed a nonlinear finite element model based on the elastoplastic finite element theory to analyze the load versus deformation (*P-Δ*) relation of steel beam to concrete filled steel tubular CFST column connections after exposure to fire. The results of the FE model were verified against the results of full scale tests performed on similar connections; and it proved to be reasonably accurate. The outcome of this research described the post-fire behavior of steel beam to CFST column connections under a constant axial load and a cyclically increasing flexural load.

Yu et al. [41] studied experimentally shear behavior of ASTM A325 and A490 bolts in fire and post-fire conditions. An electric furnace was used to heat a specimen of two bolts (7/8" diameter) under double shear while a digital video camera was used to take real-time images through an observation port. The deformations were determined based on the digital imagery using a software. The temperature of the tested bolts was kept constant during all tests while the shear load increased until failure; this was repeated for different temperatures (from 25 to 800°C in 100°C increments). As a result, shear strength reduction factors for A325 and A490 bolts during fire were obtained from the tests. It was also found that the residual shear strength of the bolts after heating would be reduced by 40%-45%.

Lu et al. [17] produced a finite element model using ABAQUS to simulate the behavior of single lap screw connections connecting two metal deck sheets in an industrial building roof. The model predicted the failure of the connection, when exposed to fire, under bearing of the screws on the metal sheets. The results were not correlated to any actual testing.

Yu et al. [18] used ABAQUS to investigate the tying capacity of web cleat connections under fire conditions. The three dimensional finite element model developed was good enough to reproduce the results of a full-scale test, up to the point of fracture. This is useful to indicate the critical locations, but not enough to predict the occurrence of component failure. A simulation of the bearing strength of bolt holes in the bolted connection was also discussed.

Rahman et al. [29] [35] used ANSYS to study the moment-rotation-temperature response of flush end-plate bare steel connections. These connections were part of a group of connections tested experimentally by Al-Jabri et al. [1] at the University of Sheffield in the UK and the finite element model results were in a very close agreement with experimental results. The finite element model utilized three-dimensional solid elements analyzed thermally and statically.

Lien et al. [39] used the Vector Form Intrinsic Finite Element (VFIFE) method to investigate the behavior of a few steel structures (two simply supported beams, a simply supported column and a five-story three-span frame with localized fire) during the heating and cooling phases of a fire. As a result, they proposed a numerical model that can effectively predict the nonlinear behavior of each structure during both heating and cooling phases. No three-dimensional modeling was performed and all the structures studied were linear elements.

Mao et al. [40] did experimental and three-dimensional finite element study of the fire response of steel semi-rigid beam-column moment connections. The experimental work for this study was performed in the fire laboratory center of the Architecture and Building Research Institute (ABRI) in Taiwan. A single cantilever w-beam attached to a vertical column was tested multiple times under two different loading conditions. The first type of loading was done by applying a constant transverse loading on the beam with increasing temperature, while in the second

type the temperature was constant with increasing transverse loading. The numerical model, developed using ANSYS, was in a very close agreement with the experimental results.

Rahman et al. [30] also used ANSYS to study the behavior of fin-plate connections in fire. Four types of element were used in the modeling of beams, column, fin-plate, and bolts. These elements were: two types of 3-D solid elements, pre-tensioning elements and contact elements. An 8-node solid brick element was used to model the entire structure and a 10-tetrahedral element with curved edges was used to model the bolts. Despite realistic results being predicted by the model, no experimental data was used to investigate its accuracy.

1.7 Problem Statement

Tension bolts in a moment-resisting steel connection, which are usually located at the top two or three rows, are more susceptible to failure during a fire than their compression counterparts. That is because the top row of bolts has to carry the applied tension load as the end plate in the connection starts to separate from the column, while in compression that same plate will help relief some of the stress on the bottom bolts.

This research examines experimentally the effects of elevated temperatures on structural A325 steel bolts under tension loading in simulated fire conditions. It also uses finite element analysis to predict the behavior of such bolts in similar conditions in order to validate the experimental results and establish a reliable FE model to study fully the bolt behavior and failure mechanism. The software used to perform the FE analysis is ANSYS Workbench, version 14.0, which is used to build a detailed three dimensional and parametric model of the tested bolts. This FE model, once calibrated, could serve as an alternative way to experimental investigation of the behavior of bolted connections under high temperatures, considering the high costs and difficult setup process for testing such connections.

1.8 RESEARCH OBJECTIVES AND SCOPE

This research aims to:

1. Develop a practical procedure and a protocol to test steel bolts under tension loads.
2. Conduct elevated temperatures tests of A325 bolts under loading and record deflection data.
3. Create a finite element model that accurately predicts the experimental results. The finite element model geometry is made to be parametric, so that future research is facilitated for any type of bolts and for different sizes. The parametric design is also useful for performing necessary sensitivity analyses.
4. Provide criteria to define the degradation in bolts strength and plot possible failure mechanisms.

1.9 DISSERTATION ORGANIZATION

This dissertation is divided into seven chapters:

- Chapter 1: the current chapter, which is concerned with introducing this work and relevant background material, defining its scope and presenting relevant literature review.
- Chapter 2: lays out a description of the thermal and mechanical material properties of steel and the effects of elevated temperatures on these properties.
- Chapter 3: details the setup and procedures used in conducting the experimental work.
- Chapter 4: covers the finite element model and analysis.

- Chapter 5: presents the results of the experimental work and the finite element model, with a comparison between the two. In addition, it also summarizes the conclusions and possible future work.
- Chapter 6: further details about the experimental setup.
- Chapter 7: lists a full description of a finite element model used in this research and details the properties and key parameters of this model.

CHAPTER 2

MATERIAL PROPERTIES

2.1 THERMAL PROPERTIES OF STEEL

Considerable research has been done to investigate the change in thermal and mechanical properties of structural steel under elevated temperatures. It is clear that the strength and modulus of elasticity of steel will decrease with the rise in temperature. However, without the need for a thermal analysis, the thermal conductivity and the specific heat of steel could be considered as constants.

The following sections present a short summary of some of the thermal properties of steel that may be relevant to finite element analyses.

2.1.1 Thermal Conductivity

The thermal conductivity is the coefficient that dictates the rate at which heat is conducted through the material. [33] There is not a significant change in thermal conductivity between different grades of steel, so the Eurocode EN 1993-1-2 describes its change with respect to temperature using an approximate linear equation [33], shown in Figure 2-1:

$\lambda = 54 - (0.0333 \times T)$ For $800^{o}\,C > T \geq 20^{o}\,C$ 2.1-a

$\lambda = 27.3$ For $1200^{o}\,C > T \geq 800^{o}\,C$ 2.1-b

Where, T is steel temperature (^{o}C)

λ is the thermal conductivity of steel (W/mK)

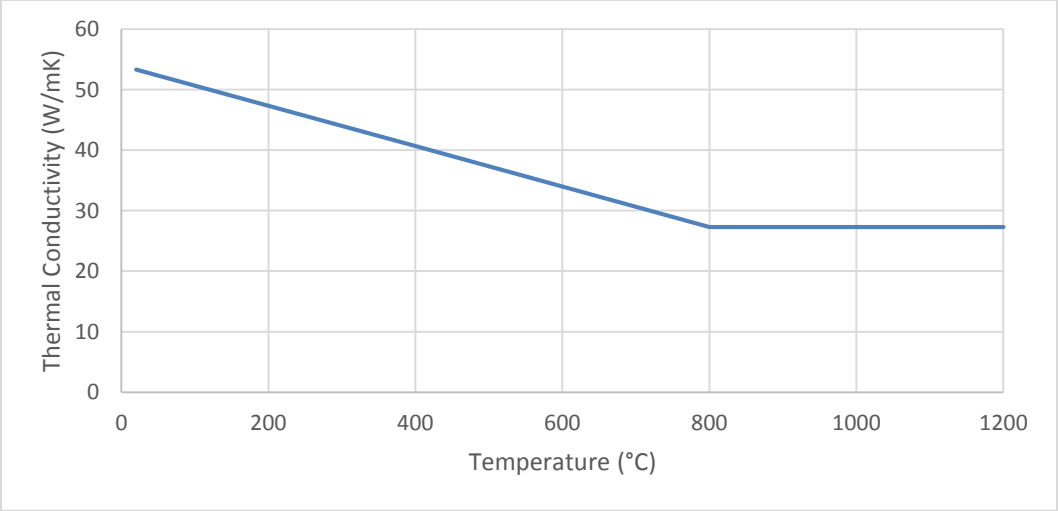

Figure 2-1 Coefficient of thermal conductivity of steel as a function of temperature (EN 1993-1-2)

2.1.2 Thermal Expansion

Thermal expansion is the rate at which a material length changes as a function of temperature. The Eurocode EN 1993-1-2 gives the following equations to determine the coefficient of thermal expansion for steel [33]:

$\alpha_s = 1.2 \times 10^{-5} T + 0.4 \times 10^{-8} T^2 - 2.416 \times 10^{-4}$ For $750^o\ C > T \geq 20^o\ C$ 2.2-a

$\alpha_s = 1.1 \times 10^{-2}$ For $860^o\ C > T \geq 750^o\ C$ 2.2-b

$\alpha_s = 2 \times 10^{-5} T - 6.2 \times 10^{-3}$ For $1200^o\ C > T \geq 860^o\ C$ 2.2-c

Where, T is steel temperature (°C)

α_s is the thermal expansion of steel

A linearized form of this equation was given in EN 1994-1-2 [33]:

$\alpha_s = 1.4 \times 10^{-5} T$

Figure 2-2 shows a graphical representation of the variation of the thermal expansion coefficient with respect to temperature.

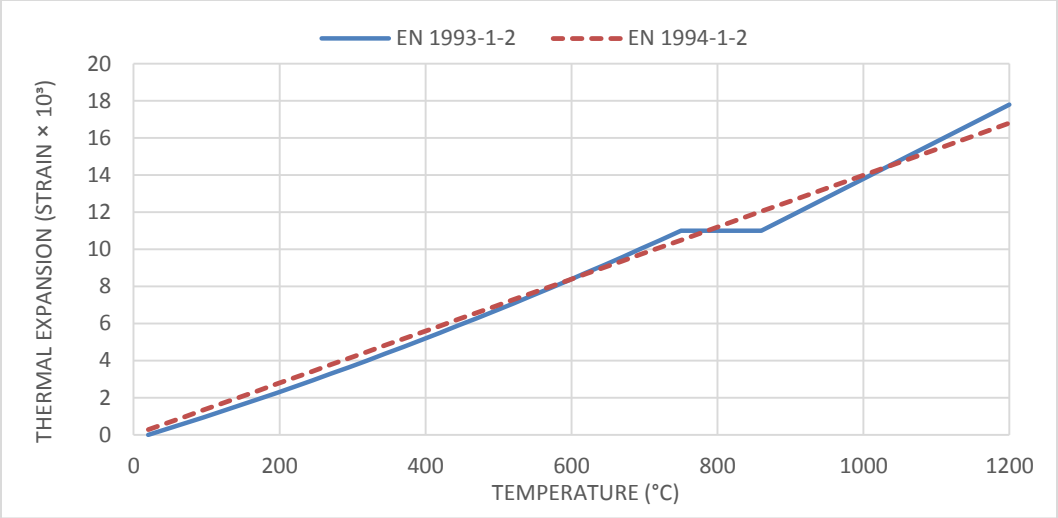

Figure 2-2 Coefficient of thermal expansion of steel as a function of temperature

2.1.3 Specific Heat

Specific heat represents the amount of energy (in joules) that a material needs to gain in order to raise the temperature of unit mass (1 kg) of the material by 1ºC [33]. The Eurocode EN 1993-1-2 suggests the following approximate equations for determining the specific heat for most steels (in J/kg.K):

$c_a = 425 + 0.773\ T - 1.69 \times 10^{-3}\ T^2 + 2.22 \times 10^{-6}\ T^3$ For $600^o\ C > T \geq 20^o\ C$ 2.3-a

$c_a = 666 + 13002/\ (738 - T)$ For $735^o\ C > T \geq 600^o\ C$ 2.3-b

$c_a = 545 + 17820/\ (T - 731)$ For $900^o\ C > T \geq 735^o\ C$ 2.3-c

$c_a = 650$ For $1200^o\ C > T \geq 900^o\ C$ 2.3-d

Where, T is steel temperature (ºC)

c_a is the specific heat of steal (J/kg.K)

Figure 2-3 shows a graphical representation of the specific heat of steel as a function of temperature.

The spike in the curve at 730° C corresponds to a phase change of steel when the steel changes from ferrite to austenite.

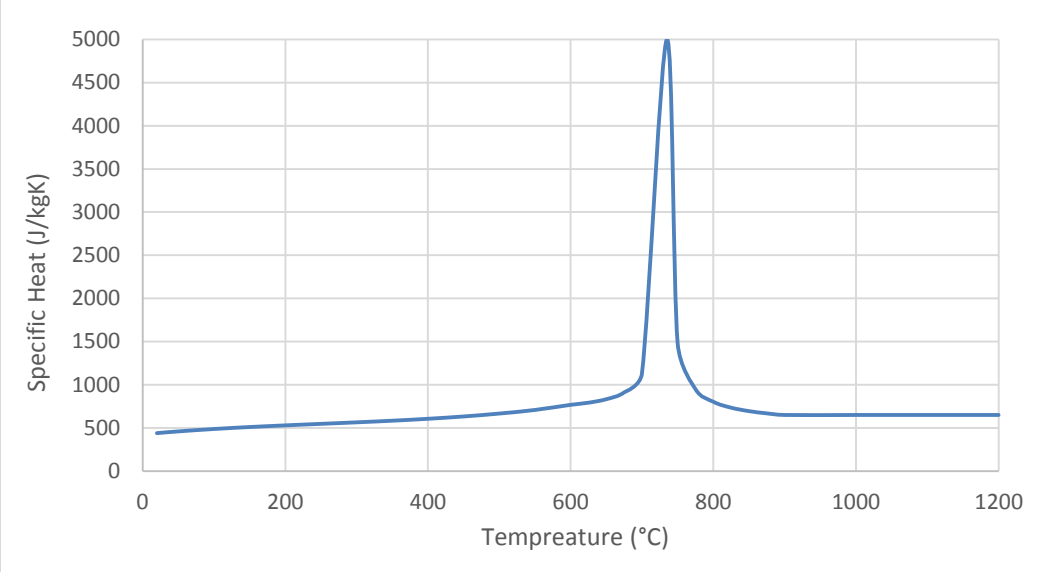

Figure 2-3 Specific heat of steel as a function of temperature

Note: Steel density and Poisson's ratio are considered independent of temperature.

2.2 Mechanical Properties of Steel

2.2.1 General Steel Properties

Under elevated temperatures the mechanical properties of steel will deteriorate, normally steel loses most of its strength at temperatures higher than 900° C. At ambient temperatures the yield point in the stress-strain curve can be easily identified, however, at elevated temperatures there is not a distinctive yield point, so the yield strength is determined based on the use of proof strength. Proof strength is the point of the stress-strain curve that intersects with a line passing through 1% strain at the same slope as the linear portion of the stress-strain curve. An example of determining the proof strength is shown in Figure 2-4.

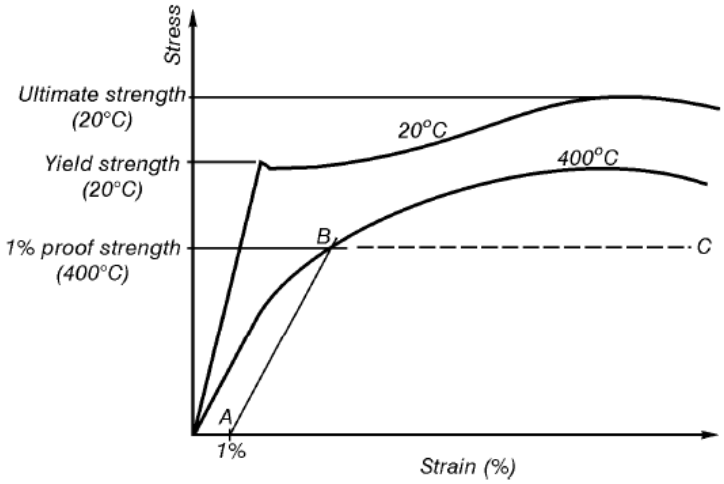

Figure 2-4 Degradation of steel properties and determination of proof strength (Buchanan [19])

To determine the stress-strain curve at elevated temperatures two methods have been commonly utilized, transient-state and steady-state methods. In transient-state method the load is applied constantly with increasing temperature, during the test a temperature-strain relationship will be recorded. While in steady-state method the test model will be heated to a specific temperature then a tensile test is performed, and the stress-strain curve is recorded during the test.

Both methods can be used to determine the mechanical properties of steel. However, it has been proven that transient-state tests results are more representative of actual behavior. Thus, the test results from this method have been adopted in the Eurocode as shown in Figure 2-5 for S275 steel.

For other types of steel, the EN 1993-1-2 provides reduction factors for stress-strain relationship of steel at elevated temperatures, these reduction factors are plotted in Figure 2-6 for yield strength, modulus of elasticity, and proportional limit.

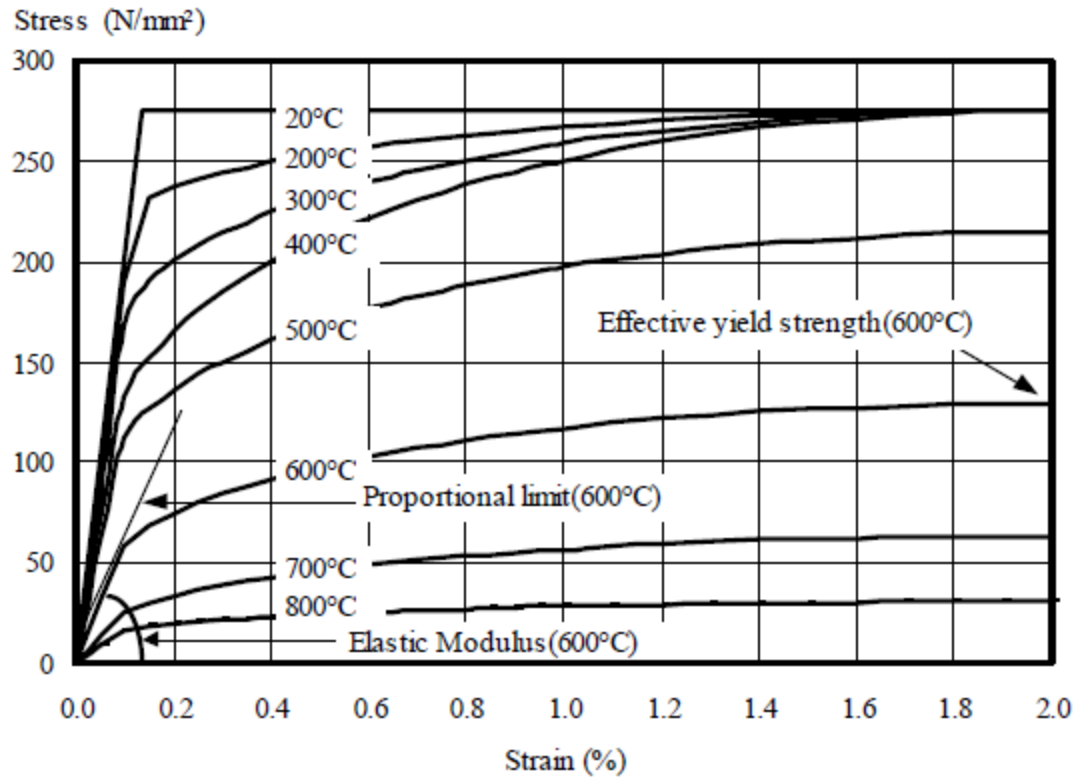

Figure 2-5 Strain-stress curves at increasing temperatures for S275 steel (EC3 curves)

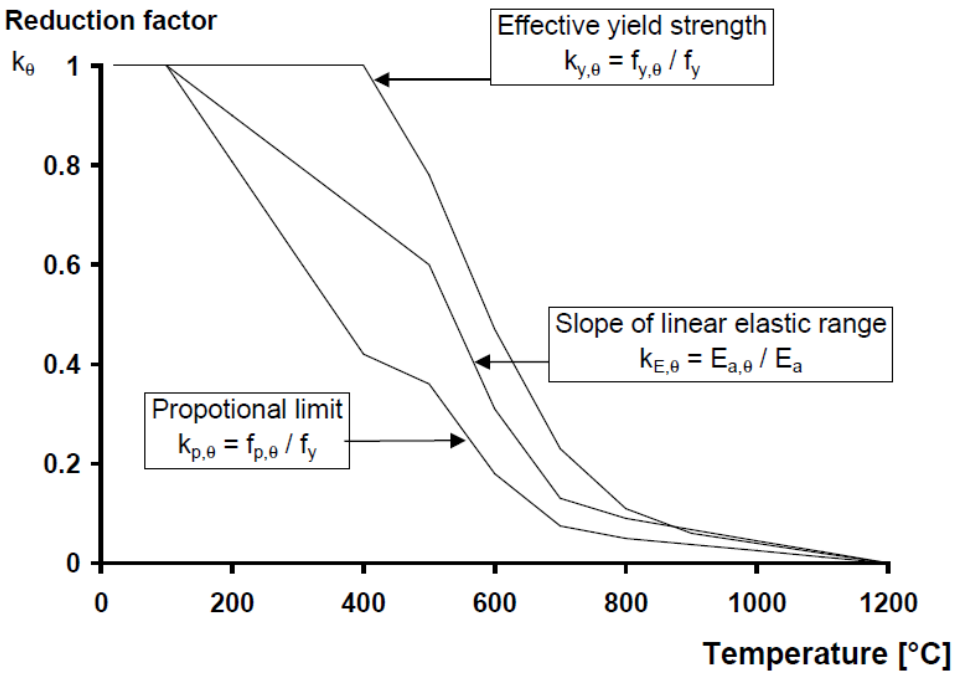

Figure 2-6 Reduction factors for stress-strain relationship of steel at elevated temperatures (EC3)

Chen et al. [36] investigated the changes in the mechanical properties of high strength and mild structural steel at elevated temperatures. The mechanical properties of steel as described in design standards is based on testing hot-rolled carbon steel with mild strength but not high strength steel. The results of their investigation showed that in general the yield strengths predicted by available design standards were conservative while the modulus of elasticity values predicted based on transient-state tests were not conservative for high strength steel.

2.2.2 Bolts and Welds Strength at High Temperature

Figure 2-7 represents the strength reduction factors for bolts (in tension or shear) due to elevated temperatures as recommended by Eurocode 3 (EN 1993-1-2:2005 Table D.1).

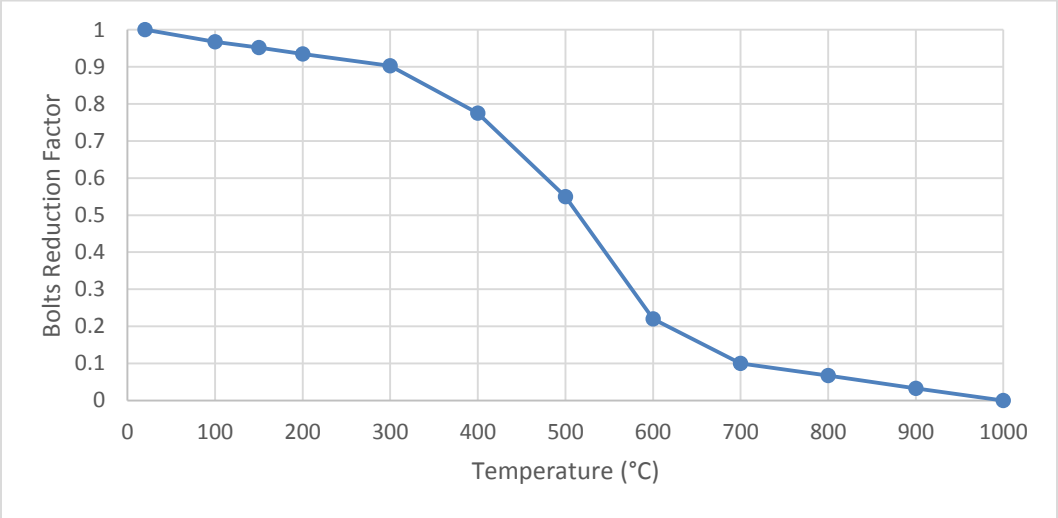

Figure 2-7 Strength reduction factors for bolts (EN 1993-1-2:2005)

The Eurocode 3 has also provided similar reduction factors for fillet welds under elevated temperatures, as shown in Figure 2-8. The design strength for butt welds, temperatures up to 700°C, should be taken as "equal to the strength of the weaker part joined using the appropriate reduction factors for structural steel."

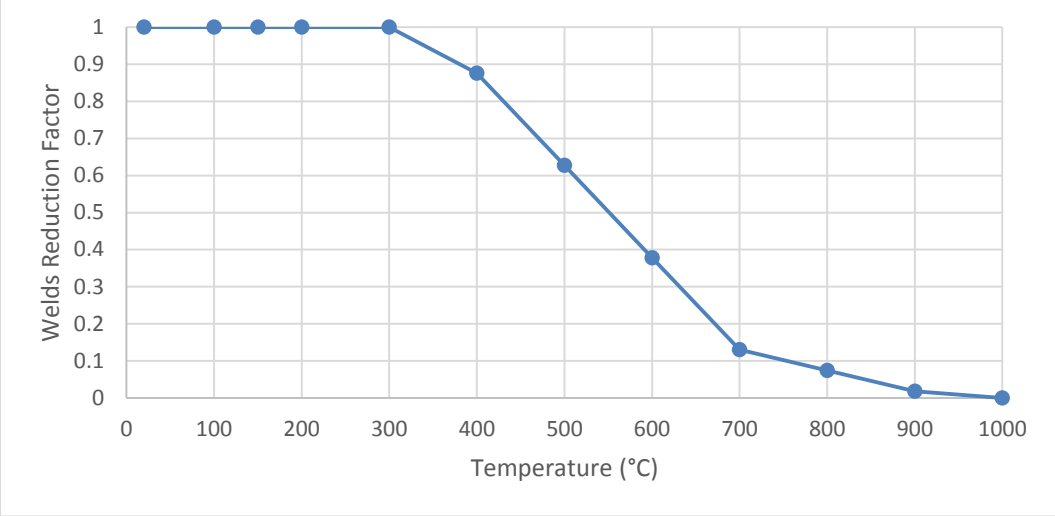

Figure 2-8 Strength reduction factors for Welds (EN 1993-1-2:2005)

2.3 JOHNSON-COOK MODEL

The Johnson-Cook constitutive model is used to represent the strength behavior of materials, typically metals, subjected to large strains, high strain rates and high temperatures. With this model, the yield stress σ_Y varies depending on strain, strain rate and temperature.

The model defines the yield stress as:

$$\sigma_Y = \left[A + B\left(\varepsilon_{eff}^{p}\right)^{N}\right](1 + C ln\dot{\varepsilon})[1 - (T_H)^{M}] \qquad 2.4$$

ε_{eff}^{p}: Effective plastic strain

$\dot{\varepsilon} = {\varepsilon_{eff}^{p}}/{\dot{\varepsilon_0}}$: Normalized effective plastic strain rate. Where $\dot{\varepsilon_0}$ is strain rate used to determine A, B and N

$T_H = \frac{T - T_R}{T_M - T_R}$: Homologous temperature

T_M: Melting temperature

T_R: Reference temperature when determining A, B and N

The expression in the first set of brackets gives the stress as a function of strain when $\dot{\varepsilon} = 1.0$ sec^{-1} and $T_H = 0$ (i.e. for laboratory experiments at room temperature). The constant A is the basic yield stress at low strains while B and N represent the effect of strain hardening.

The expressions in the second set of brackets represent the effects of strain rate on the yield strength of the material. The reference strain rate against which the material data was measured is used to normalize the plastic strain rate enhancement. 1.0/second is used by default.

The expression in the third set of brackets represents thermal softening such that the yield stress drops to zero at the melting temperature T_M. [37]

The Johnson-Cook model is used in temperature-related finite element analyses, mostly related to explicit dynamics.

2.4 Ambient Temperature Properties

Material properties for the specimen components at ambient temperature are listed in Table 2-1. These are the properties used in creating the finite element model in this research project.

Part	Ultimate Stress (ksi)	Yield Stress (ksi)	Modulus of Elasticity (ksi)×10^3
A325 bolt	120	92	29
HSS	62	50	29
Steel bars	58	36	29

Table 2-1 Ambient material properties

Note: mechanical properties of all used hollow structural sections are based on ASTM A500 Grade C.

CHAPTER 3

ELEVATED TEMPERATURE EXPERIMENTAL INVESTIGATION

3.1 INTRODUCTION

The experiments conducted in this research, and the finite element model, are focused on a small and a vital element in a big structure, the structural bolts. The application of a heat gradient (wither it is a standard fire curve or not) on a single bolt may not be used to assess the strength of an entire structure. However, it helps in understanding the response of this element and its important role in the initiation and progress of failure in a structure undergoing a fire event. Collapse of the structure begins with the weakest and most vulnerable component.

The following experiments were conducted in the Structural Lab of UW-Milwaukee. Using a tensile-testing machine (Tinius Olsen) and a custom-built electric furnace. The main objective of these experiments was to study the effects of high temperatures on standard A325 bolts and to use the results from these tests to develop a working finite element model that can possibly replace the tested bolts in a full structure.

3.2 SPECIMEN COMPONENTS AND GENERAL DESCRIPTION

In total ten tests were conducted, six of which were for the purpose of exploration of the equipment limits and testing out different bolts. Although some results from those experiments were recorded, nonetheless those results were not used to verify the finite element

model. Instead, the results from the remaining four identical tests were used with the finite element model.

In all cases the tested specimen consisted of a single ASTM A325 structural bolt connecting two square (4"x4") hollow structural steel sections (HSS), which are in turn attached to the testing machine grips through two 1"-diameter vertical bars as shown in Figure 3-1 (more details on the test setup are available in Chapter 6). In some of the experiments, a weldable high temperature strain gage was fitted to the shank of the tested bolt. In order to accommodate this strain gage, a spacer piece of steel is placed in between the two HSS. The steel bolt and the two HSS sections along with a small part of the two vertical bars were enclosed into the custom-built furnace.

Figure 3-1 The tested assembly inside the heat chamber

3.3 ELECTRIC FURNACE

The furnace used in the experimental work consists of two semi-cylindrical electric ceramic heaters with vestibules on top and bottom (2700 Watt, 240V, 12" in height, 16" outer diameter and 12" inner diameter). Two ceramic end caps were used to close the top and bottom vestibules and form a closed chamber while allowing for wires and the vertical steel bars to pass through. Figure 3-2 shows the electric furnace setting on the frame of the tensile testing machine. All parts were mounted on an adjustable steel frame that allows for positioning the furnace at suitable height while holding it firmly in place.

The temperature inside the furnace was measured by an inserted thermocouple that transmitted its data to a computerized controller unit, which could adjust the temperature in the furnace to follow a predetermined heating regime.

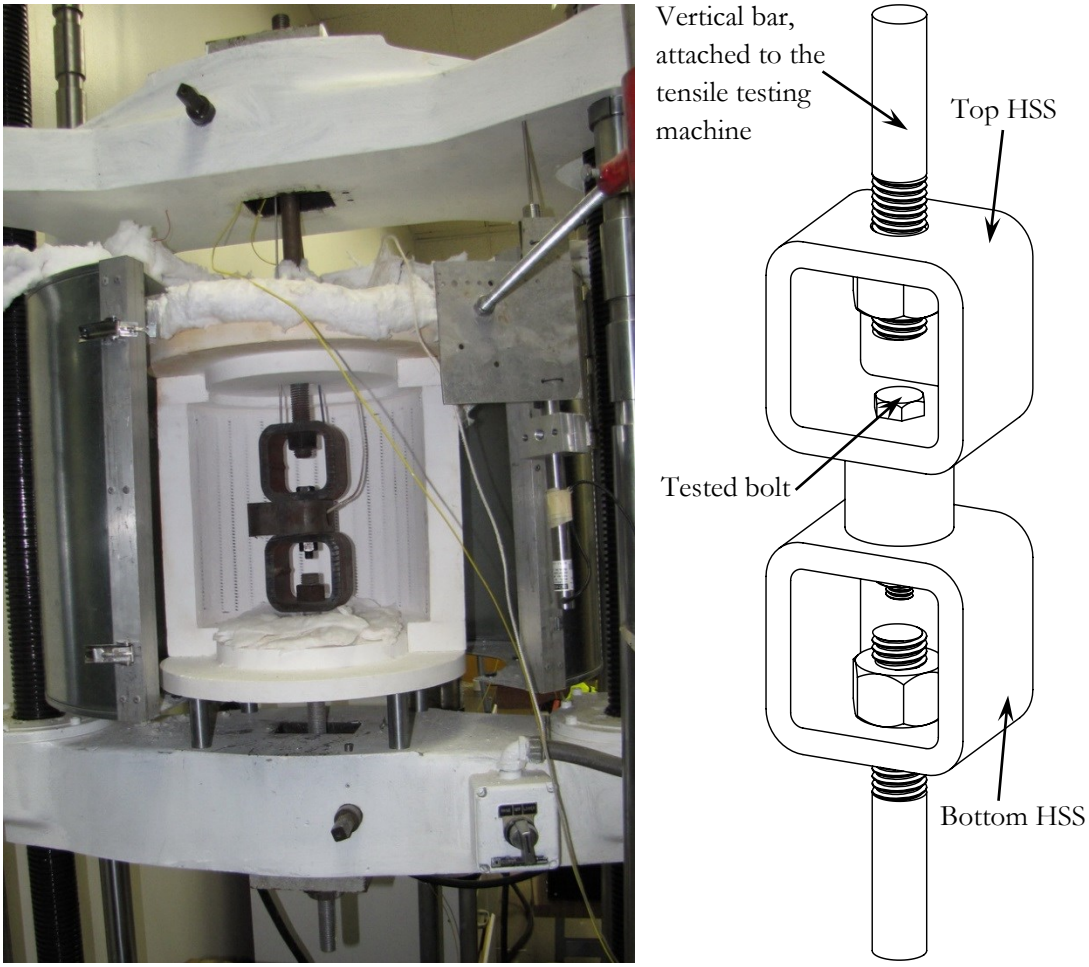

Figure 3-2 Testing rig (left), a CAD design of the test (right)

Figure 3-2 shows a comparison between the preliminary CAD design of the tested specimen and the actual one used in the experimental work. One of the two semi-cylindrical ceramic heaters is removed to expose the interior of the furnace. The furnace had electrical wiring running across its walls, which prevented a side window from being into it. The top and bottom ceramic caps were removable as well.

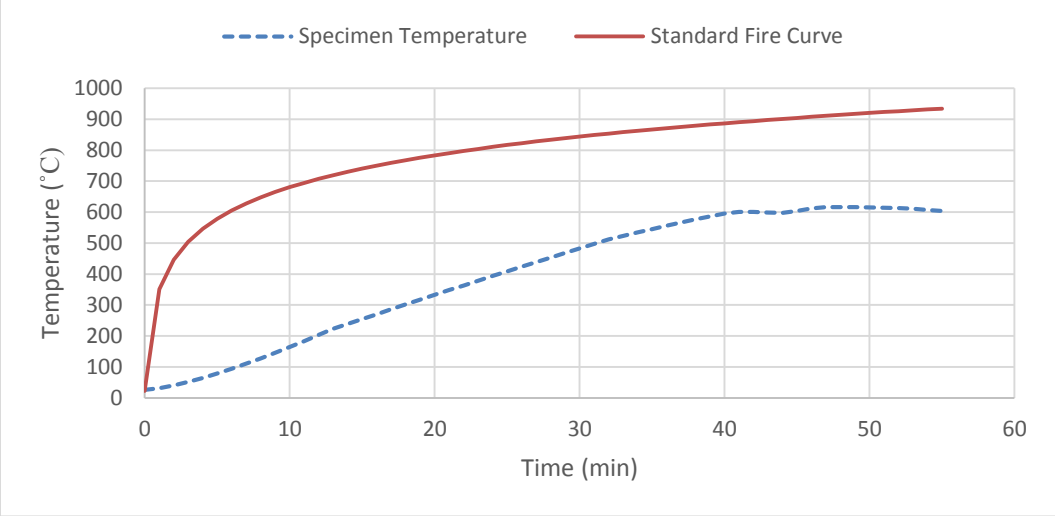

Figure 3-3 Comparison between a standard fire and the temperature of the specimen

Figure 3-3 shows the furnace-heating curve along with a standard fire curve (as presented in Chapter 1).

3.4 Test Setup

1. Strain gage installation: The bolt shank was cleaned, abraded and neutralized before fitting a strain gage to it using a capacitive spot welder.

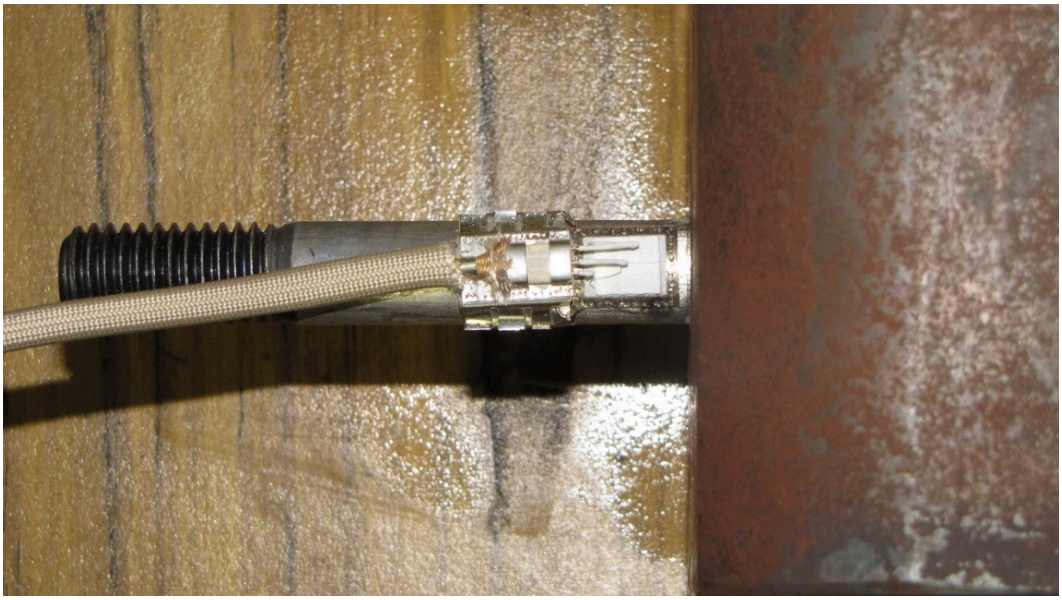

Figure 3-4 Strain gage installation

Figure 3-5 Strain gage covered with ceramic fiber and a protective cover

As shown in Figures 3-4 and 3-5, a lot of effort had been put in trying to protect the strain gage from the heat of the furnace. However, these efforts were in vain, since the strain gage kept on failing as soon as the temperature started to rise.

2. Bolt pretensioning: The tested specimen was assembled using a torque wrench to tighten the bolt between the top and bottom hollow structural sections, while the spacer piece provided enough room for the placement of the strain gage.

   The top and bottom steel bars were loosely attached to the tested specimen and the grips of the testing machine.

3. Load application: After closing the furnace and securing it inside the steel frame, a linear variable differential transformer (LVDT) was attached to the system in order to measure the vertical displacements. Afterwards, a tension load was applied to the vertical bars and increased at ambient temperature until reaching the desired load. This load was then

maintained at a constant level in order to start the next step. Figure 3-7 shows the setup just before the heat application.

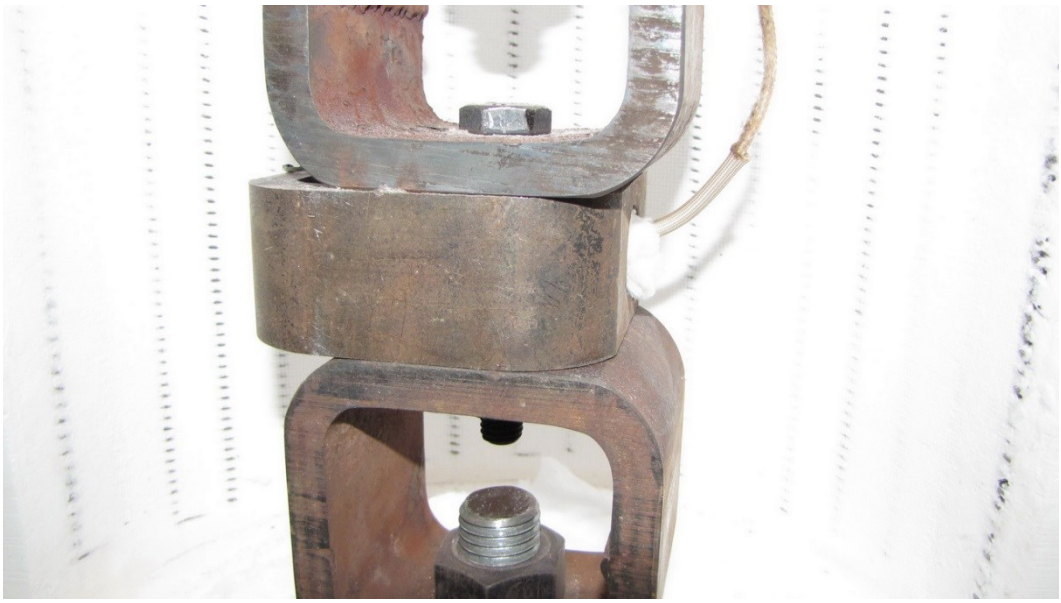

Figure 3-6 The bolt after tightening

Figure 3-7 The tested assembly just before the heat application

4. Heat application: A nonlinear temperature profile (see Figure 3-3) was adopted for the four main experiments. All the experiments were conducted using a transient-state

method, which means that the tension load was maintained at a constant level during the experiment while the temperature was increased until failure.

An attempt to follow a standard fire curve was not successful because of equipment limitations. The temperature increases in a standard fire curve so fast that the furnace components were not able to follow a similar path. It has not been fully established if creep had any significant effect on the experiments, more investigation into the effects of longer exposure to heat is recommended.

The bottom of the inside chamber of the furnace was lined with a thick layer of ceramic fiber to insure that no heat escaped from the bottom end cap and to cushion the impact of the falling parts after the specimen has failed. Outside the furnace, on the top end cap, a similar layer of ceramic fiber is also used to prevent hot fumes coming out of the furnace from melting all the electrical wires attached to and coming out of the furnace. All other parts that were in danger of exposure to high temperatures were also protected with a layer of ceramic fiber.

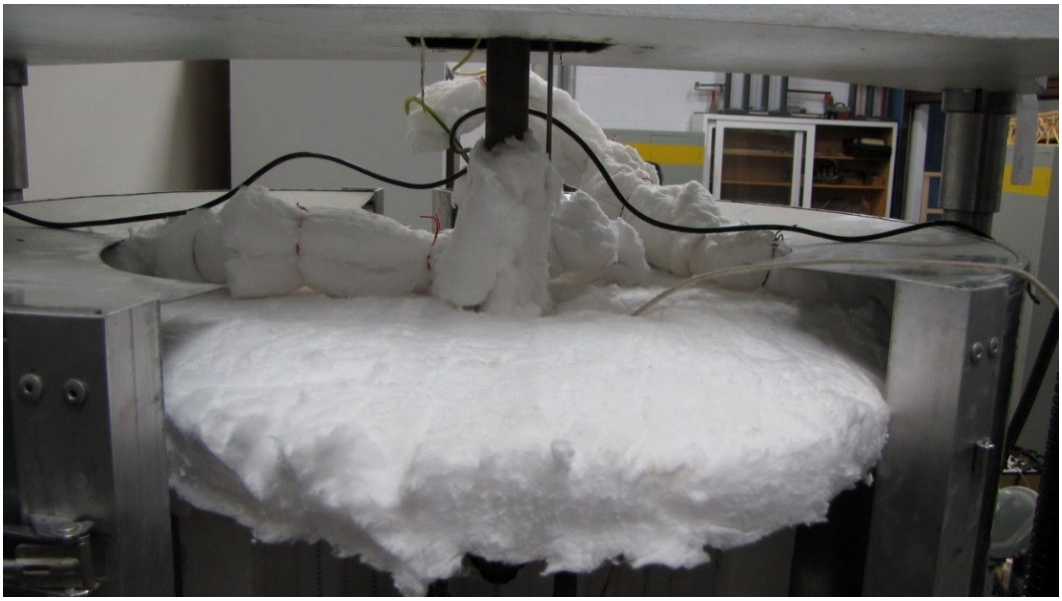

Figure 3-8 Ceramic fiber used on top of the furnace

Ambient temperature material properties were discussed in Chapter 2 and the full geometrical properties are shown in detail in Chapter 6.

3.5 DATA ACQUISITION

A data acquisition unit collected various information about the tested specimen until its failure. This information was instrumental in verifying the finite element model. The data recorded included:

1. Temperature: Two thermocouples (type K) were used to record the temperature of the steel specimen inside the furnace. The first thermocouple sent its data to the furnace controller unit, which was responsible for controlling the temperature inside the furnace. While the second thermocouple was attached to the main data acquisition unit. Both thermocouples were placed in direct contact with the top surface of the specimen as shown in Figure 3-10

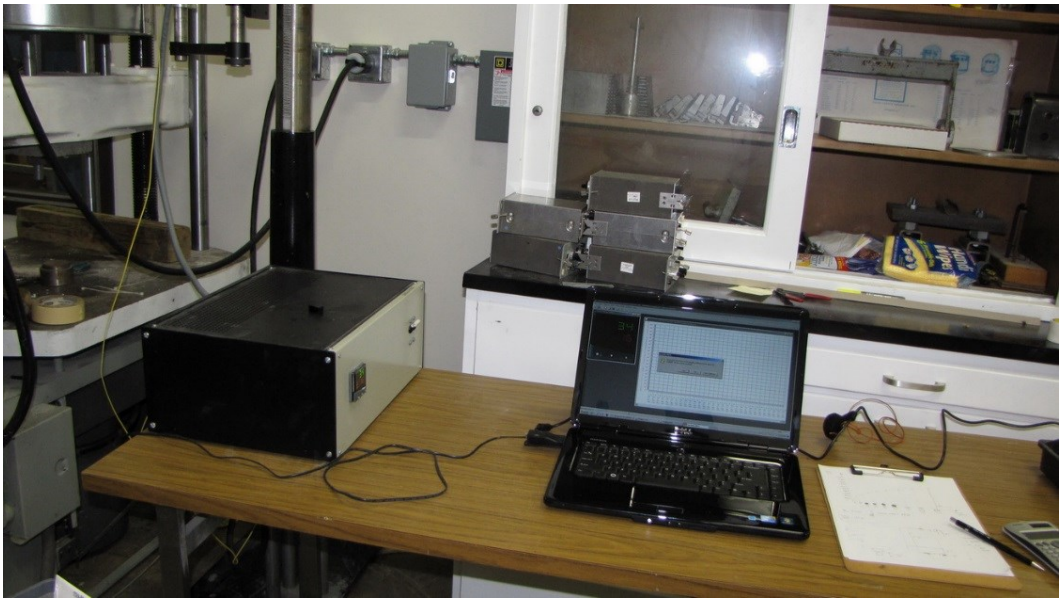

Figure 3-9 The furnace controller unit

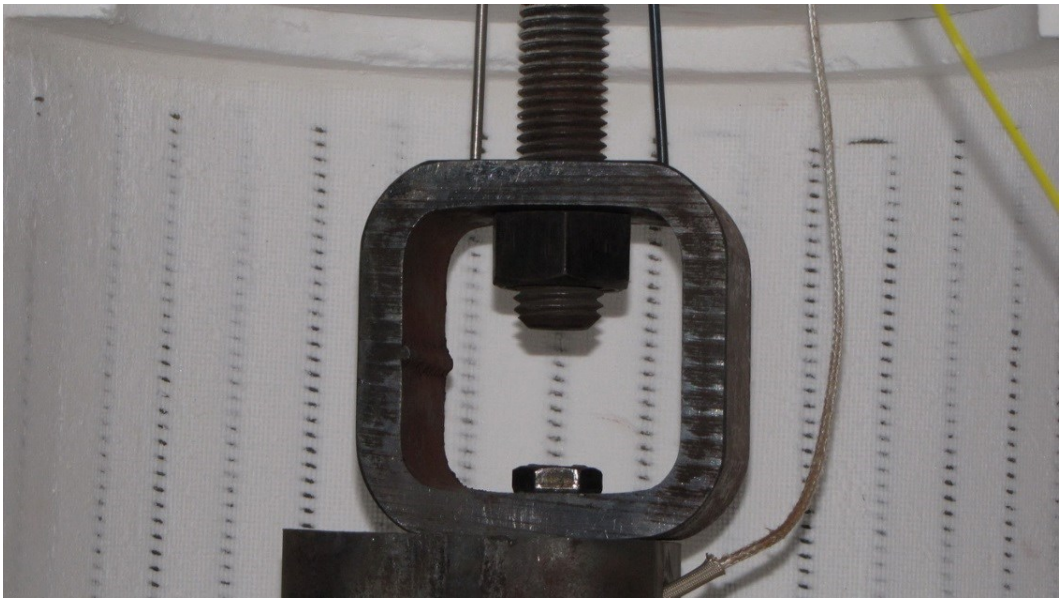

Figure 3-10 Two thermocouples resting on the top HSS

2. Load: The applied tension load was recorded through the load cell readings of the testing machine (Tinius Olsen). The readings of the load cell were verified by applying a load on a spring with a known stiffness.

3. Strain: A strain gage fitted to the shank of the tested bolt measured strains in the bolt, but as mentioned before it constantly failed at low temperatures. This is why the results of the strain gage were deemed unreliable.

4. Displacement: In order to monitor the deformations in the tested specimen until failure, a linear variable differential transformer module (LVDT) was used to measure the displacement of the tension machine. As a result, measuring the elongation in the entire specimen and not only the tested bolt. That is why it was necessary to model all the parts involved in the test.

Figure 3-11 The data acquisition unit

Other measurements of the specimen dimensions before and after each test where also recorded.

3.6 General Observations

Figure 3-12 Failure in the threaded section

The progress of each test was carefully monitored until the specimen has failed. All tested bolts failed under tension in the threaded section at the root of the nut, showing considerable deformations at high temperatures.

Figure 3-13 A comparison between the bolt before and after the test

Figures 3-12 and 3-13 show the failure patterns witnessed by all the tested bolts. The failure plane always occurred in the threaded area just under the nut. On average, ½ " –diameter bolts have elongated an extra 0.4 – 0.5 inches in length.

For most of the conducted experiments, and except for the high temperature oxidation, which was prevalent in all non-coated parts, there was no discernable damage to any of the tested parts (steel sections, bars, and nut). The only part that has failed was the bolt as mentioned above. Figure 3-14 shows the extent of the high temperature oxidation after a test.

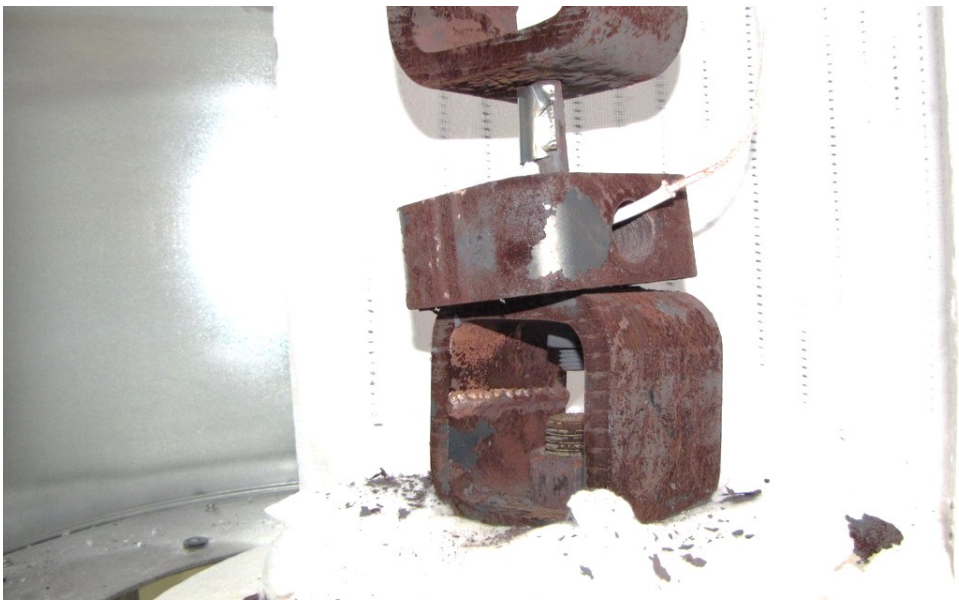

Figure 3-14 Rusted parts after the end of the test

At a closer inspection, the stain gage did not seem damaged neither did any of its wiring. Figure 3-15 shows the effect of high temperature on a strain gage.

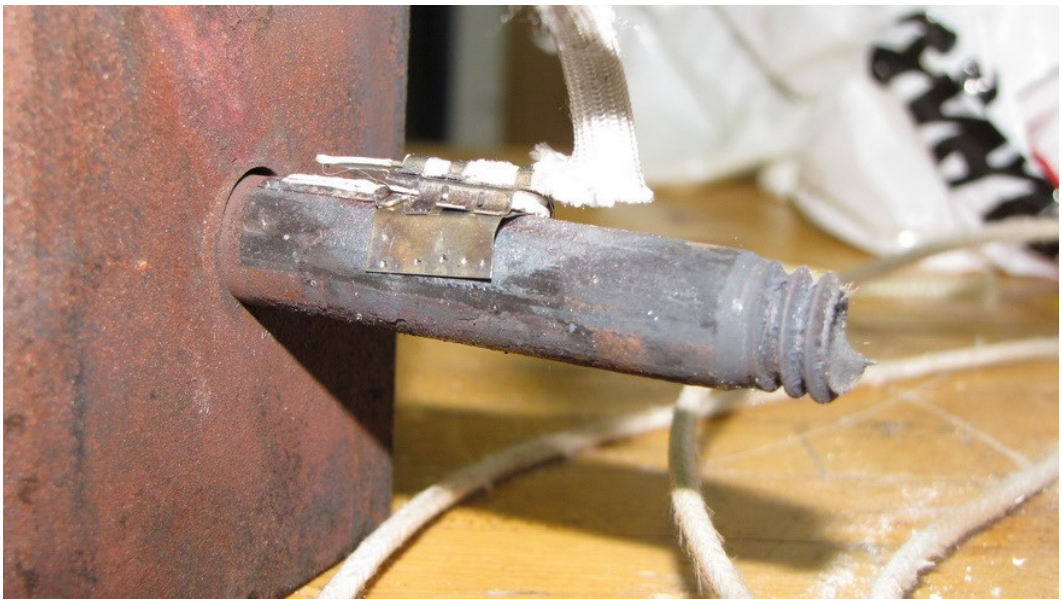

Figure 3-15 A close up look at the strain gage after the test

CHAPTER 4

3D FINITE ELEMENT MODELING OF THE A325 STEEL BOLT

4.1 THE FINITE ELEMENT SOFTWARE AND GENERAL APPROACH

The finite element package used in the analysis is ANSYS Workbench v14.0. This commercial software provides an easy and flexible working environment for developing and managing a wide array of analysis systems (transient thermal, static structural, etc.) A certain system can receive data from, or share its generated data with, other systems. The general analysis process involves:

- Creating the three-dimensional model geometry based on the given dimensions of the tested samples.
- Defining material properties of each element. Sensitivity analysis is done to choose various material property values. Especially when test data are not available or not sufficiently specific to the tested case, like the coefficient of friction or Poisson's ratio.
- Identifying contact regions between various elements and setting up their properties.
- Generating a suitable mesh of elements that represents the model with the least number of elements possible without compromising the accuracy of the analysis results.
- Applying the test loads on the model and running the analysis.
- Reviewing the results. Corrective action will be made to the problematic spots if necessary.

4.2 MODEL GEOMETRY

The tested assembly, shown in Figure 4-1, consists of two vertical bars, two hollow structural sections (HSS4×4), a single A325 bolt and a spacer piece.

The vertical bars are one-inch in diameter and although threaded on both ends in the experiments, these bars were not threaded in the finite element model since no failure or extreme deformations happened to them.

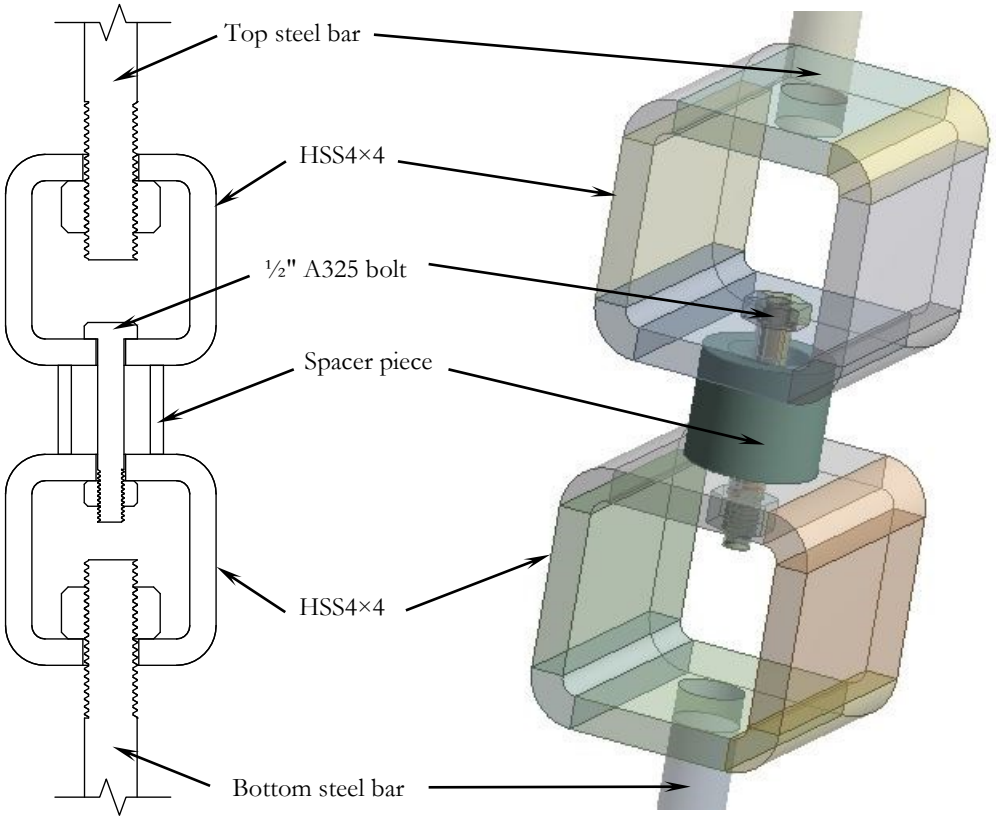

Figure 4-1 A general layout of the tested assembly

The two HSS were modeled with the exact dimensions given in the AISC. These dimensions are shown in detail in Chapter 6. Each vertical bar passes through a hole in the HSS connected to it, which has a diameter of one inch, while the hole for the bolt is $1/2" + 1/16"$ in diameter.

The spacer piece is not a structural element; hence, a simplified steel tube was used.

Since the emphasis of this analysis is placed on the behavior of the A325 bolt, extra care was given to creating an accurate model that follows closely the actual bolt-nut behavior. The dimensions used to create the bolt are shown in Table 4-1 and Figure 4-2.

The dimensions of the threads were calculated based on the Unified Thread Standard (UTS), as shown in Chapter 1.

By comparison, the modeled bolt (shown in Figure 4-3) formed a very close geometric representation of the real bolts used in the experimental work. The bolt head and the nut were simplified in shape, in order to produce a more structured mesh. Additionally, some parts of the threads were deleted to reduce the overall number of elements in the model.

Bolt Dimensions							**Nut Dimensions**		
D	**TPI**	**F**	**G**	**H**	**LT**	**L**	**A**	**B**	**E**
1/2"	13	0.875"	1.01"	5/16"	1"	3.47"	0.875"	1.01"	0.484"

Table 4-1 Dimensions of the modeled bolt

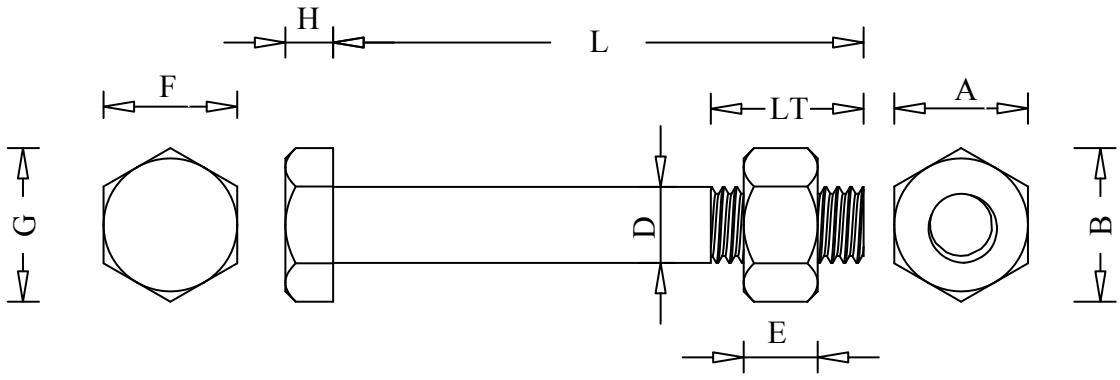

Figure 4-2 ASTM A325 bolt and nut

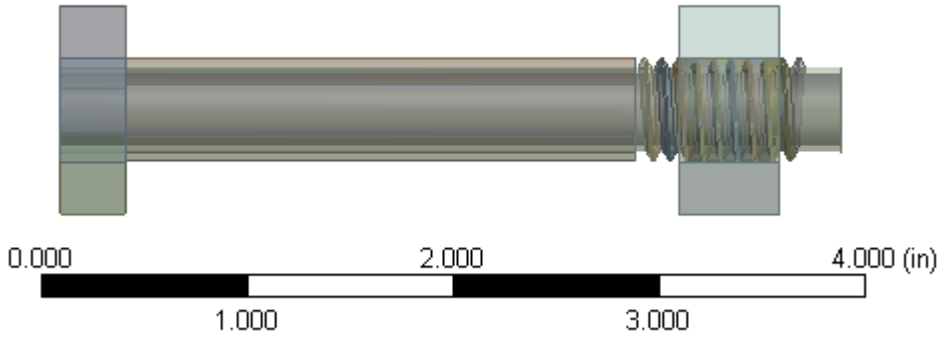

Figure 4-3 The modeled bolt

4.3 DesignModeler, Sketches, Bodies and Parts

All the previously mentioned components were modeled in ANSYS-DesignModeler. The DesignModeler is an application that provides an advanced modeling environment in which the user can create and edit 2D and 3D geometric models. The model created for this research is a "parametric model". Which means, once the model is created; all the dimensions can be modified by changing "parameters" and there is no need to repeat the long and tedious steps of modeling again.

In the DesignModeler, the model is divided into either Bodies or Parts. Each body is made up of multiple parts. This analysis utilized 5 parts and 79 bodies, as shown in Figure 4-4. Bodies were created because of the different geometric shapes involved in the modeling process and, in many occasions, in order to simplify the meshing process.

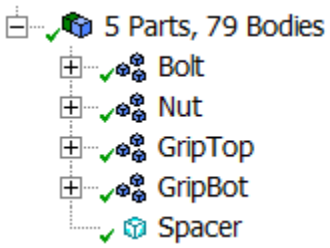

Figure 4-4 The parts and bodies used in the model

Parts, however, were created to organize bodies in a hierarchical structure easy to manipulate and they guaranteed a continuous mesh throughout each part.

All bodies were created starting from a Sketch. A sketch is a 2D dimensional profile of the body. After drawing the sketch it can be extruded, revolved, or swept to create the body. Figure 4-5 shows some of the sketches used in the modeling process; each sketch belongs to a certain coordinate system or a plane.

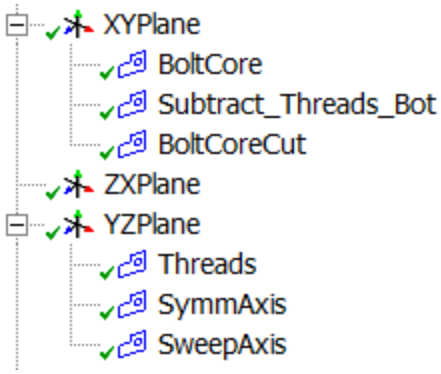

Figure 4-5 Sketches in XYPlane and YZPlane

4.4 The Model Parts

4.4.1 GripTop and GripBot

These two parts were almost identical, each consisting of a vertical bar and a single HSS. The bars were created by extruding a 1"-diameter circle sketches, and the HSS were created by extruding the profile of the hollow sections as shown in Figure 4-6, the inner sketch in the figure was extruded and then subtracted from the outer sketch.

The decision to merge the vertical bars with the attached HSS reduces the number of contact regions, since each part is meshed as a whole without discontinuities in the mesh.

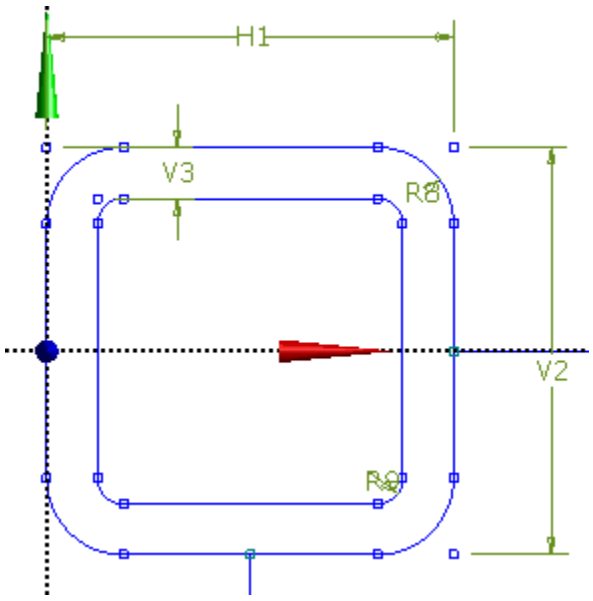

Figure 4-6 Sketches used to create the HSS

4.4.2 Spacer

Figure 4-7 shows the two sketches that were used to create the spacer piece between the two HSS. Both sketches were extruded to the desired height, and then the inner cylinder was subtracted from the outer one to create the final model.

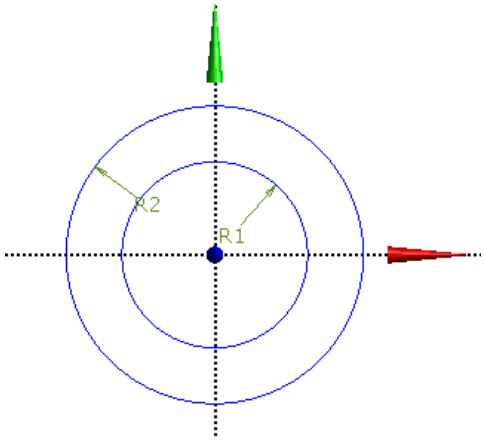

Figure 4-7 Sketches used to create the spacer piece

4.4.3 Bolt

To simplify the bolt geometry and make the meshing process easier, the bolt was divided into smaller bodies. These bodies can be grouped into four distinctive components:

1. Bolt Head

The bolt head was extruded from a hexagon, sliced into six different bodies and then an inner core was subtracted as shown in Figure 4-8.

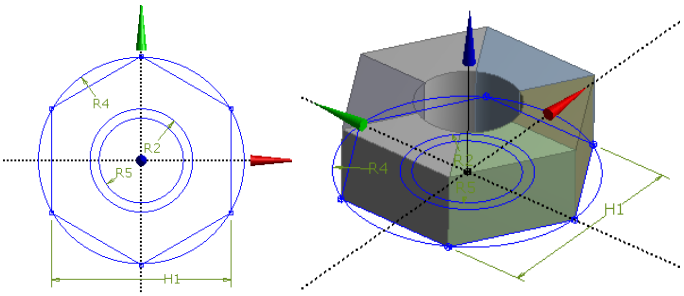

Figure 4-8 Bolt head

2. Bolt Shank (up to the threaded part)

The outer shell of the bolt shank up to the threads was modeled separately. This way an inner cylindrical core extending all the way from the top of the bolt to the bottom could be created as illustrated in the next step. The bolt shank was also sliced into six pieces to help in the meshing process.

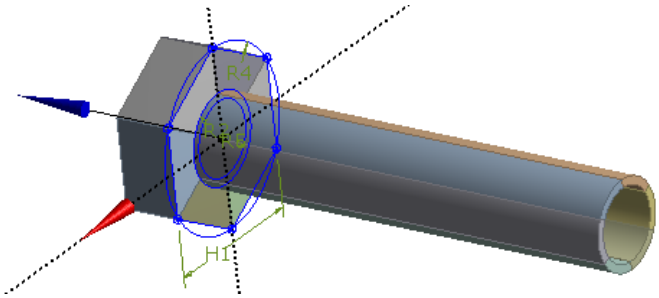

Figure 4-9 Bolt shank shell

3. Bolt Core

Providing a single cylindrical body for the core of the bolt was very useful in applying the pretensioning load and in the meshing process as well. This core was later sliced further to provide a transitional body during the meshing process.

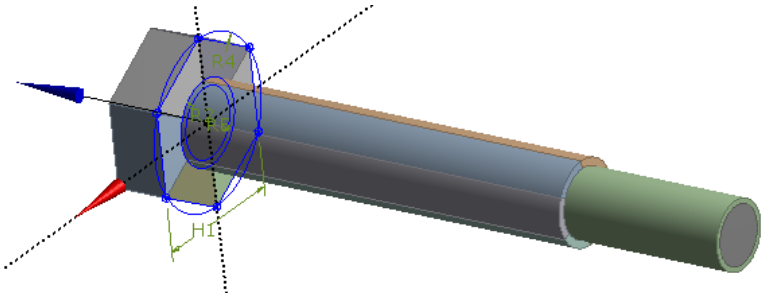

Figure 4-10 Bolt core

4. Bolt Threads

The profile and pitch of the threads, shown in Figure 4-11, were based on the dimensions of threads as presented in Chapter 1. The threads were created using a "sweep" command on a helical path.

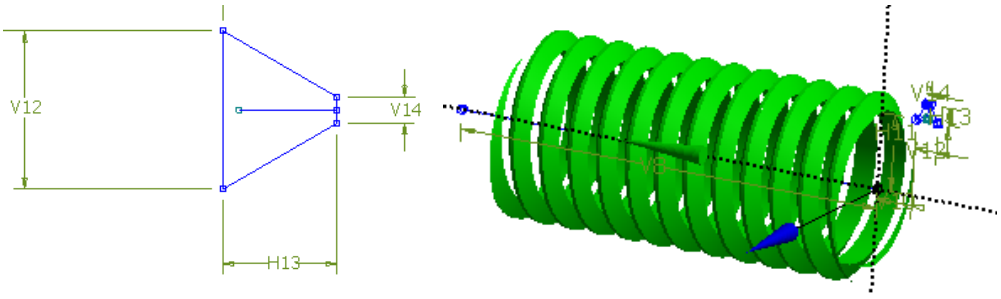

Figure 4-11 Threads profile and the threads body

Like all the previous bodies, creating a single body for threads was not practical. Slicing this body and creating multiple half-revolution threads allowed greater control over the threads. The threads beneath the nut were deleted since they did not have any structural value; this helped in reducing the amount of elements in the model significantly.

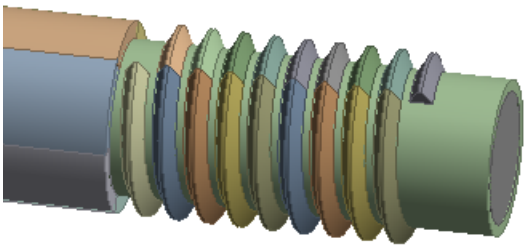

Figure 4-12 Deleted threads at the bottom and top of the threaded section

4.4.4 Nut

The nut was created by extruding a hexagon and then subtracting the bolt geometry from it. The threads in the nut have also been separated from its body and sliced to form smaller half-turn bodies.

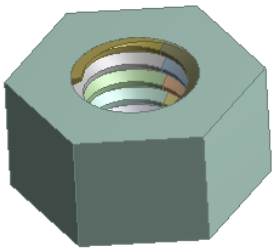

Figure 4-13 The nut model

4.5 Design Parameters

As previously mentioned, all the dimensions of the bodies created in the DesignModeler were parameterized. That also included the locations of geometric planes and symmetry lines. Changing these parameters and refreshing the model will make the remodeling process much faster and easier to manage.

The "Design Parameters" were coded into the DesignModeler as shown below. To help explain each line of code, descriptive comments have been inserted into the code preceded by the hash symbol "#".

```
# (All units are in inches)
# Bolt Dimensions

BoltR = 0.25
BoltH = 3.785


BoltThreadH = 0.0451
BoltThreadTotalH = 1.0
BoltThreadTop = 0.0104
BoltThreadBot = 0.0625
BoltThreadPitch = 0.0833

# Bolt head circumscribed polygon circle radius
BoltHeadCCR = 0.4375
BoltHeadH = 0.3125


# Nut Dimensions

NutH = 0.4844
NutCCR = 0.4375

# HSS Dimensions

HSSThickness = 0.5
HSSHeight = 4.0
HSSWidth = 4.0
HSSLength = 3.0

# Gap between the top & bot HSS sections
# (spacer height, does not include thickness of sections)
GapH = 1.6875

# Bars Dimensions
# Top Bar Length (including thickness of HSS)
TopBLength = 19.4375

# Bot. Bar Length (including thickness of HSS)
BotBLength = 17.75

# Bar radius
BarR = 0.5

# HSS position and extrusion
XYPlane_HeatedBBar.FD1 = 0
XYPlane_HeatedTBar.FD1 = 0
ZXPlane_HSS_Side.FD1 = HSSLength/2
HSS_Ext2.FD1 = HSSLength
HSS_Int2.FD1 = HSSLength
```

4.6 PARAMETER/DIMENSION ASSIGNMENT

The following is the code used to create the model based on the previously defined parameters.

Comments are also present and preceded by the hash symbol "#".

```
#Calc. Core Radius
BoltCoreR = @BoltR - @BoltThreadH

#Calc. Shank w/o threads length
BoltClearShank = @BoltH - @BoltThreadTotalH - @BoltHeadH

# Calc. Grip: thickness of the two plates clamped by
# the bolt and nut + spacer height
Grip = @GapH + 2 * @HSSThickness


# Bolt Core
XYPlane.R1 = BoltCoreR

# Bolt inner core slice radius
XYPlane.R4 = 0.85 * BoltCoreR

# Bolt inner core slice height
InnerCoreSlice.FD1 = @BoltH

# Arbitrary (used for trimming threads)
XYPlane.R2 = 2 * @BoltR

#Bolt Thread Dimensions
YZPlane.V14 = @BoltThreadTop
YZPlane.V12 = @BoltThreadBot
YZPlane.H13 = @BoltThreadH
YZPlane.H11 = BoltCoreR

# Sweep Axis length (make 20% longer then trim)
YZPlane.V8 = 1.2 * @BoltThreadTotalH

# used to create bolt head
XYPlane_BoltHeadBot.H1 = 2 * @BoltHeadCCR

# Bolt cover outside radius
XYPlane_BoltHeadBot.R2 = @BoltR

# Arbitrary (used for trimming threads)
XYPlane_BoltHeadBot.R4 = 2 * @BoltR

#Bolt cover inside radius
XYPlane_BoltHeadBot.R5 = BoltCoreR

# Plane at the bottom of bolt head
XYPlane_BoltHeadBot.FD1 = @BoltH - @BoltHeadH

# Plane at top of bolt head
XYPlane_BoltHeadTop.FD1 = @BoltH

# Used to cut bolt core
XYPlane_BoltHeadTop.R1 = BoltCoreR

# Bolt creation commands
BoltHead2.FD1 = @BoltHeadH
BoltHeadCut.FD1 = @BoltHeadH
ShankShell.FD1 = BoltClearShank
ShankShellCut.FD1 = BoltClearShank
Shank.FD1 = @BoltH
SweepThreads.FD6 = @BoltThreadPitch
ThreadsCutTop.FD1 = BoltClearShank
```

```
# Nut creation commands
XYPlane_NutTop.FD1 = @BoltH - @BoltHeadH - Grip
XYPlane_NutTop.H1 = 2 * @NutCCR
XYPlane_NutTop.R2 = @BoltR
Nut2.FD1 = @NutH
NutCut.FD1 = @NutH
NutThreads2.FD1 = @NutH

# Bolt hole dia. = bolt dia. + 1/16"
XYPlane_TopHSS_InTop.R1 = @BoltR + 1/32

# HSS creation commands

# Setup the plane for top HSS sketch
ZXPlane_HSS_Side.FD1 = @HSSLength/2

# Extrude and subtract
HSS_Ext2.FD1 = @HSSLength
HSS_Int2.FD1 = @HSSLength

# Set bottom of creation plane at the bottom of bolt head
ZXPlane_HSS_Side.FD2 = @BoltH - @BoltHeadH - @HSSThickness

# Set plane to inner top surface of top HSS.
XYPlane_TopHSS_InTop.FD1 = @BoltH - @BoltHeadH + @HSSHeight -2 *
@HSSThickness

# Set mirror plane to create bottom HSS
XYPlane_HSS_MirrorPlane.FD1 = @BoltH - @BoltHeadH - @HSSThickness -
@GapH/2

# Set slice plane for top of the Bottom HSS
XYPlane_HSS_CutH3.FD1 = - @HSSHeight - @GapH - 0.25
# Bar hole/Bar radius
XYPlane_TopHSS_InTop.R2 = @BarR

# Top and bottom bars creation commands
# Set Top Bar Length
Bar.FD1 = @TopBLength

# Cut Bottom Bar to real length
# Create a plane then slice and suppress bottom part
# If top bar is shorter, you need to reverse the operation
XYPlane_CutBotBar.FD1 = - @GapH/2 - @HSSHeight - @BotBLength +
@HSSThickness

# Spacer creation commands
# Place plane at bottom of top HSS
XYPlane_Spacer.FD1 = - @HSSThickness

# Outer radius. (random dimension - just make it large enough)
XYPlane_Spacer.R2 = 4 * @BoltR
# Inner radius. (random dimension)
XYPlane_Spacer.R1 = 2.5 * @BoltR


# Create spacer
Spacer_Ext2.FD1 = @GapH
Spacer_Int2.FD1 = @GapH

# Part of the top and bottom bars is inside the furnace
# To assign proper temperature, a final cut was necessary
```

```
# The clear height of the heated area is 13"
# Since it's a fixed number, it was not assigned to a variable

XYPlane_HeatedBBar.FD1 = - 13/2
XYPlane_HeatedTBar.FD1 = 13/2
```

4.7 Modeling Tree Outline

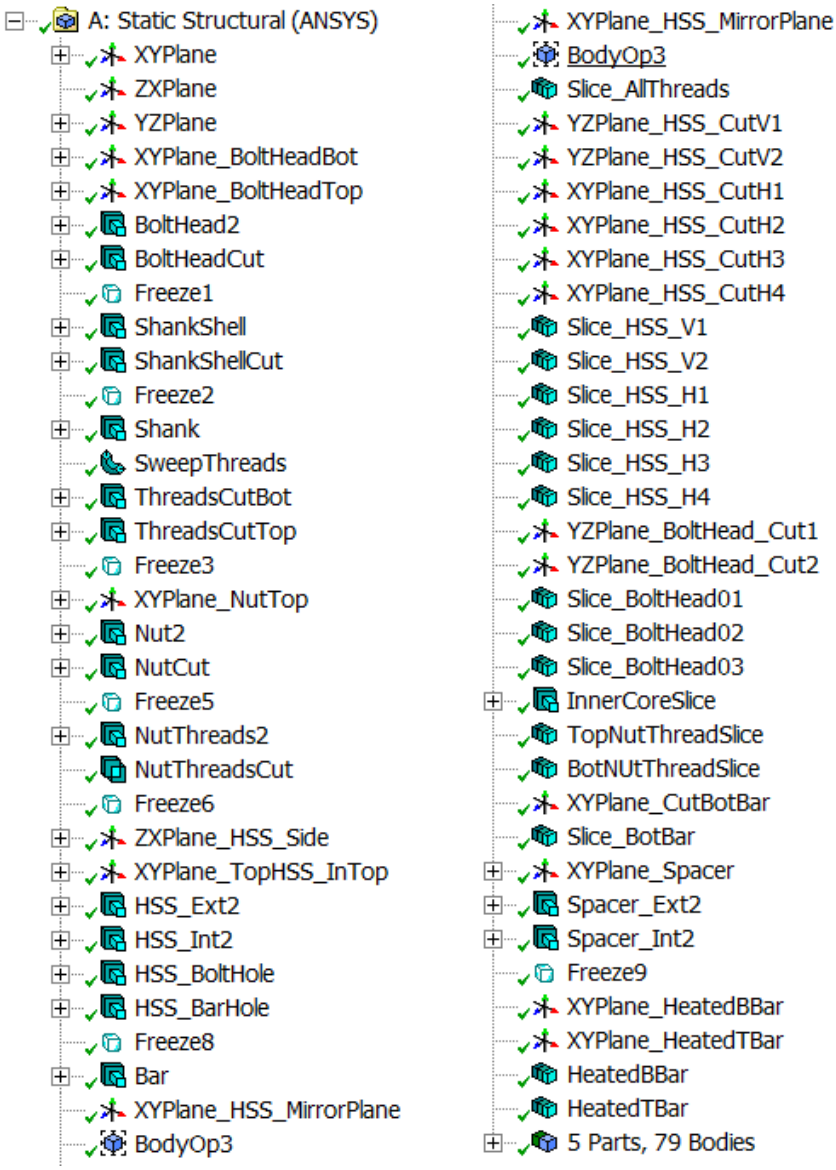

Figure 4-14 Modeling tree outline

The modeling tree outline is a graphical representation of all the steps and operations involved into the process of creating the model. The details of each step are not shown, but can easily be deduced from the code listed above.

4.8 MATERIAL PROPERTIES

The normalized reduction factors for steel properties, provided by the European Code, as explained in Chapter 2, were used to determine steel properties at different temperatures, which the software will assign to each element based on its temperature. The reduction factors for yield strength and modulus of elasticity of steel are listed in Table 4-2 and the computed values of those properties are presented in Table 4-3.

Poisson's ratio is assumed to be temperature-independent for steel. All available research has pointed towards small and inconsistent variations of the value of Poisson's ration, which supports the previous assumption.

Temperature (ºC)	Reduction factor for effective yield strength (relative to f_y)	Reduction factor for bolts yield strength (relative to f_y)	Reduction factor for the elastic modulus (relative to E)
22	1	1	1
100	1	0.968	1
200	1	0.935	0.9
300	1	0.903	0.8
400	1	0.775	0.7
500	0.78	0.55	0.6
600	0.47	0.22	0.31
700	0.23	0.1	0.13
800	0.11	0.067	0.09
900	0.06	0.033	0.0675
1000	0.04	0.00	0.045

Table 4-2 Reduction factors for steel stress-strain relationship at elevated temperatures

Steel Temperature, ºC	Young's Modulus (ksi)	Tensile Yield Strength (ksi)		
		Bolts	HSS	Bars
22	29000	92	50	36
100	29000	87.6	50	36
200	26100	86.0	50	36
300	23200	83.1	50	36
400	20300	71.3	50	36
500	17400	50.6	39	28.08
600	8990	20.2	23.5	16.92
700	3770	9.2	11.5	8.28
800	2610	6.2	5.5	3.96
900	1957.5	3.0	3	2.16
1000	1305	0.0	2	1.44

Table 4-3 Computed steel yield strength and modulus of elasticity

A list of other general properties of steel, used in this analysis, is provided in Table 4-4.

Property	Steel	Unit
Poisson's Ratio	0.3	–
Density	490	lb/ft^3
Thermal Expansion	1.2×10^{-5}	1/ºC
Thermal Conductivity	60.5	W/m.ºC
Specific Heat	434	J/kg.ºC

Table 4-4 General material properties

The stress-strain relationship of steel was assumed to be nonlinear. A multilinear kinematic hardening curve was used to represent this relationship. The linear segment in the curve derives its slope from interpolating a value for the modulus of elasticity based on the assigned temperature of each element. The nonlinear (plastic) part of the stress-strain curve had a single slope defined by a temperature-reduced ultimate stress. The reduction factors used for the ultimate stress were the same ones used for the yield stress, which is an approximation.

4.9 CONTACT REGIONS

When two bodies meet, a contact condition is formed. This contact can transfer structural loads and heat flows.

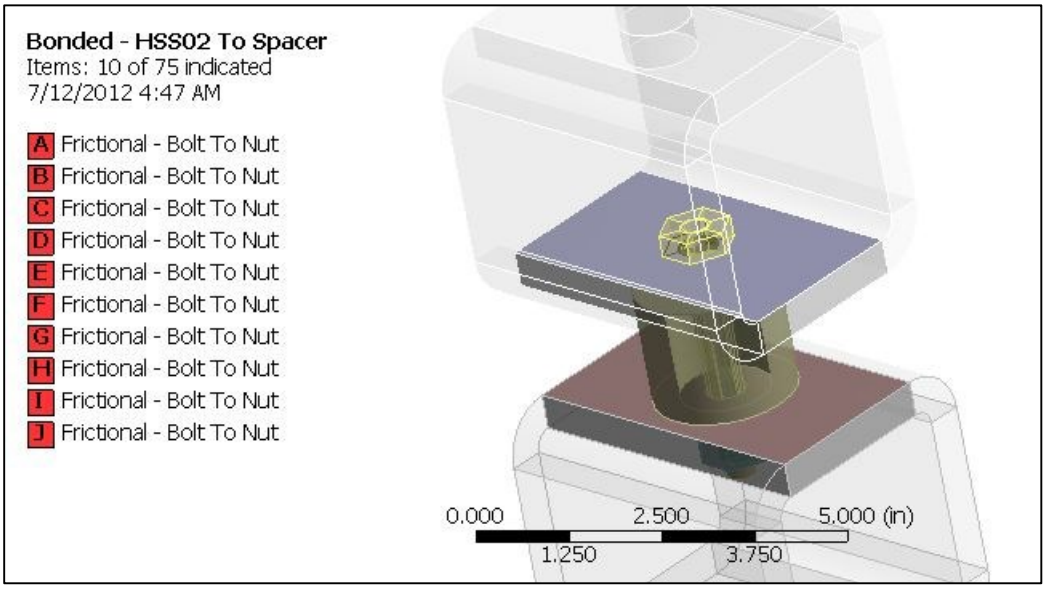

Figure 4-15 Contact regions

Depending on the type of contact, the analysis can be linear or nonlinear. Although, nonlinear analysis can increase runtime significantly, this could not be avoided because of the nature of the analyzed model where nonlinear behavior is evident and cannot be overlooked.

When the assembled model was imported from ANSYS DesignModeler into ANSYS Mechanical (the application used to perform the analysis), contact regions were automatically detected and the following contacts were generated:

- Bar and HSS contact: a bonded contact region type was adopted. This means that the top and bottom bars will always be glued to the hollow sections, and the relationship at the contact region will be linear, since there will be no gap or change in the length/area of the contact region.

- Bolt and nut contact: This contact will provide force transfer between the bolt threads and the nut through mutual friction and pressure. A gap will occur and the nature of this contact will be nonlinear. Hence, a frictional contact region was used to represent this interaction.

  Determining an accurate friction coefficient can be a daunting and tedious task. This is because, even with the availability of test data for the coefficient of friction at ambient temperatures, such data is not readily available at higher temperatures and measuring this coefficient at higher temperatures may pose some serious challenges to the researcher. As suggested by Al-Jabri et al. a value of 0.15 has been used.

  To ensure that the bolt will apply pressure on the nut without witnessing any significant penetration and vice versa, a normal stiffness value should be used for each contact region. The normal stiffness values range usually between 0.1-10. Smaller values will provide easier convergence but with more penetration. After some trials and due to convergence problems encountered when using small values for the normal stiffness, a value of 5 has been adopted. This value is also permitted to be updated automatically, in every equilibrium iteration, if necessary.

- Bolts and HSS contact: This contact is similar to bolt-nut contact; hence, similar values were used.

- Spacer piece and HSS contact: Also considered similar to the bolt-nut contact.

4.10 CREATING THE MESH

4.10.1 General Guidelines for Mesh Creation

- The mesh must be refined near all points of interest. The main points of interest are those where stresses (or deformations) are to be monitored or calculated. In this case, it is the area between the threads of the bolt and nut.

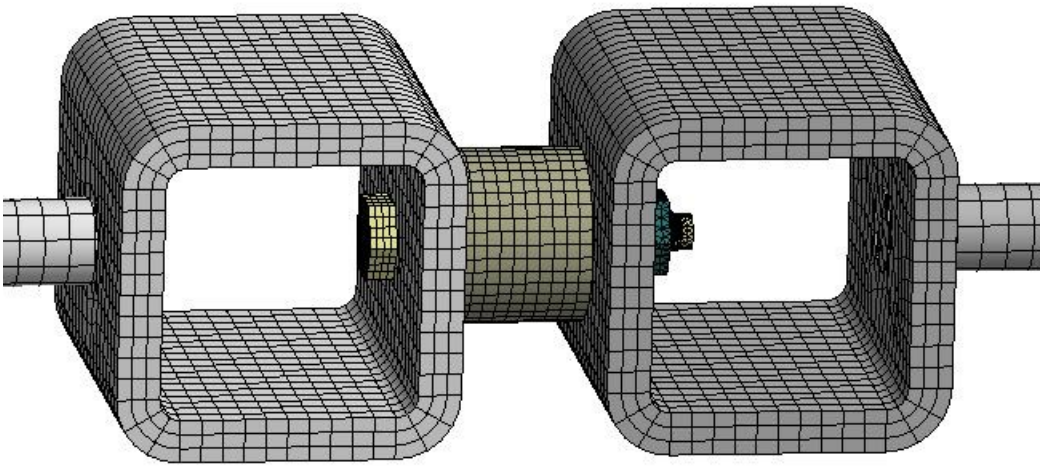

Figure 4-16 The HSS mesh

- The mesh must be refined where there is a sudden change in geometry. For example, around bolt holes and the area where the bars are attached to the hollow sections.

- Smaller objects require finer mesh.

- A continuous mesh between different parts is desirable whenever possible. If that is not possible, then a refined mesh on one side may be sufficient to produce good results. For instance, the contact between the bolt and all the other parts required a fine mesh on at least one side of the contact surface. This helped in defining the physical relationship between the different parts and prevented undesirable penetrations.

- Enough elements on the shank of the bolt were provided to allow for the application of the pretensioning load.

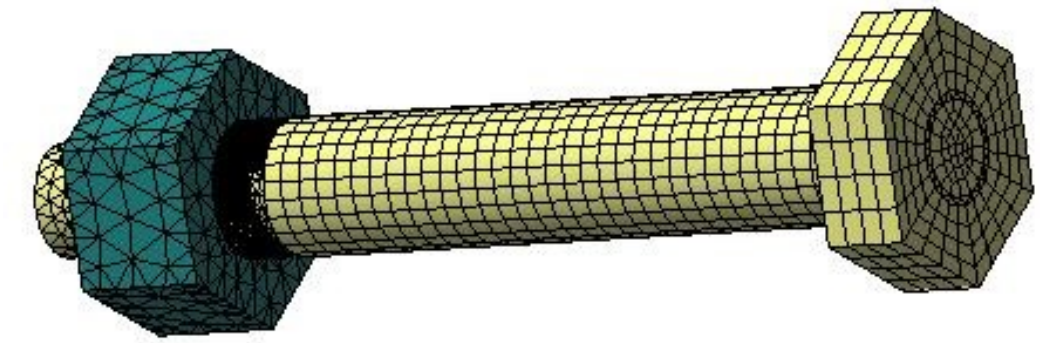

Figure 4-17 The bolt shank mesh

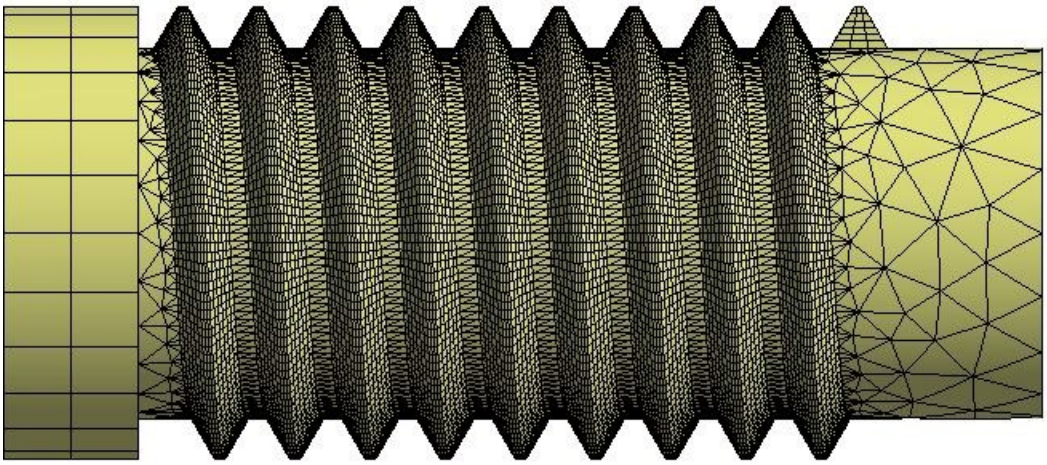

Figure 4-18 The threaded section mesh

4.10.2 Element Types

Three different categories of elements were used in the model:

- Solid elements: two types of solid elements were used in general, SOLID185 and SOLID187.

- Pretension element: known as PRETS179, assigned automatically to all elements with a pretension load.
- Contact elements: CONTA174 and TARGE170, used for the contact surface and target surface respectively.

More information about these element types can be found in the ANSYS Inc. documentation files [20].

4.10.3 Mesh Metrics

ANSYS Workbench can provided advanced mesh statistics through its mesh metrics option. The element quality bar graphs show a quality factor ranging between 0 and 1. This metric is based on the ratio of the volume to the edge length for a given element. A value of 1 indicates a perfect cube or square while a value of 0 indicates that the element has a zero or negative volume.

During the meshing process, multiple meshing scenarios were considered, while trying to obtain a good quality mesh with the least number of nodes possible. Here are a few of those scenarios:

1. A bolt with mostly Tet10 elements

The total number of nodes for this case was about 234000. Not many meshing controls were required to produce the mesh. However, the mesh quality dropped below 0.5 for a considerable number of elements and at critical locations. Besides, the overall mesh did not conform to the geometry very closely, although this could have been avoided by adding some sizing controls, but that would have increased the number of nodes required for the analysis.

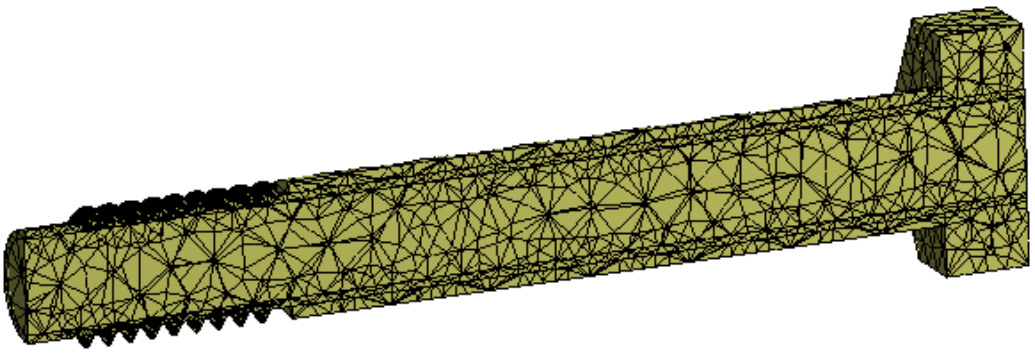

Figure 4-19 Tet10 mesh

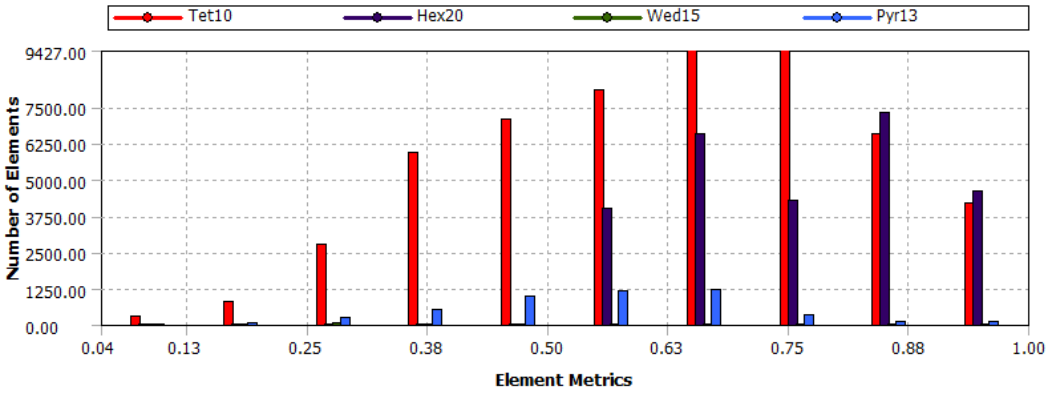

Figure 4-20 Tet10 element metrics

Figure 4-21 shows the distribution of elements that had a quality factor of 0.38 throughout the bolt. Many of those elements were located near the threaded section.

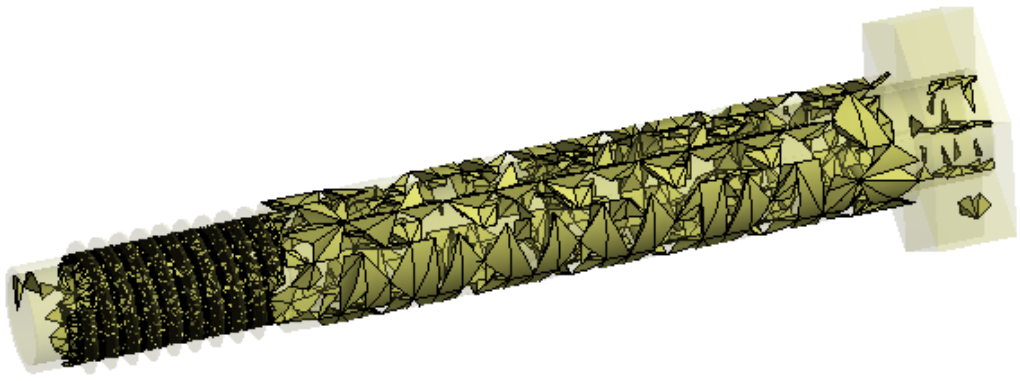

Figure 4-21 Elements with element quality factor of 0.38

2. A bolt with mostly Hex20 elements

This model had about 230000 nodes, with remarkably structured elements and excellent mesh quality. The mesh was achieved by separating the threads from the bolt and nut, and assigning them to two independent parts, which allowed for almost all the bodies in the model to be meshed through the "sweep" command. The connection between the bolt and its threads was accomplished using bonded contact regions; this is where the disadvantage of this model lay.

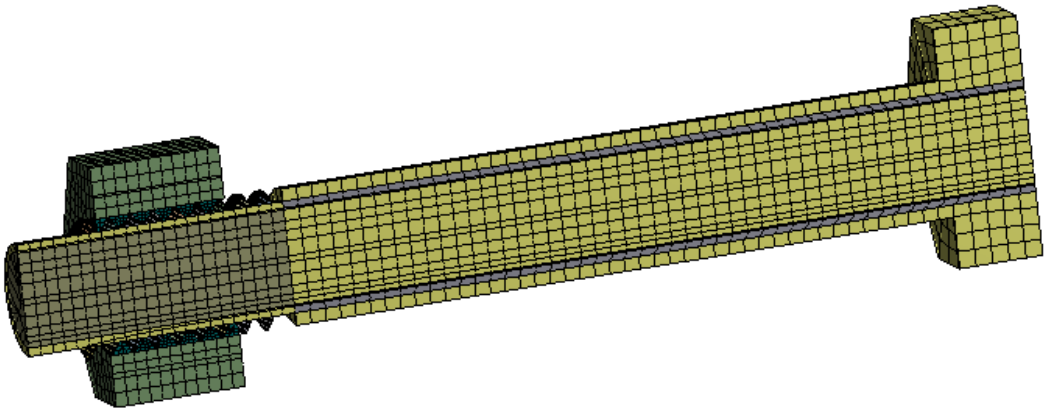

Figure 4-22 Hex20 mesh

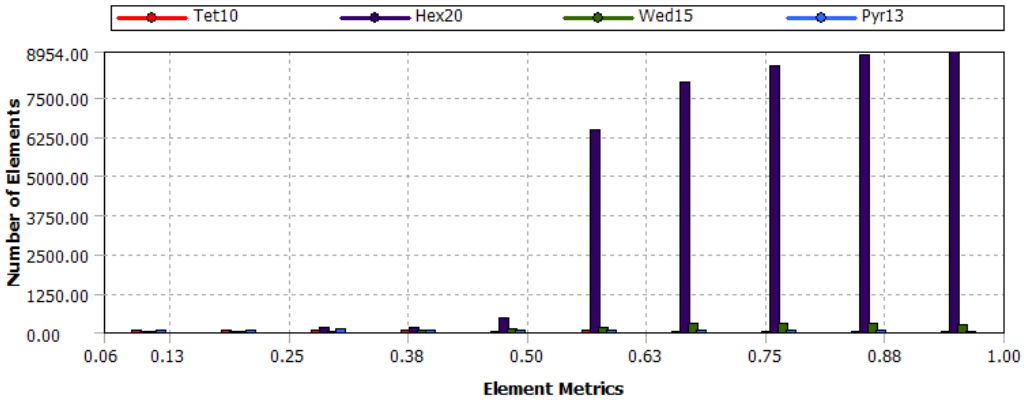

Figure 4-23 Hex20 element metrics

The contact regions in this model suffered from various issues of convergence and penetration, especially at high temperatures when the model became extremely nonlinear.

3. A bolt with a combination of Tet10 and Hex20 elements

This model had about 248000 nodes. Although it could not produce a completely structured mesh like the previous case, but it was able to keep the mesh quality within acceptable levels while at the same time maintain the continuity of the mesh between the bolt/nut and their threads. This mesh was the one chosen for this analysis; therefore, it will be discussed in detail.

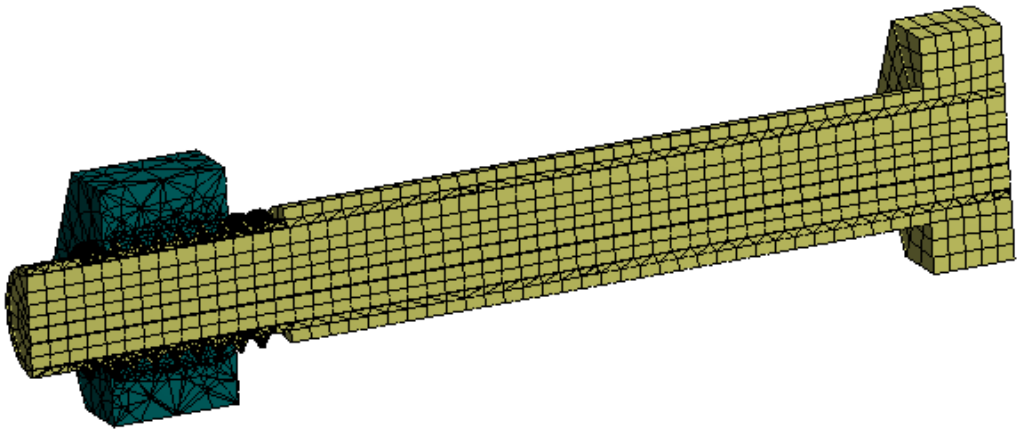

Figure 4-24 Tet10 and Hex20 mesh

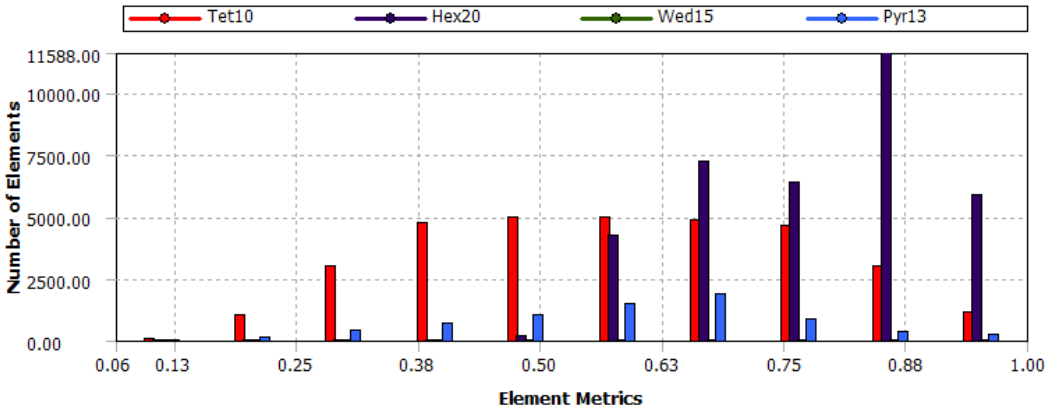

Figure 4-25 Tet10 and Hex20 element metrics

4.10.4 Mesh Details

As explained in the discussion about mesh metrics, "good" elements are close to being perfect cubes. The best way to produce cube-like elements is by using the "sweep" method. During

the meshing process, the sweep method was used whenever possible. That included almost all the bodies in the analysis, except for those in close proximity to the threads (whether in the nut or bolt).

For example, each HSS was split into multiple bodies that ANSYS could easily mesh using the sweep method. Figure 4-26 shows the bodies that make up a single HSS and their mesh. In the actual model, these bodies were not separated and their mesh was continuous. The continuity of the mesh was a direct result of merging all these bodies into a single part.

Because of its simplicity, the processing time for this mesh was relatively short.

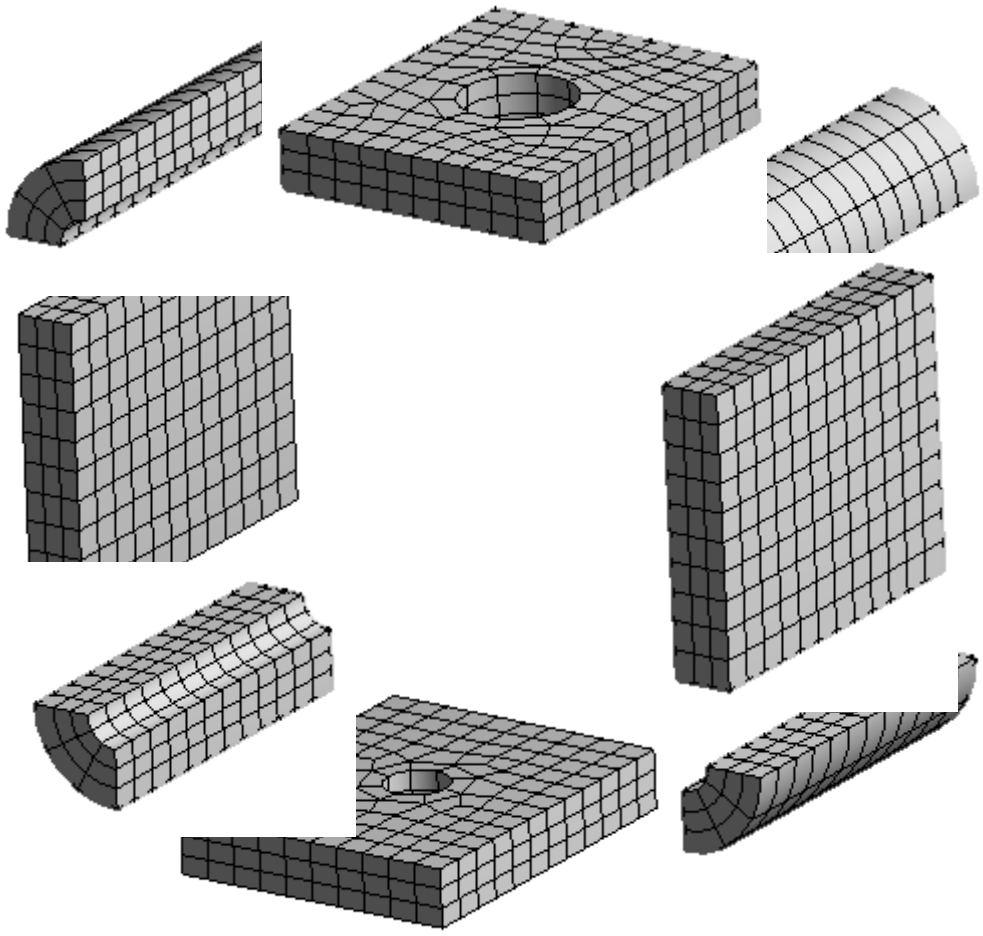

Figure 4-26 Meshed HSS bodies

Most of the mesh elements and nodes were concentrated in the threads, which had a tricky spiral geometry. By splitting the threads, smaller pieces with two end-faces were formed, which helped in implementing the sweep method on most of the threads. Figure 4-27 shows a meshed thread body, this body had about 7300 nodes.

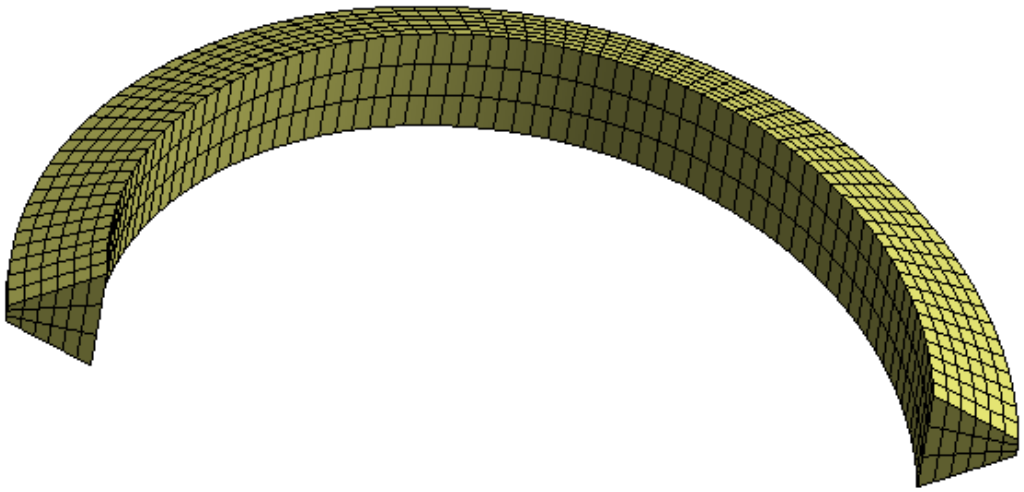

Figure 4-27 Thread mesh

The sweep method, however, could not be used for all of the threads. In particular, some of the threads on the nut were irregular in shape and a free-form meshing method had to be used. These threads were necessary to predict accurate behavior of the nut and could not be avoided.

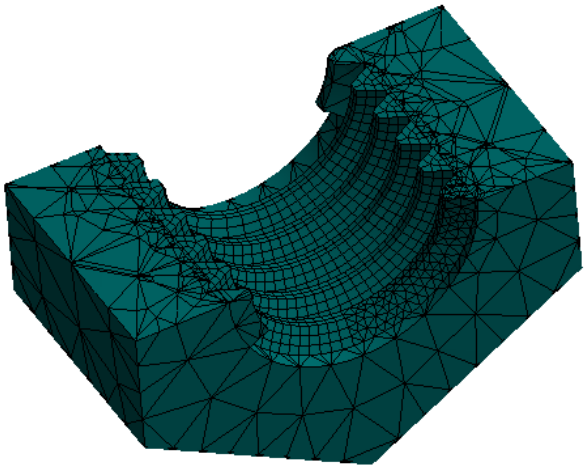

Figure 4-28 The nut mesh

Figure 4-28 shows also how the nut mesh could not be made uniform without considerably increasing the number of elements. This is because of the spiral geometric nature of the threads and the relative small dimensions of the nut. The interior of the nut did not witness any extreme stresses or strains, so this mesh was also accepted.

The same problem was faced in the bolt as well, and to resolve it the central core had an outside shell that worked as a transitional mesh connecting the core to the threads with a somewhat irregularly shaped elements.

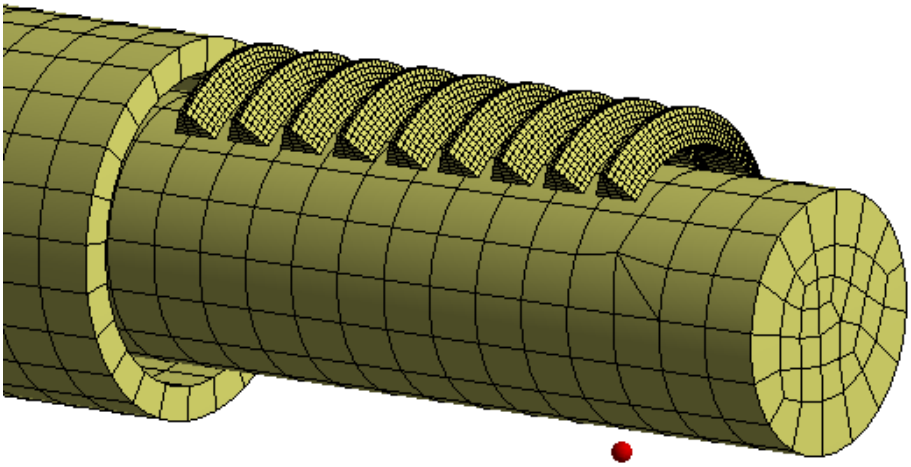

Figure 4-29 Bolt-core and threads mesh

Figure 4-29 shows the uniform mesh of the bolt core and threads, where the shell connecting them is hidden. Figure 4-30 shows a small layer of elements extending between the threads and the central core of the bolt with less-than-ideal shape factor. The performance of this meshing arrangement proved to be relatively stable and it kept the mesh size within reasonable limits.

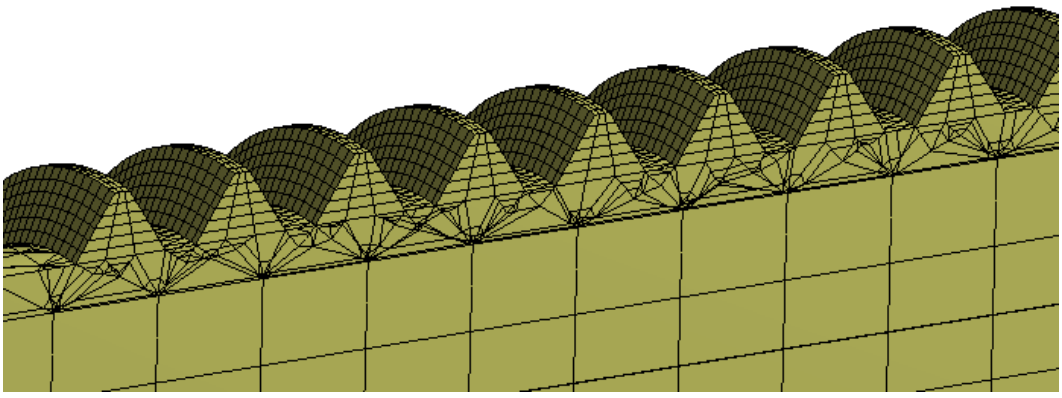

Figure 4-30 Mesh transition between the bolt-core and the threads

Figure 4-31 shows the mesh at the bolt head and across the non-threaded section. Slicing the bolt head and the shank cover simplified the meshing process and produced a very good quality mesh in this area.

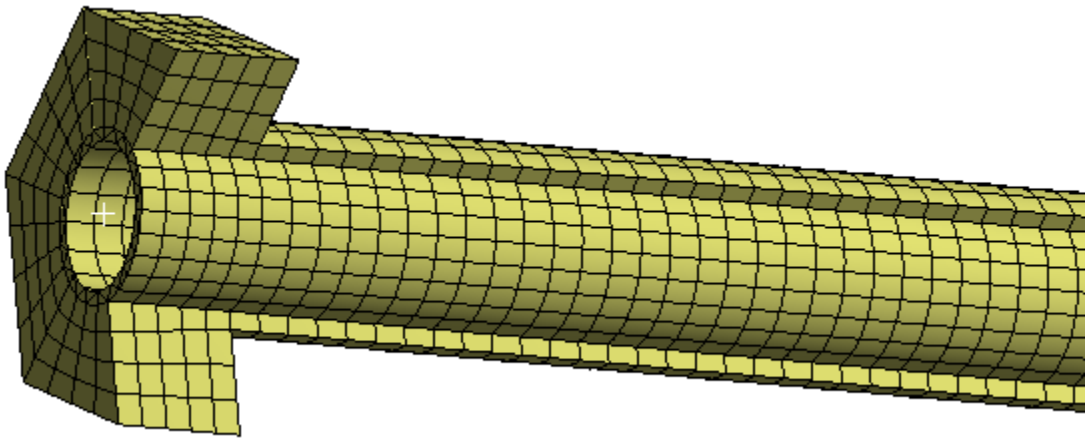

Figure 4-31 Mesh of the bolt head and non-threaded section

4.11 Load Application and Analysis

The loads carried by the tested connection were applied on the finite element model in three consecutive sub-steps. In the first step, the pretensioning load in the bolt was applied along with the self-weight (gravity loads) of all members, this step mimics the assembly phase of the

connection where the connection gains its strength after tightening the bolt. In the next load step, the tension load was applied on the vertical bars until reaching the constant level used in the experiments; which represents the phase just before turning on the heat in the furnace. In the final load step, the temperature was increased gradually and equally, for the parts that were inside the furnace, up to failure. The following sections describe briefly the loads used in each sub-step.

4.11.1 Bolt Pretensioning and Boundary Conditions (Load Step 1)

The tested assembly was fixed at the bottom end of the bottom vertical bar and pinned at top end of the top vertical bar. The top vertical bar was allowed to move upward in the direction of the applied tension force. Similar boundary conditions were implemented in the finite element model as well.

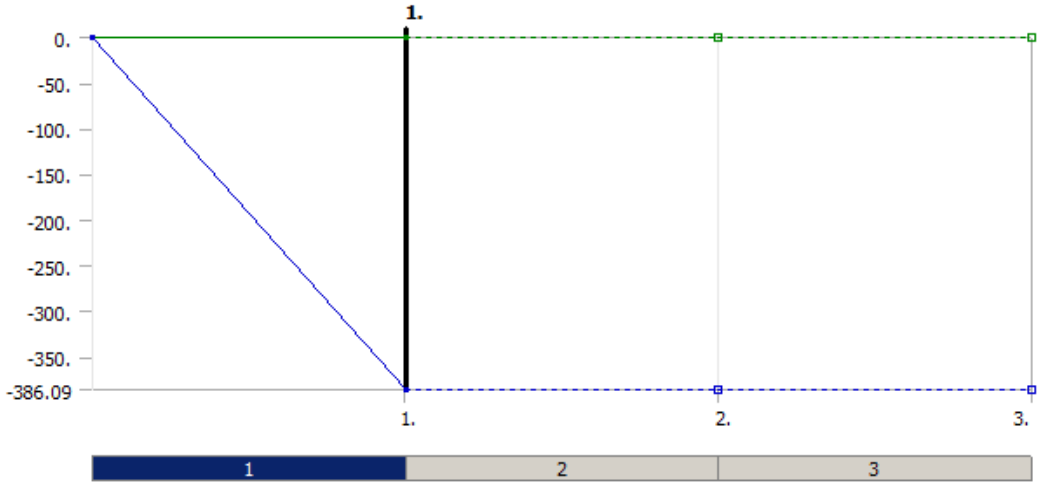

Figure 4-32 Force of gravity – load step 1

Figure 4-32 shows the application of the force of gravity during the first time step. The force was applied linearly and in increments at every sub-step.

The pretension load needed to be applied in the first load step because there were no other forces or boundary conditions that existed to hold the different parts together, instead these

parts were allowed to move freely in space and this movement was only restricted after the bolt had been tightened. If the stiffness of the contact regions was chosen correctly, then the multiple bodies in the model will be held in place without penetrating each other or falling apart.

During the experiments, the bolt was tightened using a torque wrench, and the force in the bolts was estimated to be 2500-lb.

4.11.2 Tension Force (Load Step 2)

After the end of the first load step, a constant force of 2000-lb was applied in the vertical direction (z-direction) at the top end of the top vertical bar. Figure 4-33 shows the application of this force, just like the force of gravity the tension force was applied linearly and in increments at every sub-step. After entering the third load step, this force remained constant.

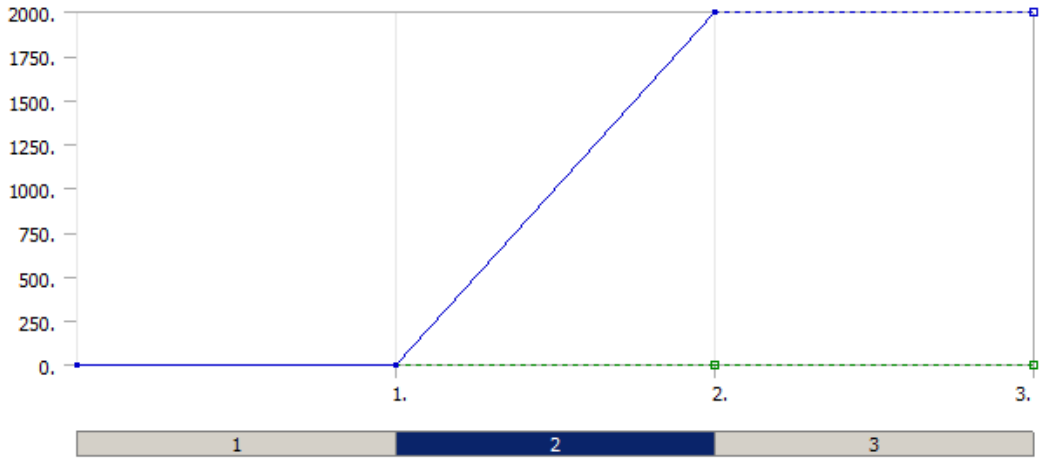

Figure 4-33 Tension force – load step 2

Figure 4-34 shows the location of the applied forces and boundary conditions on the finite element model.

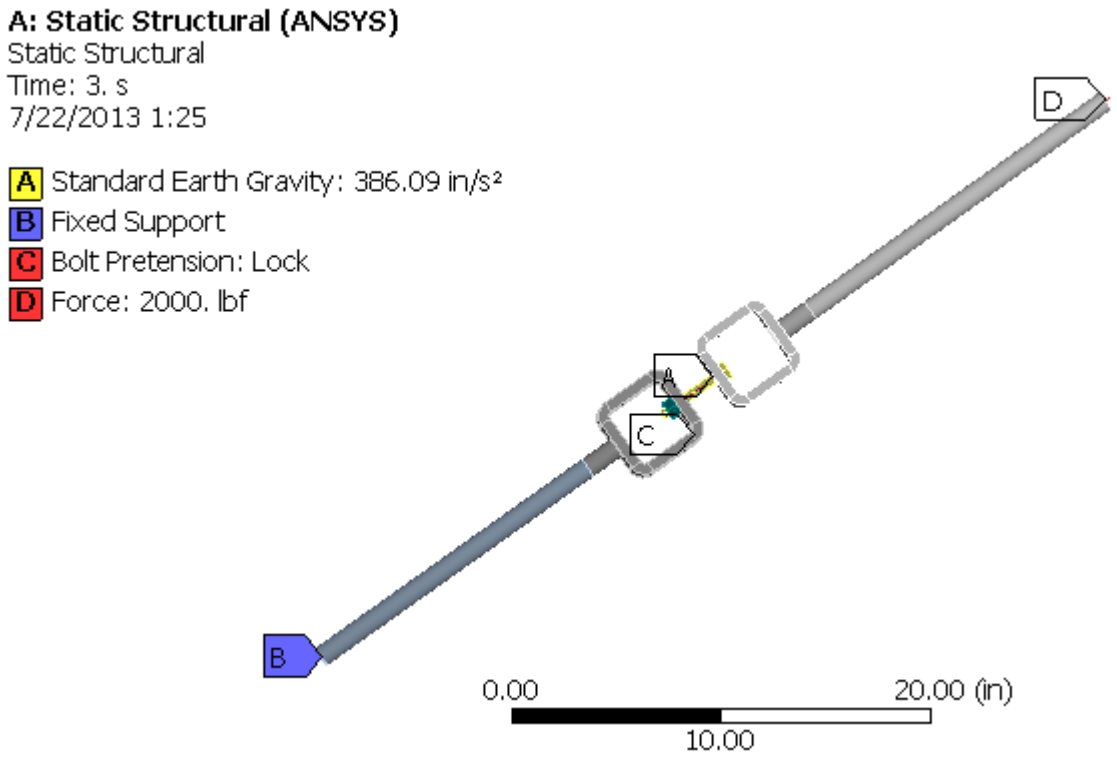

Figure 4-34 Location of the applied force and boundary conditions

4.11.3 Thermal Condition (Load Step 3)

A thermal condition was added to the parts that were inside the furnace, as shown in Figure 4-35, this excluded parts of the top and bottom vertical bars.

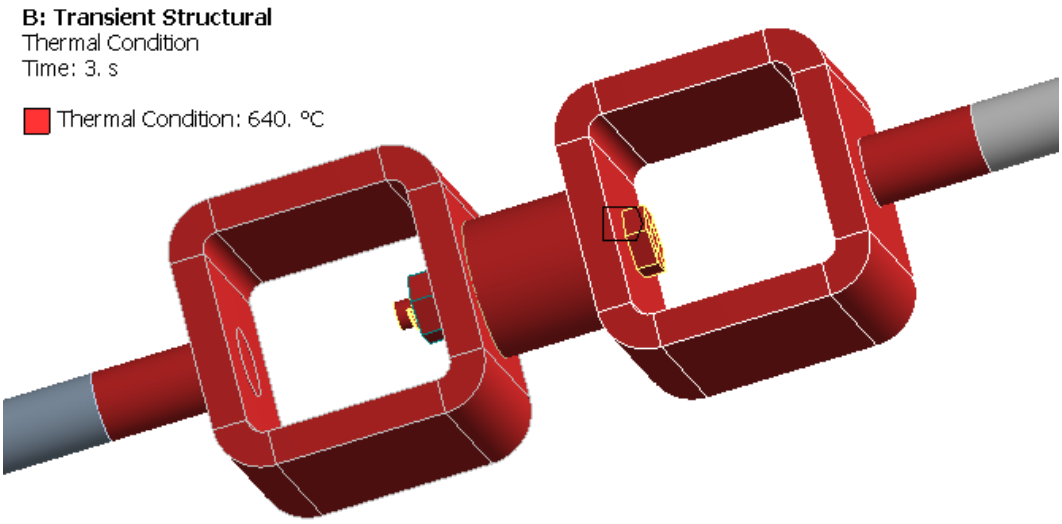

Figure 4-35 Bodies under the thermal condition

The thermal condition was not applied linearly, instead its slope flattened a little towards the end of the load step. This was done to enhance the solution process and it is tantamount to applying the thermal load linearly but in two different load steps with different time stepping controls. Every load step is governed by a predefined minimum time step that cannot be changed during the analysis. Choosing a smaller slope at higher temperatures effectively works as a reduction in the minimum time step used.

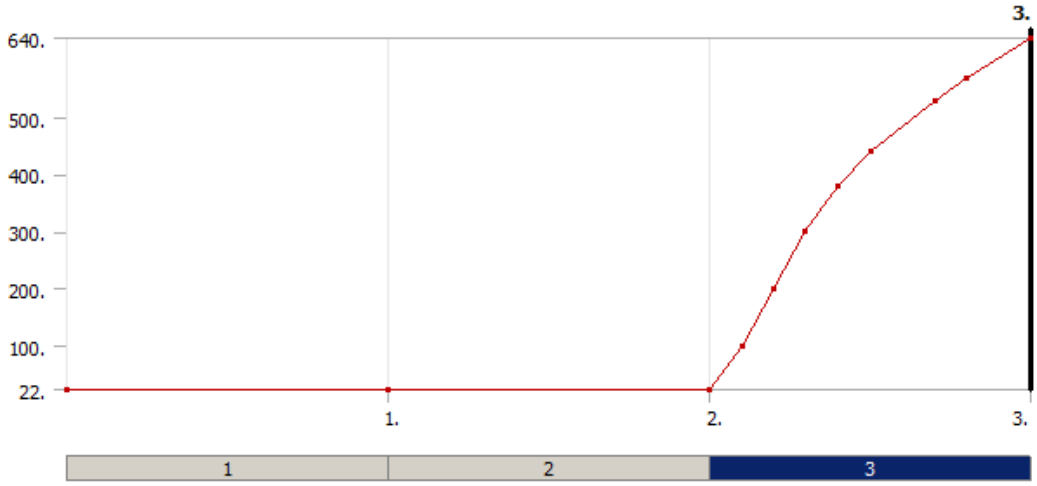

Figure 4-36 Thermal condition (°C) – load step 3

CHAPTER 5

RESULTS AND CONCLUSIONS

5.1 INTRODUCTION

This chapter presents the results of the conducted experimental work and the finite element analysis, in addition to a comparison between the two. The results recorded during the experiments are limited only to displacement, applied load, temperature and time. While in the finite element model, we have a greater flexibility in exploring the results of the analysis. For example, stress contours can be plotted in places difficult to monitor during the actual tests.

5.2 EXPERIMENTAL RESULTS

In the initial stages of testing, and in order to calibrate the testing equipment, the first group of tests were not identical and were used for the sole purpose of investigating the effects of changing the heating speed, choosing the optimum heating regime and to compare different bolt diameters. In the second group of tests, all the experiment parameters were the same for four different tests. The results of these tests were then plotted, compared and used for calibrating the finite element model.

The following sections discuss in detail the results obtained from both test groups.

5.2.1 First Test Group

In total, six of the experiments conducted belong to this group. For example, one of these experiments was performed at ambient temperature before running any tests under high temperatures. It was meant to check the integrity of the tested assembly by applying a simple

tension load within the yield limit and then removing it. The results from two of these tests are listed below.

- **Test 01**

In this test, the tested specimen had the same dimensions described in Chapter 3. Those are the dimensions used for the finite element model with a ½"-diameter A325 bolt. However, the load was increased to 6000-lb instead of 2000-lb.

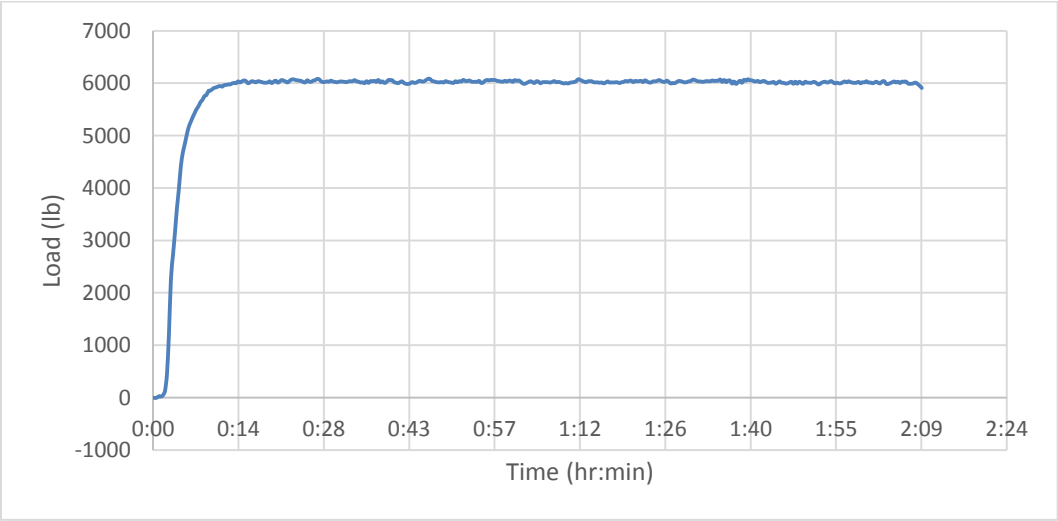

Figure 5-1 Load vs. Time chart (Test01 – First Group)

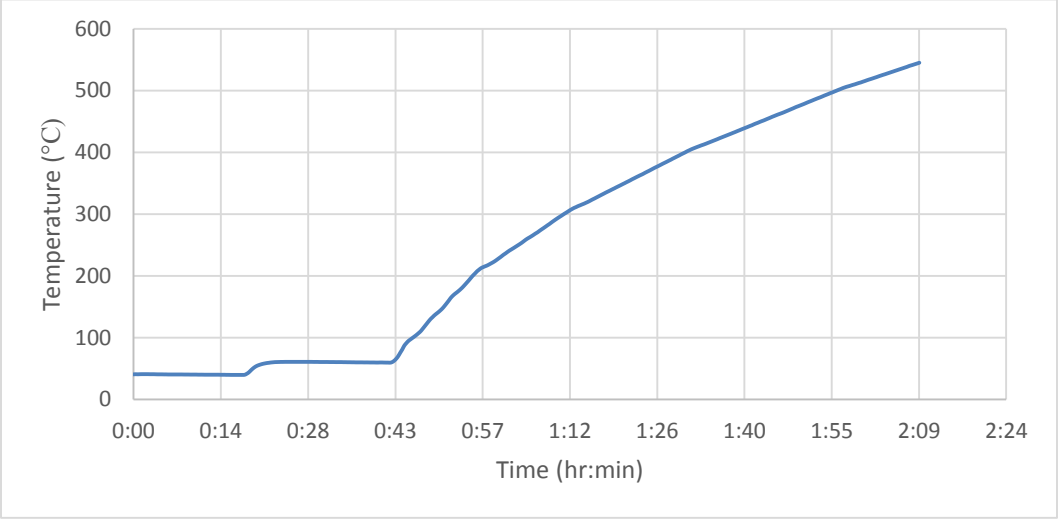

Figure 5-2 Temperature vs. Time chart (Test01 – First Group)

Figures 5-1 and 5-2 show the load and heat application during the period of the test. This test was meant to see what effect a larger load would have on the experiment if all other parameters were the same. The failure of the bolt occurred when the temperature reached 545°C, for similar experiments and a reduced load of 2000-lb the lowest temperature to cause failure was about 590°C which was expected. The failure mechanism however did not change.

Figure 5-2 also shows a period where the temperature in the furnace was kept constant for a while. This was done to examine the effects of time on the displacements of the specimen. Since the heat program chosen did not adhere to a standard fire curve, instead it took the average experiment about 40 minutes to reach a temperature of 600°C while in a standard fire the temperature after 40 minutes would be about 880°C.

Figure 5-3 shows that for a short period if the temperature was kept constant, we can safely assume that the increase in displacements, if any, is negligible albeit at low temperatures.

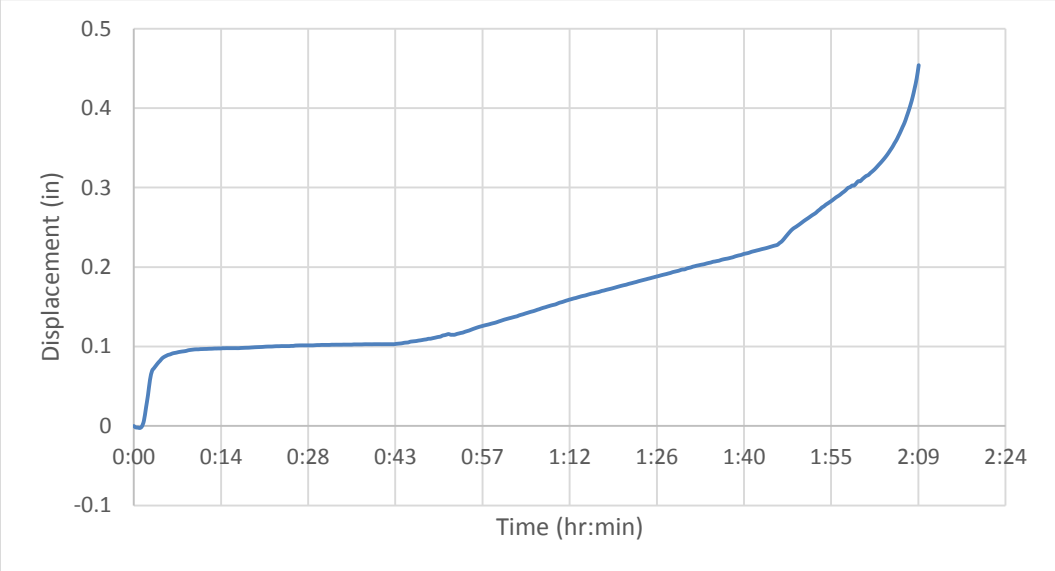

Figure 5-3 Displacement vs. Time chart (Test01 – First Group)

- **Test 02**

This experiment used the same general arrangement to test a ¾"-diameter A325 bolt. With a setup identical to the one previously used, including the applied tension load of 2000-lb. Figures 5-4 and 5-5 show the failure in the bolt and the distorted dimensions of the HSS.

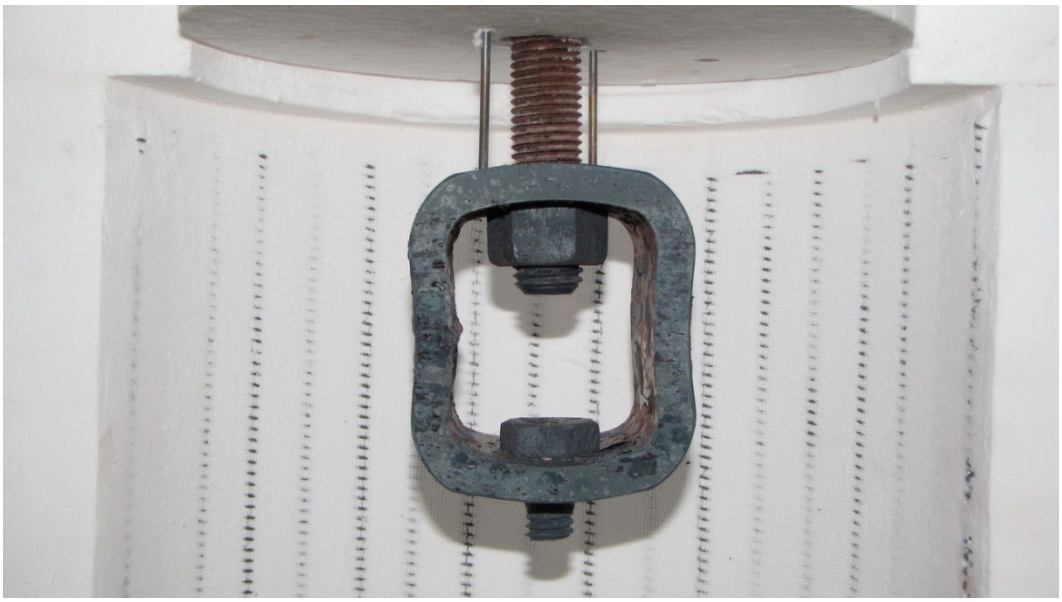

Figure 5-4 Failure in top section of the specimen (Test02 – First Group)

Figure 5-5 Failure in bottom section of the specimen (Test02 – First Group)

Failure in this case occurred at about 880°C in the threaded section of the bolt and in a similar fashion to that of the ½"-diameter bolts. However, the two HSS were severely deformed while the vertical bars did not suffer any discernable changes in dimensions.

Figure 5-6 shows that a maximum displacement of more than 1.2 inches was recorded before failure. The maximum displacement recorded in the case of the ½ "-diameter bolts was in the range of 0.5 inches, although it is expected for a higher temperature to produce more strains but this larger displacement is heavily affected by the vertical elongation of the hollow sections which did not deform much at lower temperatures.

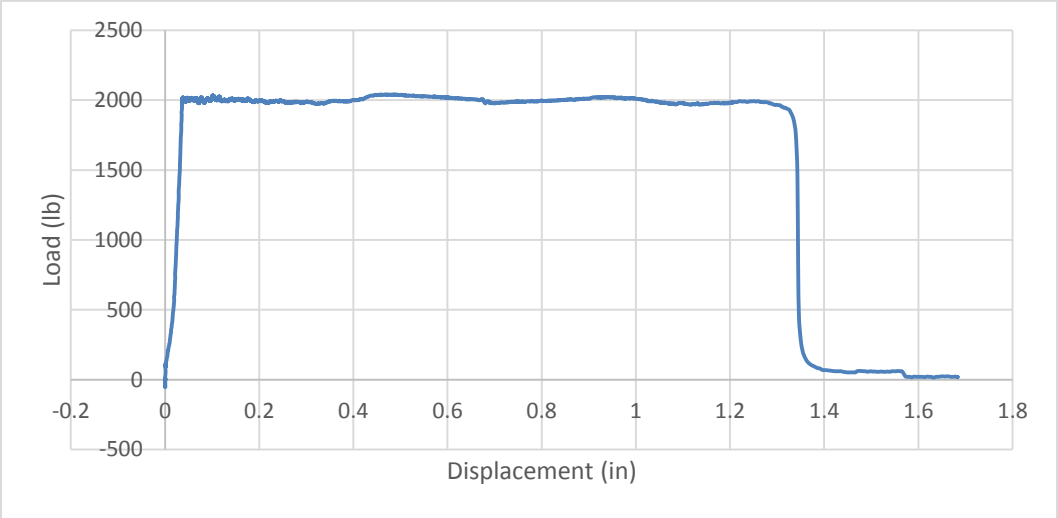

Figure 5-6 Load vs. Displacement chart (Test02 – First Group)

This test also was meant to try to program a standard fire curve into the furnace, as defined by Equation 1.1. That however did not work out; as Figure 5-8 shows that in spite of reaching a temperature of 900°C inside the furnace, the furnace components could not achieve that temperature as fast as a standard fire should. The maximum temperature for which the furnace components were designed is 900°C, and pushing the temperature close to that limit caused few cracks to appear in the corners of the ceramic heaters. This is why, for all other

experiments, the temperatures in the furnace were at a lower level. The choice of applied load and bolt diameter allowed us to test the bolts at high temperatures without damaging the equipment and in many cases without damaging the vertical bars and the two hollow sections, which were reused in other experiments.

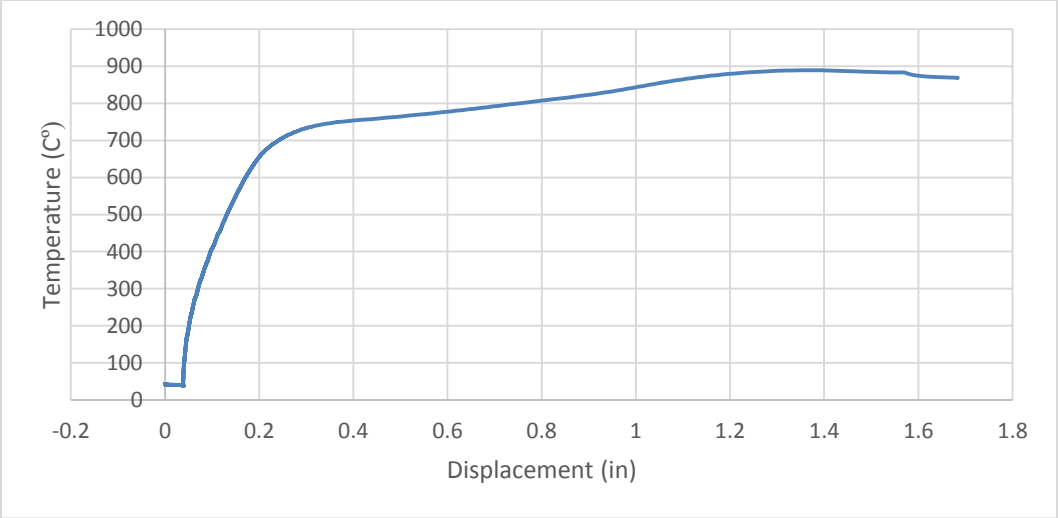

Figure 5-7 Temperature vs. Displacement chart (Test02 – First Group)

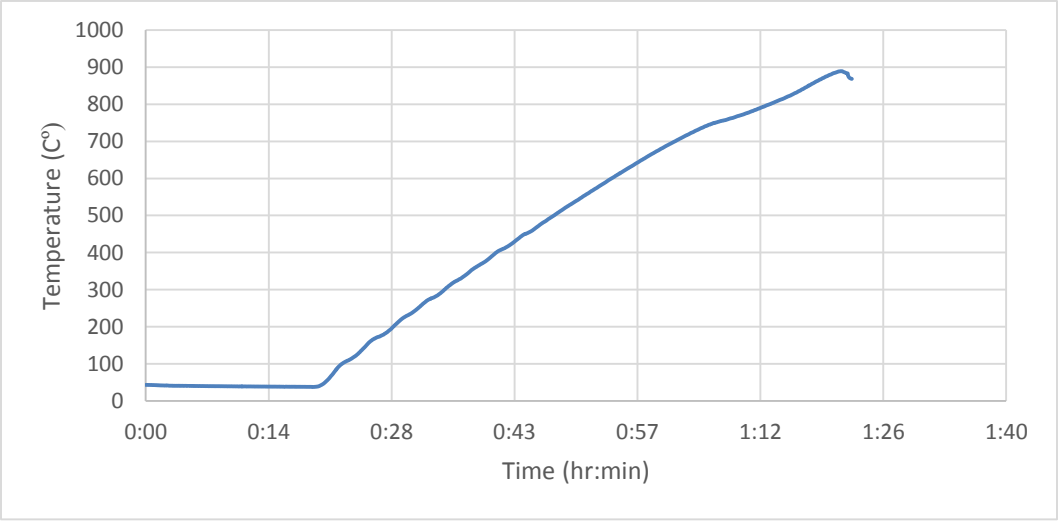

Figure 5-8 Temperature vs. Time chart (Test02 – First Group)

5.2.2 Second Test Group

This group of tests consisted of four experiments conducted under almost identical conditions. The tested bolts were ½ " in diameter and the applied tension load was 2000-lb. The exact dimensions and conditions of the experiments are discussed in Chapters 3 and 6.

Figures 5-9 through 5-13 show the detailed results of these experiments.

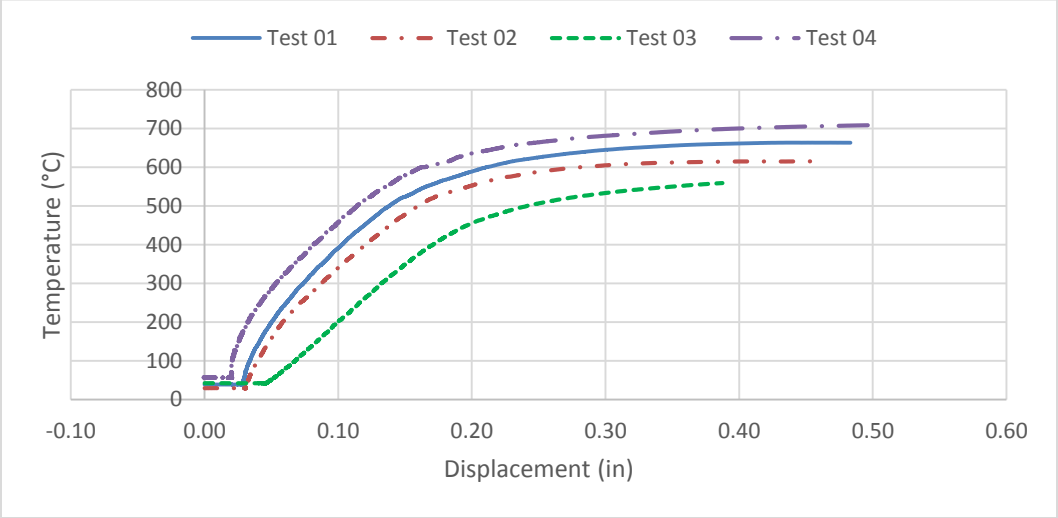

Figure 5-9 Temperature vs. Displacement chart (Second Group)

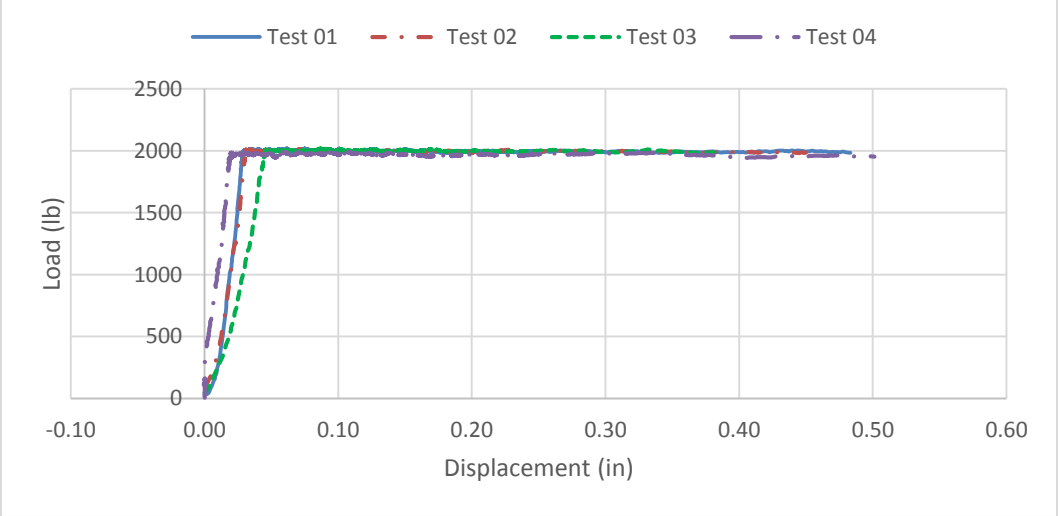

Figure 5-10 Load vs. Displacement chart (Second Group)

The cutoff point (or the end-of-test point) for each graph has been chosen at the location where the tension load had its first sudden drop off. Figure 5-6 illustrates the full range of recorded data per experiment. The end-of-test point was also confirmed by measuring the dimensions of each specimen components before and after the test.

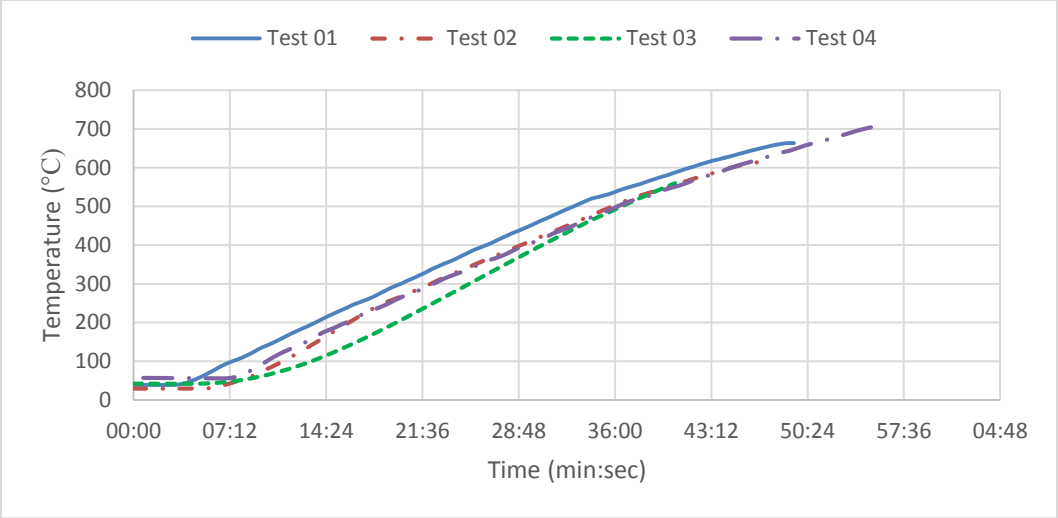

Figure 5-11 Temperature vs. Time chart (Second Group)

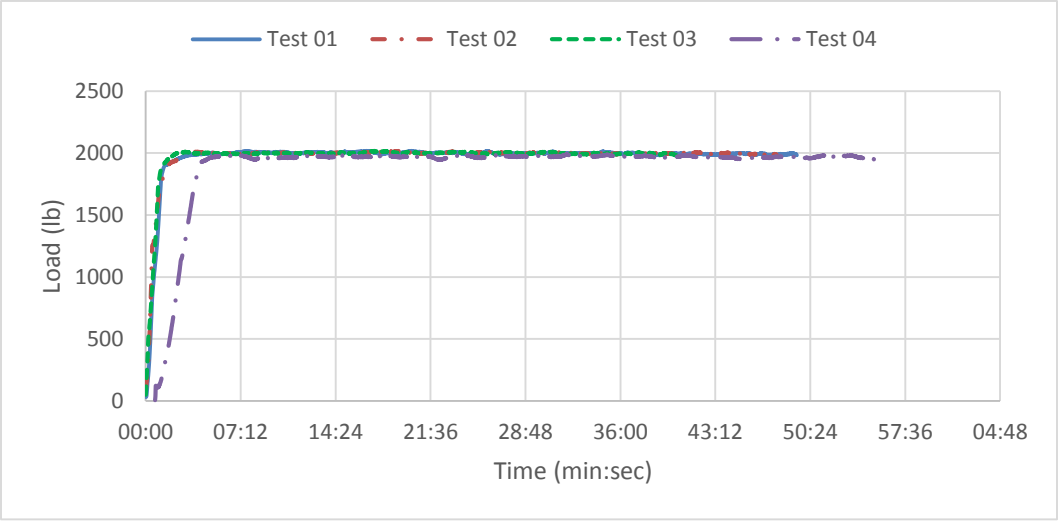

Figure 5-12 Load vs. Time chart (Second Group)

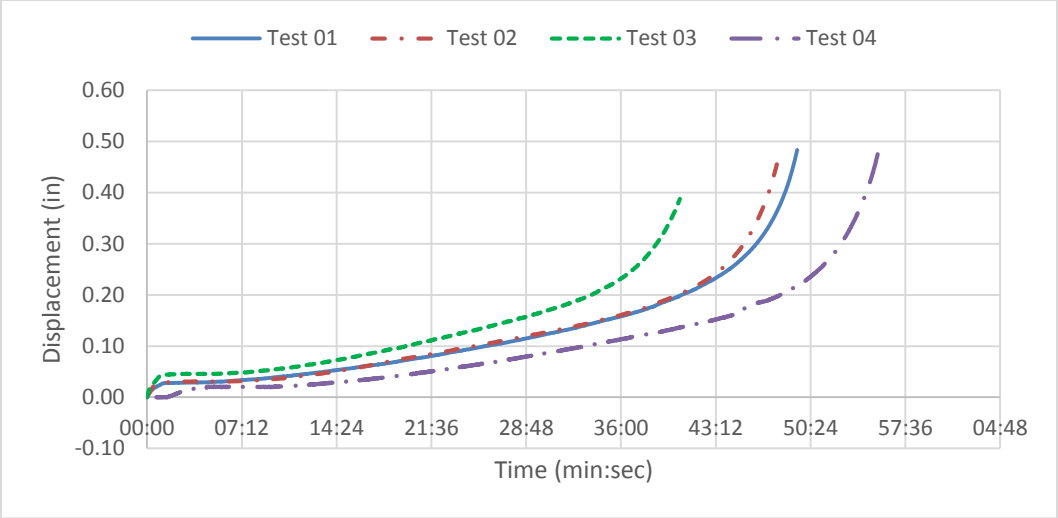

Figure 5-13 Displacement vs. Time chart (Second Group)

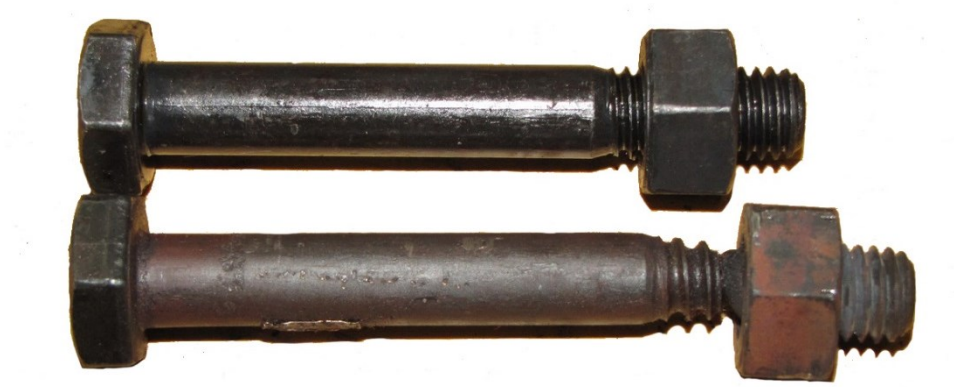

Figure 5-14 A comparison between the bolt before and after the test

The results of the FEA were correlated to the results shown in Figures 5-9 and 5-10, that is the Load vs. Displacement and Temperature vs. Displacement chart. Since time had no real effect on the FE model, the remaining charts were not used. However, those remain important to have a full understating of how close the results of those tests. Figure 5-12, for example, shows that the loading rate in that test was slightly slower than the others.

Although the results from all four experiments seem to be close, but the results of Test 03 have deviated the most. This was attributed to using a previously tested bolt that may have residual stresses present prior to testing. Due to this reason, Test 03 results will be excluded.

5.3 COMPUTATIONAL RESULTS

5.3.1 Analysis Systems and Force Convergence Diagram

The solution of the finite element model was controlled by many parameters like the coefficient of friction, the stiffness of the contact regions, time stepping controls and the refinement of the mesh. In addition, the nonlinearity of the model stemmed from the nonlinear frictional contact regions, geometric nonlinearities and the nonlinear material properties. All of these factors have contributed to creating a highly sophisticated analysis that required a considerable amount of time and computational resource.

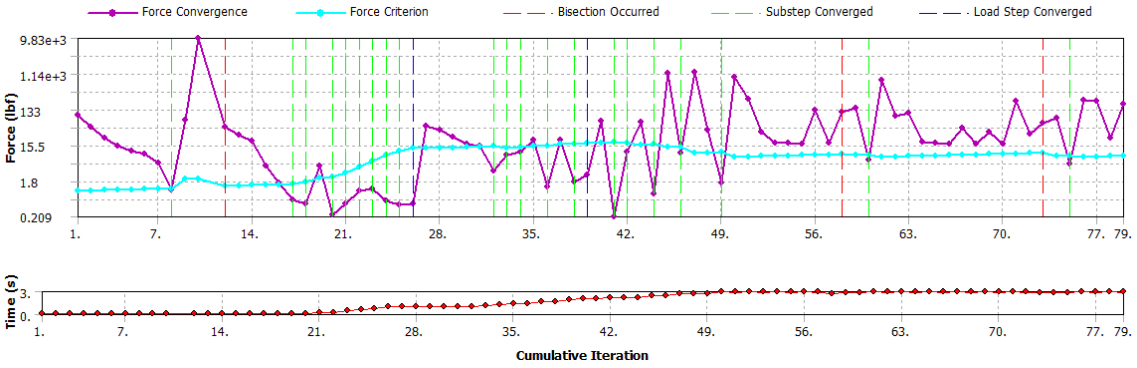

Figure 5-15 Force convergence in a Static Structural system

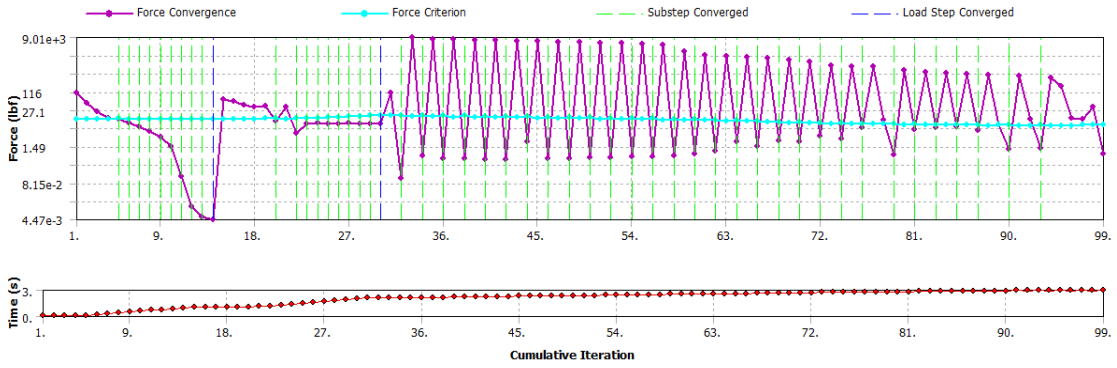

Figure 5-16 Force convergence in a Transient Structural system

Two independent systems of analysis were chosen to solve the FE model, a Static Structural system and a Transient Structural system. Both of which produced very comparable results.

Figures 5-15 and 5-16 illustrate force convergence diagrams for both of those systems. Although the Transient Structural system took more iterations to reach a solution but each sub-step has converged without the need for any bisections. The results shown in this chapter are from a Transient Structural analysis system.

5.4 CONTACT REGIONS

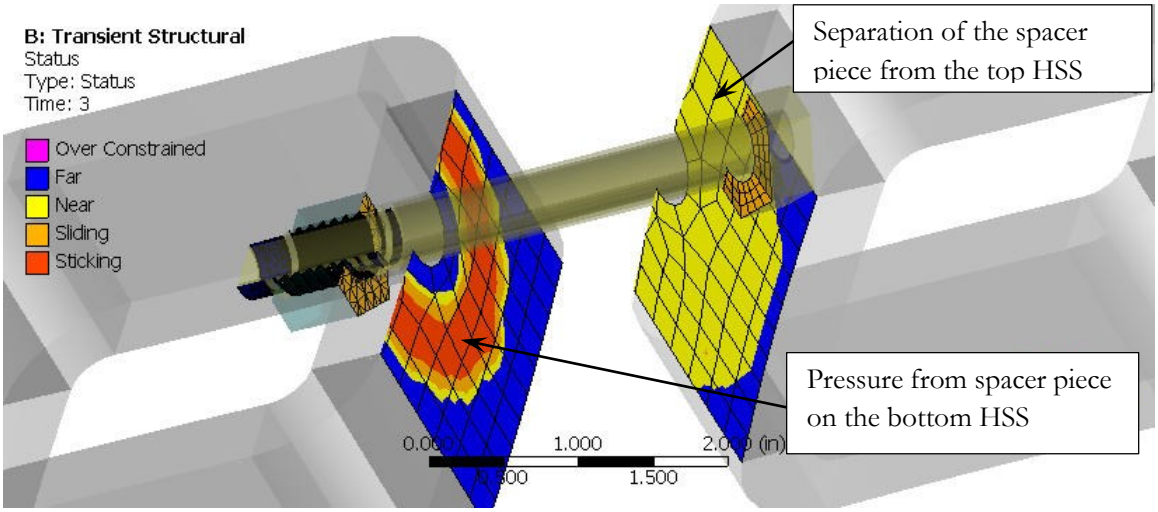

Figure 5-17 The status of the contact regions

Contact regions were closely inspected since contact stiffness controls the penetration relationship between any two surfaces in the model. The more stiffness the contact surface has, the less penetration it will experience. However, that would come at the cost of increasing the number of iterations necessary to achieve load convergence.

To choose a reasonable value of stiffness, different models were run with different stiffness values. Then an optimum value of 5 was chosen based on the duration of the analysis and inspecting the status, pressure and sliding distance of each contact surface. Figure 5-17 shows an example of the status contours for some of the contact regions in the model.

Figure 5-18 shows the maximum penetration values between the bolt-nut contact regions throughout the three time steps required to perform the analysis. A maximum value of about 2×10^{-5} in. was reached at the end of the second time step and this value was deemed within acceptable levels relative to the smallest dimensions in the geometry.

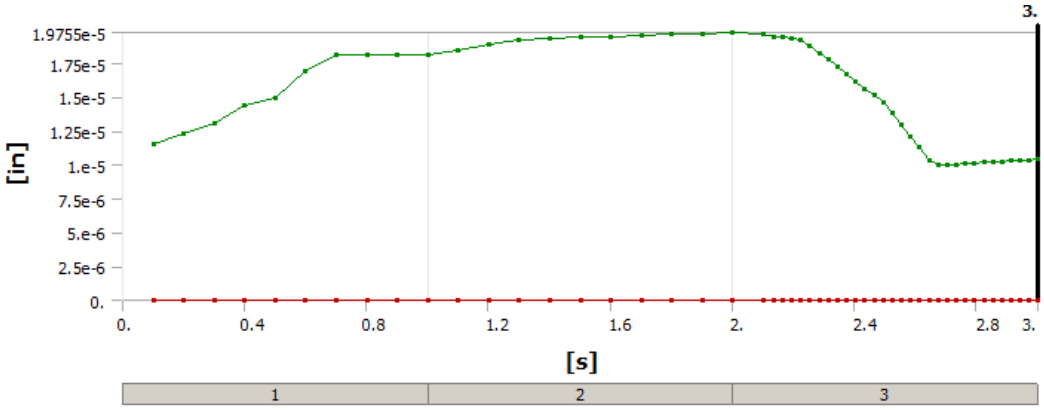

Figure 5-18 Penetration values between bolt and nut threads

5.5 STRESSES

5.5.1 Equivalent Stress (von Mises)

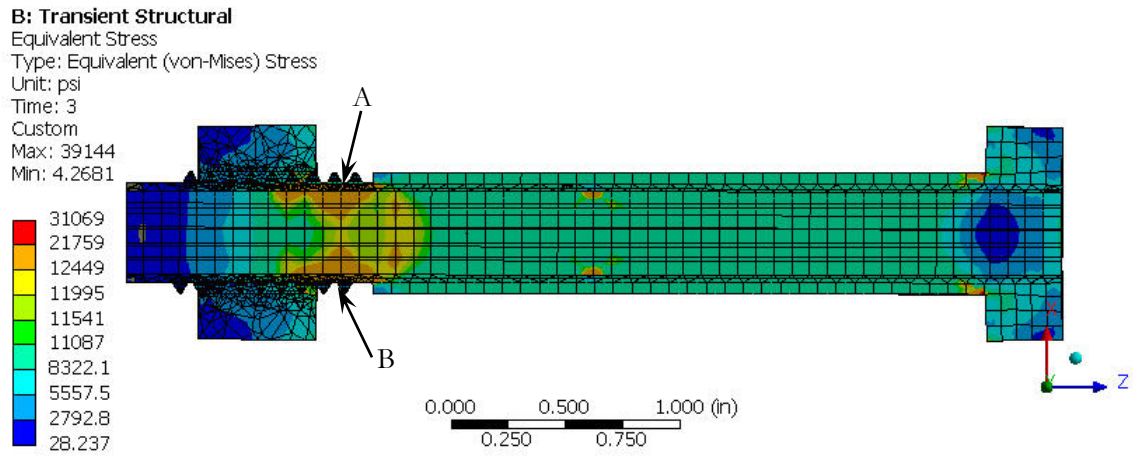

Figure 5-19 von Mises stress

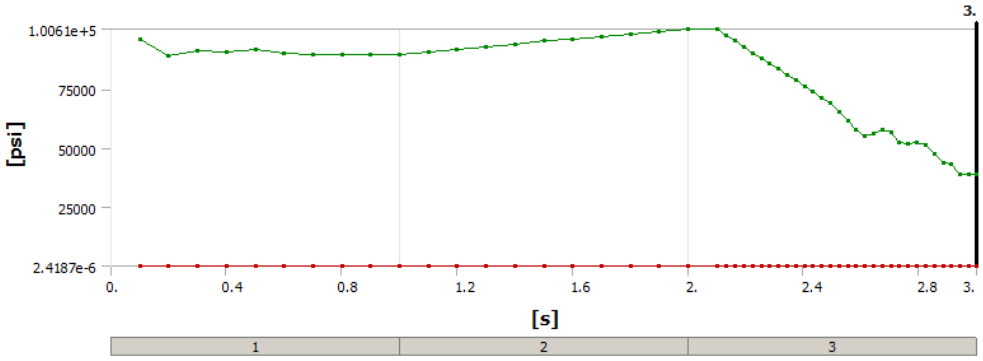

Figure 5-20 Maximum and minimum von Mises stresses throughout the analysis

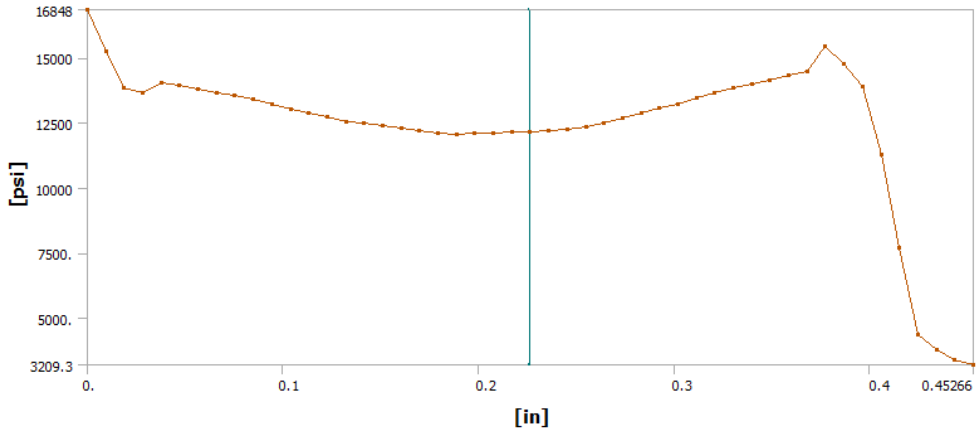

Figure 5-21 von Mises stress for a path extending between points A and B

5.5.2 Maximum Shear Stress

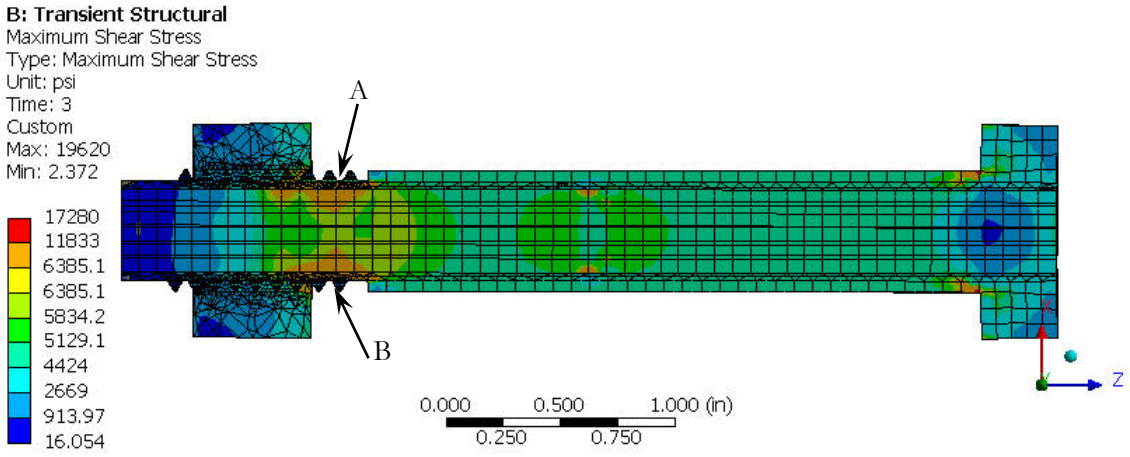

Figure 5-22 Maximum shear stress

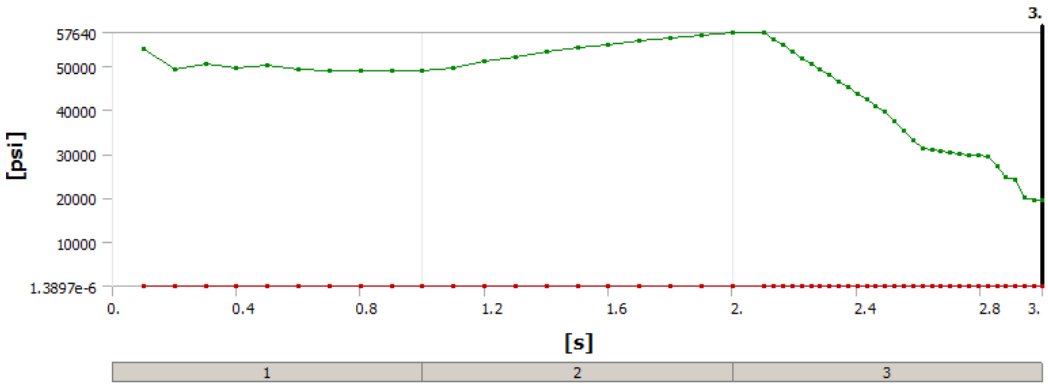

Figure 5-23 Maximum and minimum shear stresses throughout the analysis

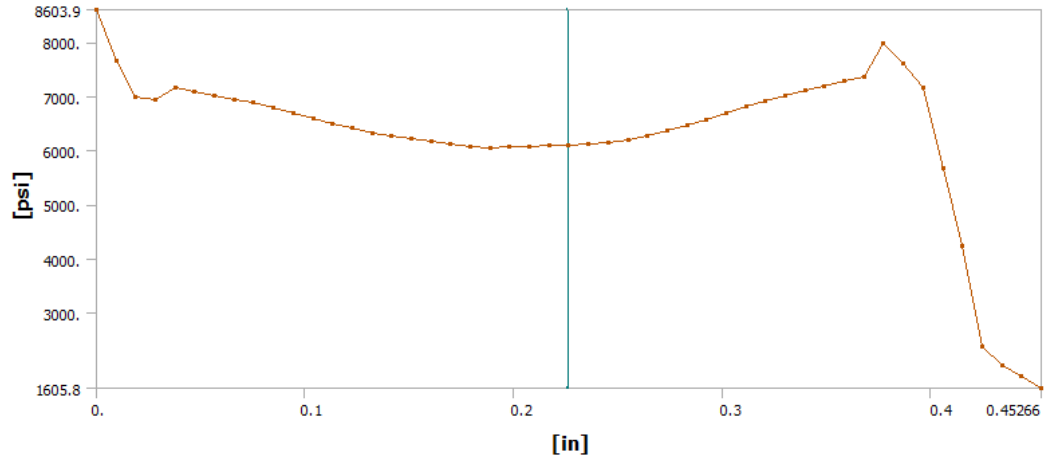

Figure 5-24 Maximum shear stress for a path extending between points A and B

The type of bolt failure as illustrated in Figure 3-12 is a ductile fracture, in which large plastic deformations take place just before failure causing the phenomenon known as "necking" and resulting in a cup-and-cone shaped failure surface. A look at the stresses (von-Mises and the shear stress are chosen) shows clearly the formation of large stresses in the failure plane vicinity, forming a conically shaped stress contour just above the location of the nut where the fracture is supposed to happen.

Figures 5-20 and 5-23 show stress relaxation (reduction in maximum stresses) during the heating time step. While Figures 5-21 and 5-24 show stress-concentration profiles at the failure section.

A look at the stress distribution across the axis of the bolt, as shown in Figures 5-25 and 5-26, shows very small stresses at the bottom of the bolt head and a large concentration of stress at the critical section above the nut. This response would not have been captured if the bolt and nut modelling was to mirror that of the bolt head.

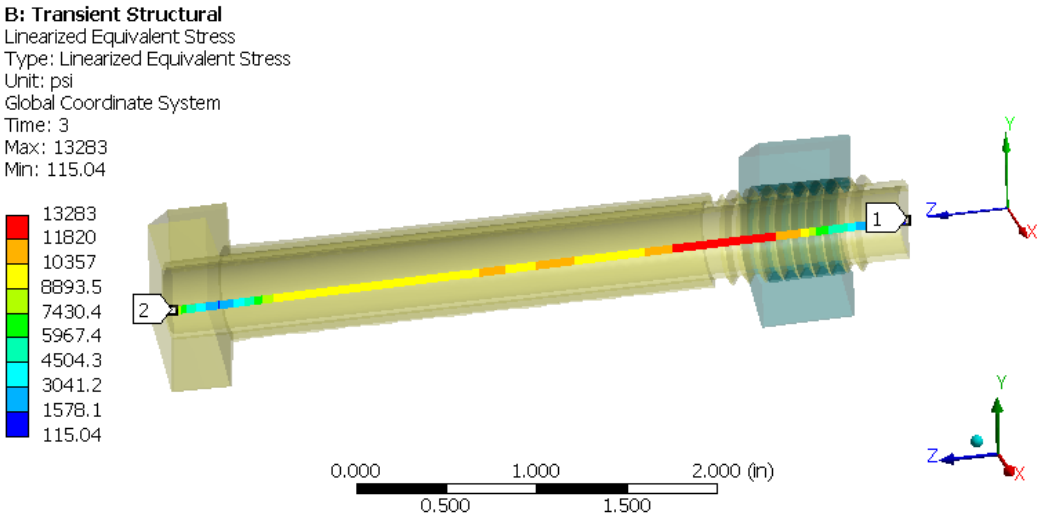

Figure 5-25 von-Mises stress across the axis of the bolt

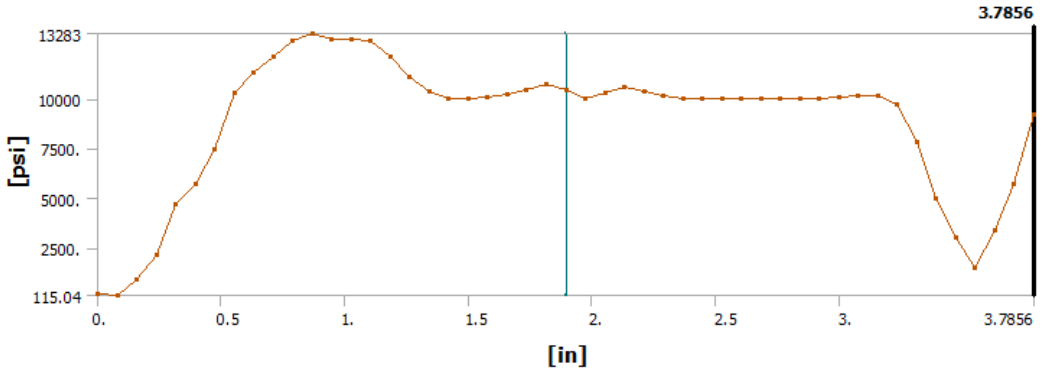

Figure 5-26 Linearized von-Mises stress across the axis of the bolt

5.6 Plastic Strain

Figure 5-27 shows that plastic strain has formed in excessive amounts near the necking area. Although the entire bolt has developed some plastic strains of lesser value. This just confirms our previous conclusion about the formation of a cup-and-cone surface forming in this area.

Necking also can be observed near the areas with high plastic strain, this is the same location where the bolt eventually breaks.

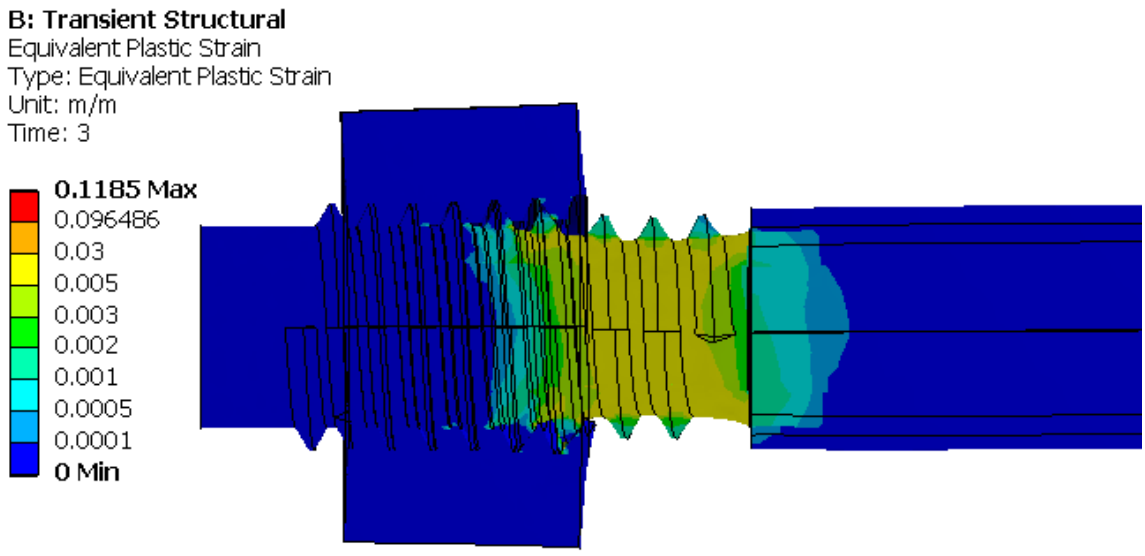

Figure 5-27 Equivalent plastic strain

Furthermore, plastic strain has appeared in other parts of the specimen (the HSS and the two vertical bars) but in smaller amounts. This has also been recorded, since the dimensions of all the elements in the specimen were taken before and after each test; even when there were not any deformations visible to the naked eye, small but permanent changes in those dimensions were recorded after each test.

Figure 5-28 shows the formation of plastic strains at the bolt head corners. Although plastic strains may form at these locations because of the high stresses resulting from stress concentrations. However, the values shown in the FE model may depend on the refinement of the mesh around those corners. Since these strains did not have a predominant effect on the experiments, further refinement of the mesh was not necessary.

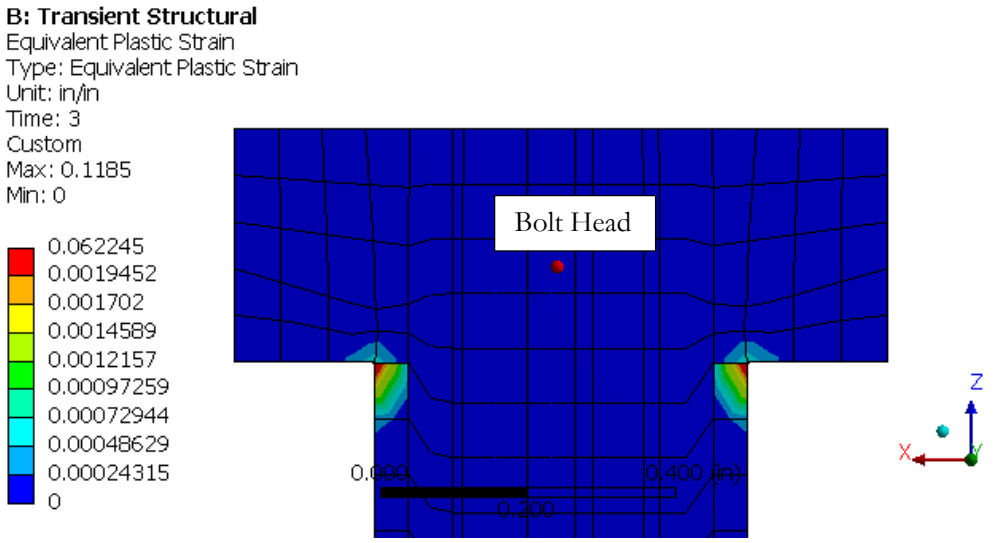

Figure 5-28 Plastic strain at the bolt heat

Figures 5-29 and 5-30 show the plastic strains at the axis of the bolt. A clear spike in the values of plastic strain was observed at the critical section just above the nut. Elsewhere on the axis of the bolt, the plastic strain values remained close to zero. Figures 5-31 and 5-32 show the distribution of plastic strains across the critical section. Plastic strains in the threads were not relatively very large, however their values increased towards the center of the bolt and at the roots of the bolt threads.

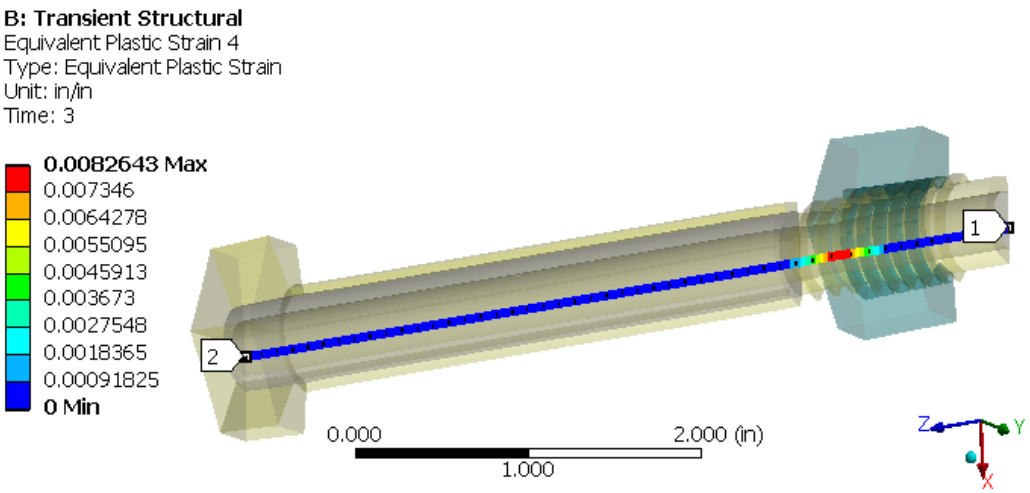

Figure 5-29 Plastic strain across the axis of the bolt

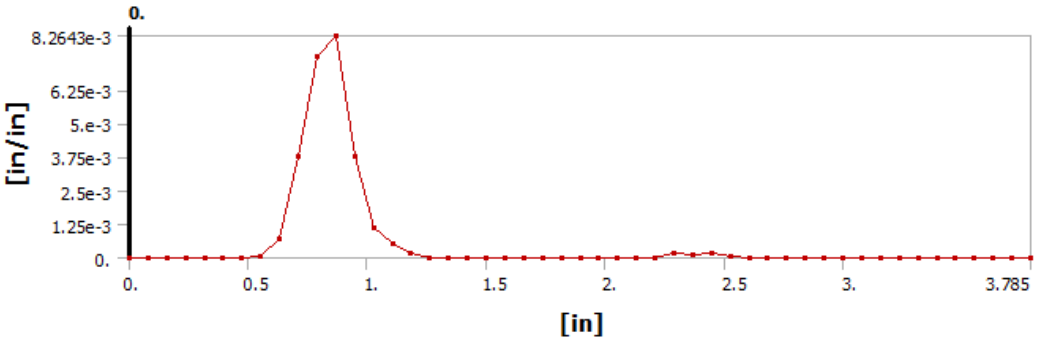

Figure 5-30 Linearized plastic strain across the axis of the bolt

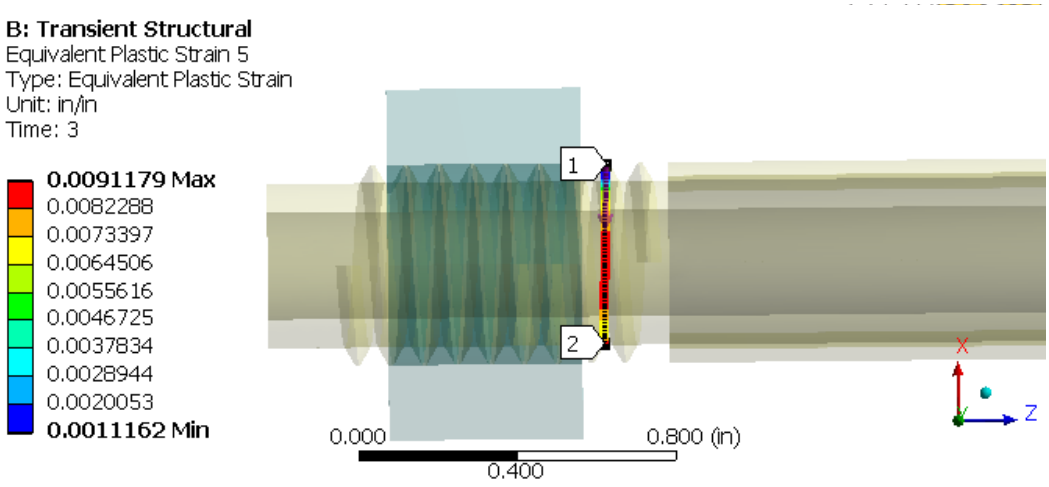

Figure 5-31 Plastic strain at the critical section

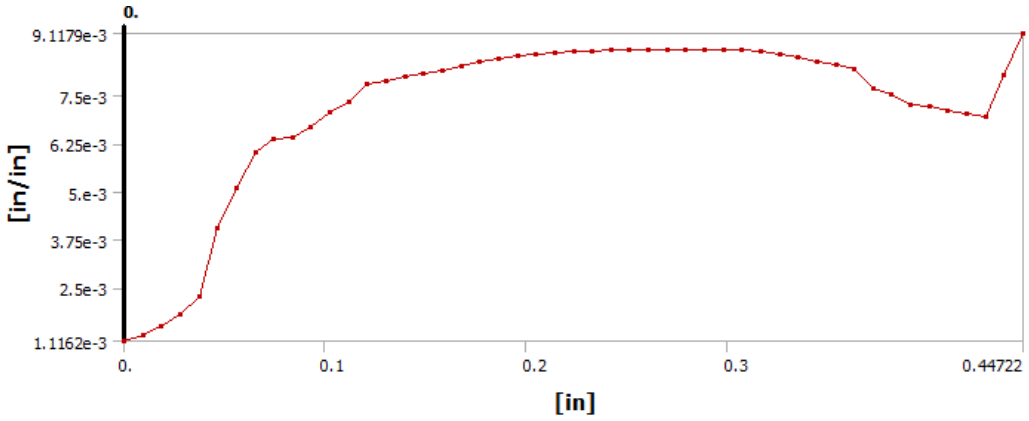

Figure 5-32 Linearized plastic strain at the critical section

5.7 DEFORMATIONS

Tables 5-1 and 5-2 list the deformation (upward movement) of the top point of the model. All readings have been adjusted by adding the amount of 2.45×10^{-5} in., which is the equivalent of the compression caused by bolt pretensioning in the first load step. These tables also show the incremental application of loads (tension or temperature) during each time step. As mentioned in Chapter 4, these increments were chosen in a way that facilitates the convergence of the model.

The time shown in Tables 5-1 and 5-2 does not represent real time. It represents the time step length, which was chosen to be 1 second and it is only used for the purposes of performing the iterative solutions. The maximum temperature that could be reached without divergence in the solution was 640°C.

Time (s)	Load (lb)	Deformation (in)
1	0	0.0000000
1.1	200	0.0008000
1.2	400	0.0016605
1.3	600	0.0024566
1.4	800	0.0033486
1.5	1000	0.0042218
1.6	1200	0.0051109
1.7	1400	0.0059887
1.8	1600	0.0068734
1.9	1800	0.0077559
2	2000	0.0086379

Table 5-1 Deformation of the top end during the second step of loading

Time (s)	Temperature (°C)	Deformation (in)	Time (s)	Temperature (°C)	Deformation (in)
2.00	22	0.0086379	2.55	464	0.0953619
2.10	100	0.0212539	2.58	477	0.0987969
2.13	133	0.0268149	2.61	491	0.1024279
2.16	163	0.0318299	2.64	504	0.1063279
2.19	193	0.0368699	2.67	518	0.1105879
2.22	223	0.0419159	2.70	531	0.1151779
2.25	253	0.0469859	2.73	543	0.1185379
2.28	283	0.0520709	2.76	555	0.1221379
2.31	311	0.0571839	2.79	567	0.1260379
2.34	335	0.0623099	2.82	578	0.1294479
2.37	359	0.0674739	2.85	589	0.1328979
2.40	382	0.0726589	2.88	599	0.1366879
2.43	400	0.0778809	2.91	610	0.1409079
2.46	418	0.0831359	2.94	620	0.1456779
2.49	436	0.0884399	2.97	630	0.1508579
2.52	450	0.0920839	3	640	0.1569379

Table 5-2 Deformation of the top end during the third step of loading

By comparing the deformed model shown in Figure 5-33 to the deformations of the real tested specimen shown in Figures 5-4 and 5-5, we can see that the FE model has deformed in a similar fashion.

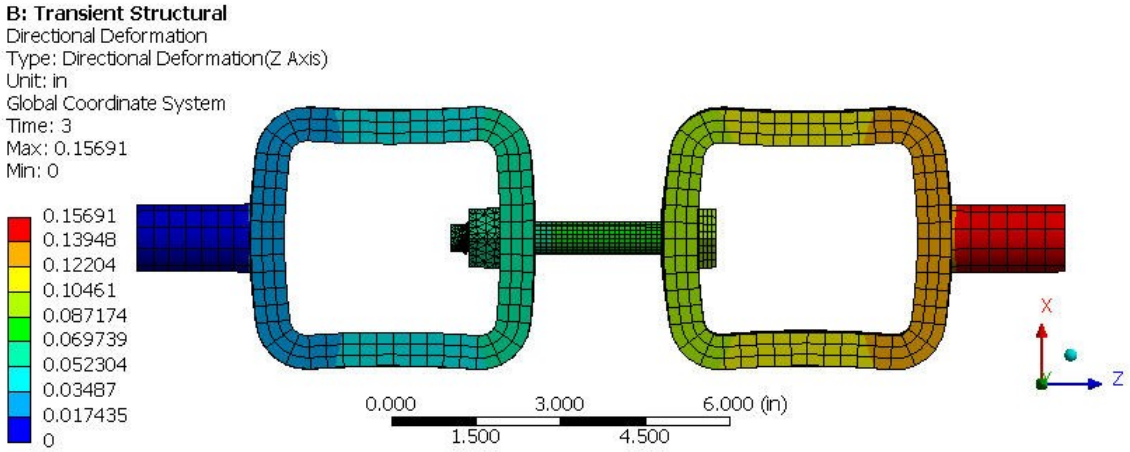

Figure 5-33 Deformed shape of the specimen

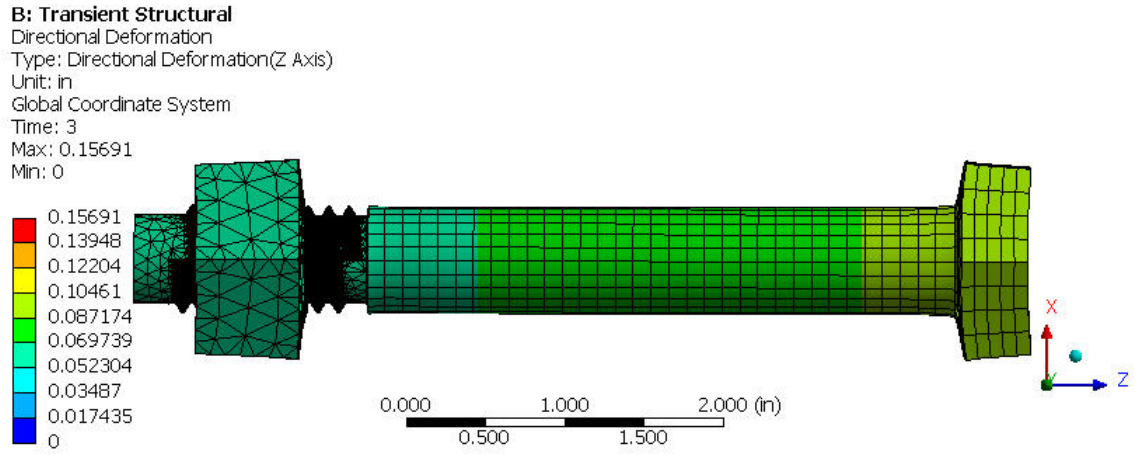

Figure 5-34 Deformed shape of the bolt

Figure 5-35 illustrates the relationship and separation between the nut and bolt threads. At ambient temperatures, it has been estimated [42] that bolt failures are more likely to occur at three different locations; 15% under the head, 20% at the end of the thread, and 65% in the threads at the nut face. In all these places, the main culprit in causing failure is stress concentrations due to sudden geometric changes.

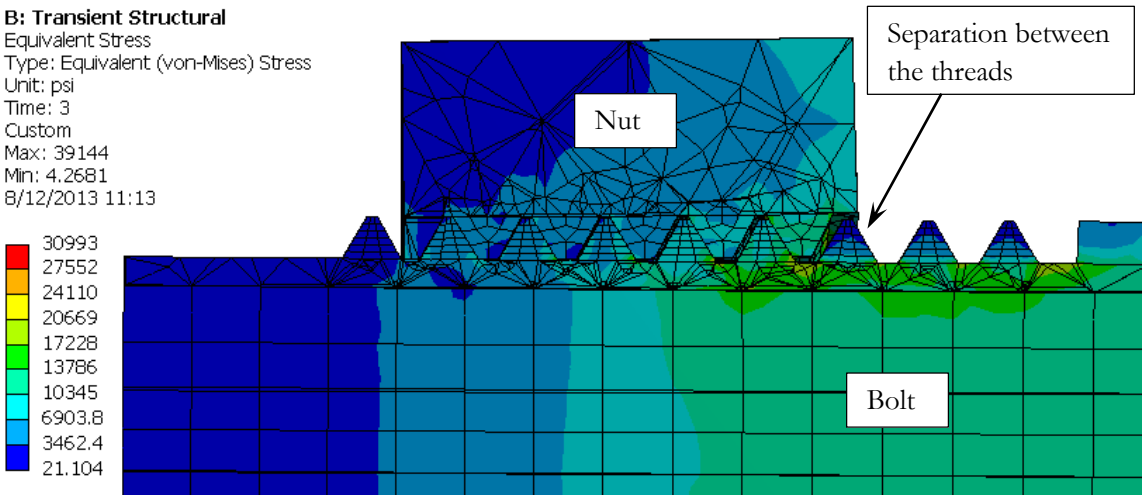

Figure 5-35 Nut and bolt separation

The accurate modeling of the nut and bolt threads allows for near realistic behavior during the analysis. Modeling the nut and bolt as a single object does not permit the two to separate and

it does not capture all the changes in the geometry of the bolt, thus leading to a reduction in the accuracy of the measured deformations and stresses. Furthermore, the modeling of a threaded bolt can be used in analyzing the fatigue strength of steel bolts as well.

5.8 COMPARISON

5.8.1 Temperature-Displacement

Figure 5-36 shows a comparison between the Temperature-Displacement charts from the finite element model (load step 3) and the experimental results. The FE model showed very good agreement with the experimental results especially up to a temperature of 500°C.

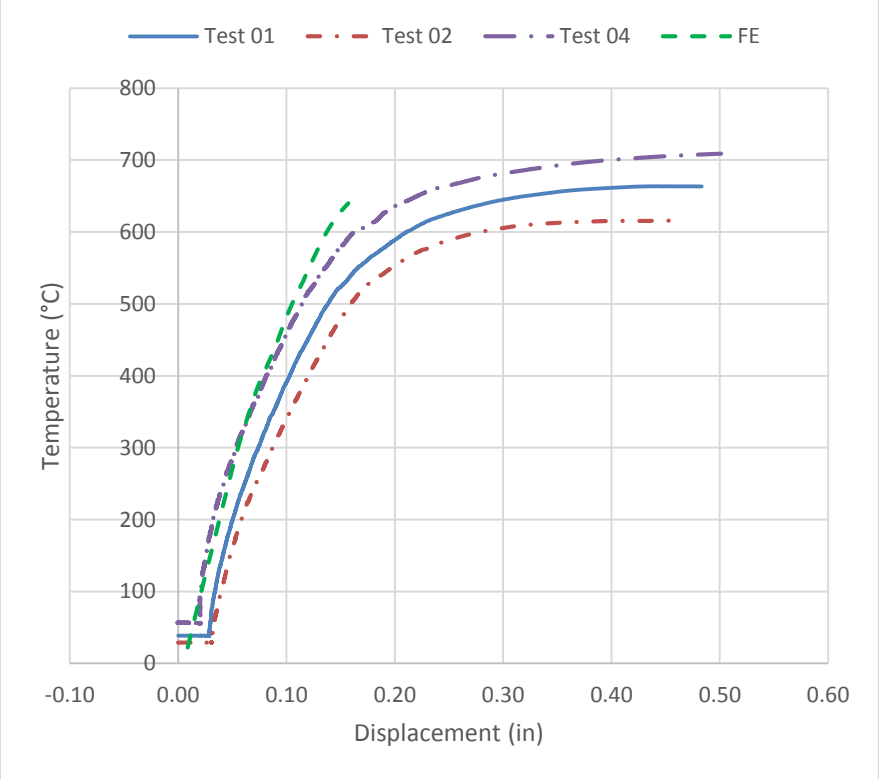

Figure 5-36 Temperature vs. Displacement comparison

After that, it displayed some signs of increased stiffness; this is because the FE model has no residual internal stresses, does not reflect impurities in the used materials, assumes continuous connectivity between components, and assumes ideal geometric and boundary conditions.

In most FE analyses, the finite element results are generally stiffer than experimental results.

Additionally, the FE model response could not be obtained beyond 640°C and if that was possible, it is expected that the response will continue to be stiffer than the one obtained through experiments.

5.8.2 Load-Displacement

Figure 5-37 shows a comparison between the Load-Displacement charts from the finite element model (load step 2) and the experimental results. The FE model seems to have a much stiffer response than any of the other experimental curves. However, the reason behind this is that during the experiments and at very low loads, there are some significant deformations recorded before the load picks up. This may have resulted in adding some extra deformations to the experimental values. At any rate, the FE model would still be a little bit stiffer in comparison to the experimental specimen for the same reasons mentioned before.

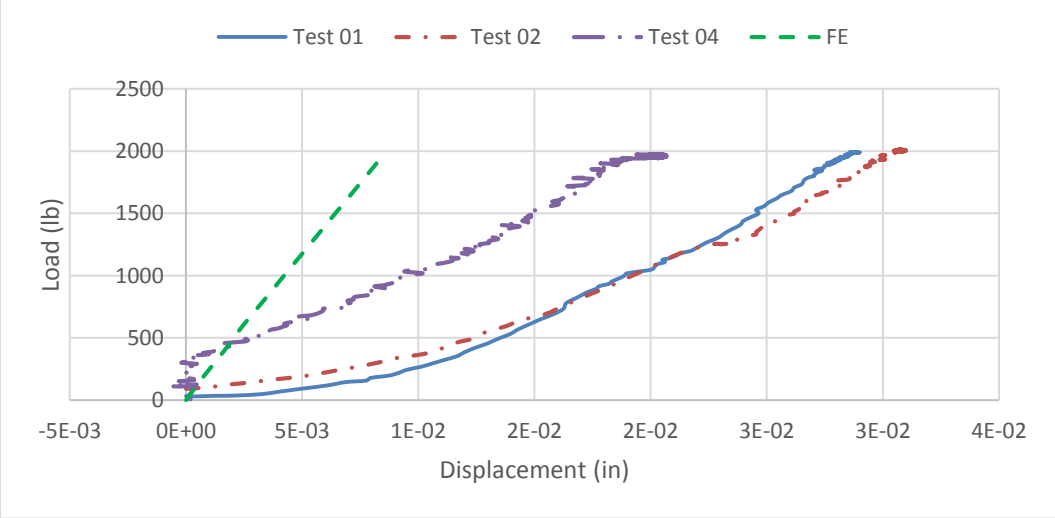

Figure 5-37 Load vs. Displacement comparison

5.9 CONCLUSIONS

This work develops a simplified procedure for testing bolts in tension under simulated fire conditions. Performing such tests on a large scale is a daunting task let alone very expensive one. In addition, the conducted experiments predict a mode of the failure mechanism of similar structural bolts under elevated temperatures.

The results from the experimental work show that the tested bolts are likely to collapse after the temperature has reach 600°C – 700°C, and below 600°C the bolts will deform quite visibly. However, this result is dependent upon the bolt diameter and the applied load. It would be useful if we were able to quantify the relationship between the bolt diameter, temperature and the applied tension load. However, that requires many more experiments and maybe done as a future work.

In an effort to simulate fire conditions, all experiments were conducted in a relatively short period of time. In situations where bolts are subjected to extended high levels of heat exposure, more research is required in order to know the exact effects of that prolonged heat exposure.

Using the data obtained from the experimental work, a very highly detailed finite element model of the bolt has been developed. This model handles a multitude of different nonlinear behaviors that bolts exhibit during a fire. Moreover, this model lays the foundation for creating a very detailed FE model of different types of steel connections in order to investigate the response of the connection as a unit under similar circumstances. Especially since it was parametrically created.

The response of the FE model was found to be in good agreement with the experimental results, particularly at elevated temperatures and that was the original intent of this research.

The finite element model was built on using ideal material properties, ideal boundary conditions and load application, which removed from it all the imperfections and residual stresses found in reality. That resulted in a relatively stiffer response when compared to the experimental results.

With a reliable finite element model, we have the tool to explore more about the response (stress, strain and deformation) of the bolt during a fire. Which may not be practical due to the experimental limitations.

5.10 Future Work

5.10.1 Moment-Resisting Frame Connections

This research, which studied the effects of tension on a single steel bolt, can be expanded to include all components of a moment-resisting steel connection. The beams, columns, bolts and end-plates. All of which would have a different effect on the behavior of the connection under elevated temperatures.

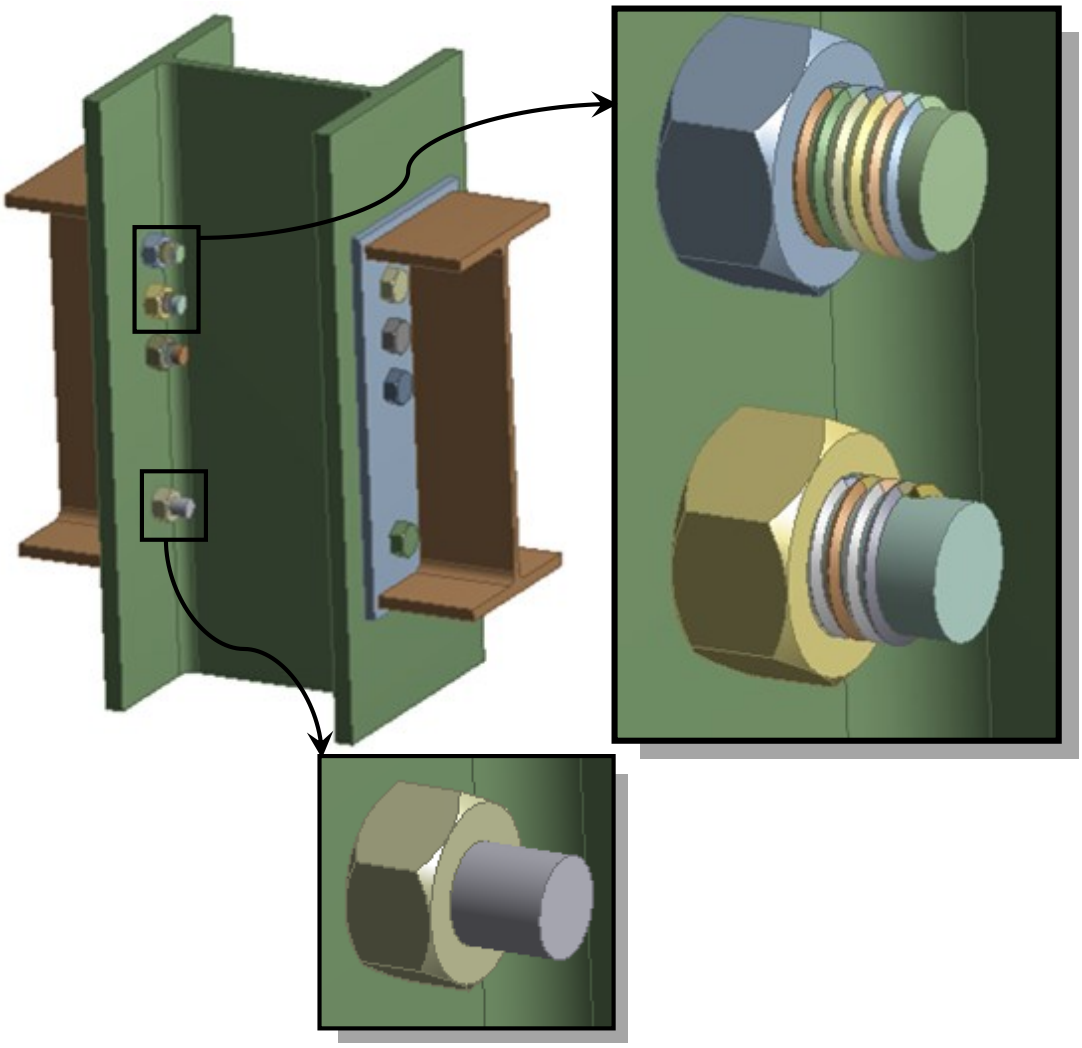

Figure 5-38 A proposed future-model of a moment-resisting connection

5.10.2 Performance of Steel Frames under Fire Effects

Conducting fire tests on isolated connections helps in understanding how much strength the connection will lose under certain temperatures. Although studying the isolated connection is more convenient and economic than testing full-scale structures, a full understanding of how fire affects buildings cannot be achieved without looking into the structure as a whole. When a steel connection is integrated into a structure, it may have a better chance surviving fires; since it may get less heat exposure and, in case of failures, the loads get redistributed to other healthier member.

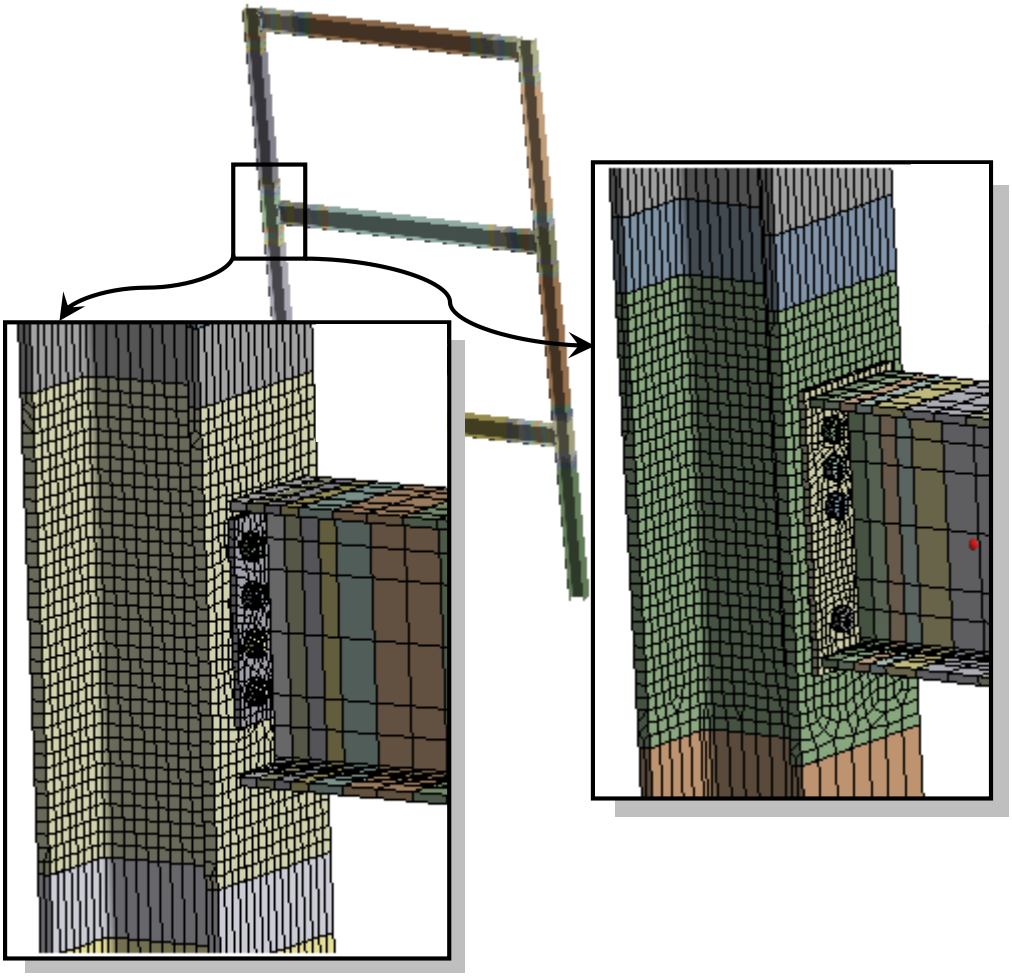

Figure 5-39 A proposed future-model of a steel frame

5.10.3 Elevated Temperatures Effects on Composite Connections

The use of composite sections is a very common design practice that increases the efficiency of the structural design by allowing a better use of concrete and steel sections. On the other hand, the addition of a concrete slab to bare steel connections provides a significant improvement on the fire-resistance front. The concrete slab cast on the top flange of a steel beam behaves like an insulation layer; thus reducing its temperature and enhancing the overall fire resistance of the structure. It has been found that the upper flange in a floor beam supporting a concrete slab will not be heated as much as the rest of the beam. In fact, it may be 40% cooler than the bottom flange.

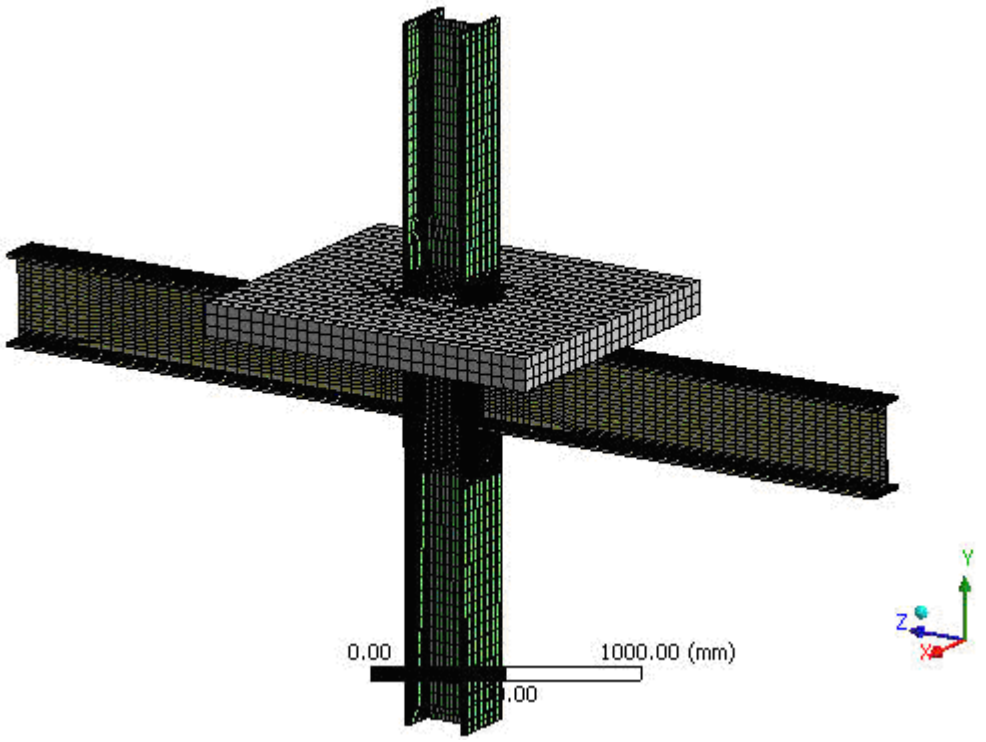

Figure 5-40 A proposed future-model of a composite connection

5.10.4 Shear tests at elevated temperatures

Using a similar testing methodology to the one followed in this research, the behavior of bolts under shear (single or double) can be investigated in simulated fire conditions.

Figure 5-41 A shear test specimen

CHAPTER 6

ELEVATED TEMPERATURE TESTS - EXPANDED

6.1 FURNACE COMPONENTS

6.1.1 Parts

Table 6-1 lists all the components used in building the furnace. This list is useful for future repairs and upgrades. A laptop computer was also necessary to run the application used to write heating programs and communicating with the CN9600 controller through a universal serial bus port.

Quantity	Part Number	Description
1	RMJ-K-S	Miniature, round hole, square face, thermocouple panel mount.
1	EXFF-K-24-25	Type K thermocouple extension wire, 24 AWG, 25ft.
2	CRWS-1212/240-C-A	CRWS Series Semi-Cylindrical Ceramic Heaters, with vestibule; 2700 Watt, 240V, 12" h, 16" OD, 12" ID.
1	SSRL 240 DC 50	Solid State Relay, DC control signal, 240V, 50 amp.
1	FHS-2	Finned Heat Sink 1.2°C/W for SSR.
1	SMPW-CC-K-M	Thermocouple Connector, miniature size, flat 2-pin includes integral cable clamp cap, male.
1	SMPW-CC-K-F	Thermocouple Connector, miniature size, flat 2-pin includes integral cable clamp cap, female.
1	KMQXL-125G-12	12" long, 0.125-dia, Type K, OmegaXL sheath, grounded, male miniature connector.
1	CN96621TR-C4	CN9600 1/16 DIN triple output ramp/soak, process 10V input controller, 10 Vdc output, DC pulse.
1	CN9-SW-GRAFIX	Graphical software for CN9600 series controller.
1	CN9-C2-CABLE-10	RS232 cable with female DB9 10-ft.
1	CN7-485-USB-1	Mini-node communication signal converter.
2		Insulation vestibule end caps / blocks (AVB-8761; 16"OD x 10"OD x 2" machined plug.

Table 6-1 List of furnace components

6.1.2 Dimensions

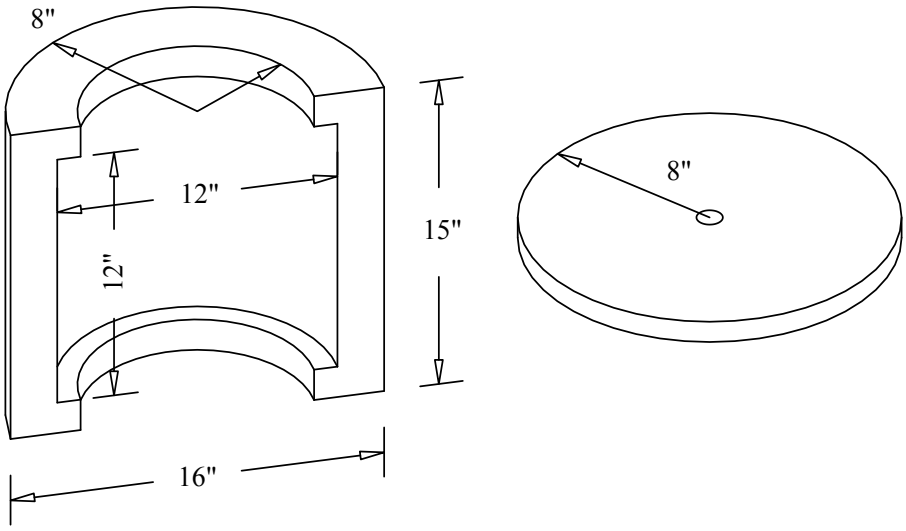

Figure 6-1 Dimensions of the ceramic heater and cap

The heat chamber is cylindrical with an inner diameter of 12" and a height of 12". The outside diameter is 16" and the total height is 15". Both top and bottom caps have a diameter of 16" as well and a total thickness of 2".

6.1.3 Steel frame

In addition to the parts listed above, a steel frame was built to hold and position the ceramic heaters around the tested specimen. This frame allowed for vertical and side-way motion without disrupting the work flow in the vicinity of the specimen.

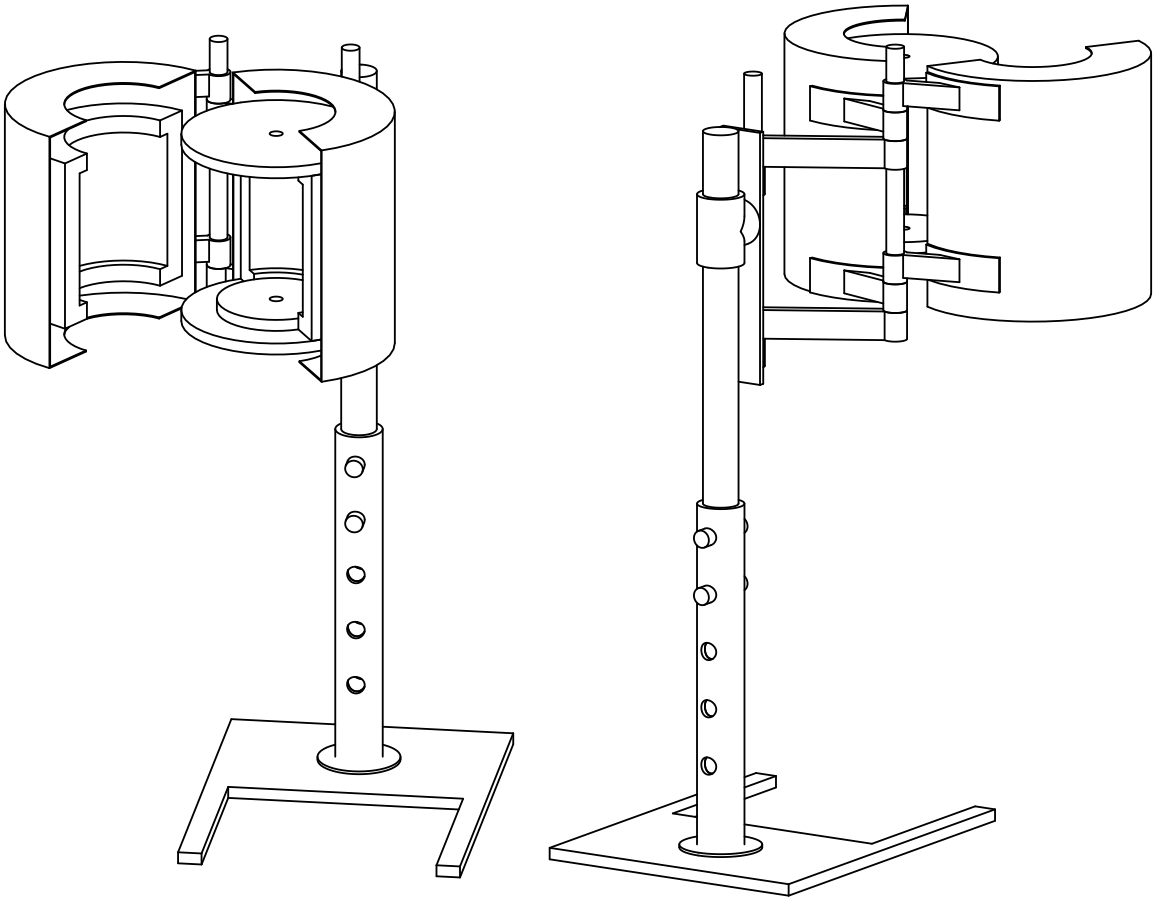

Figure 6-2 The furnace enclosed in its steel frame (back and front views)

6.2 SPECIMEN DIMENSIONS

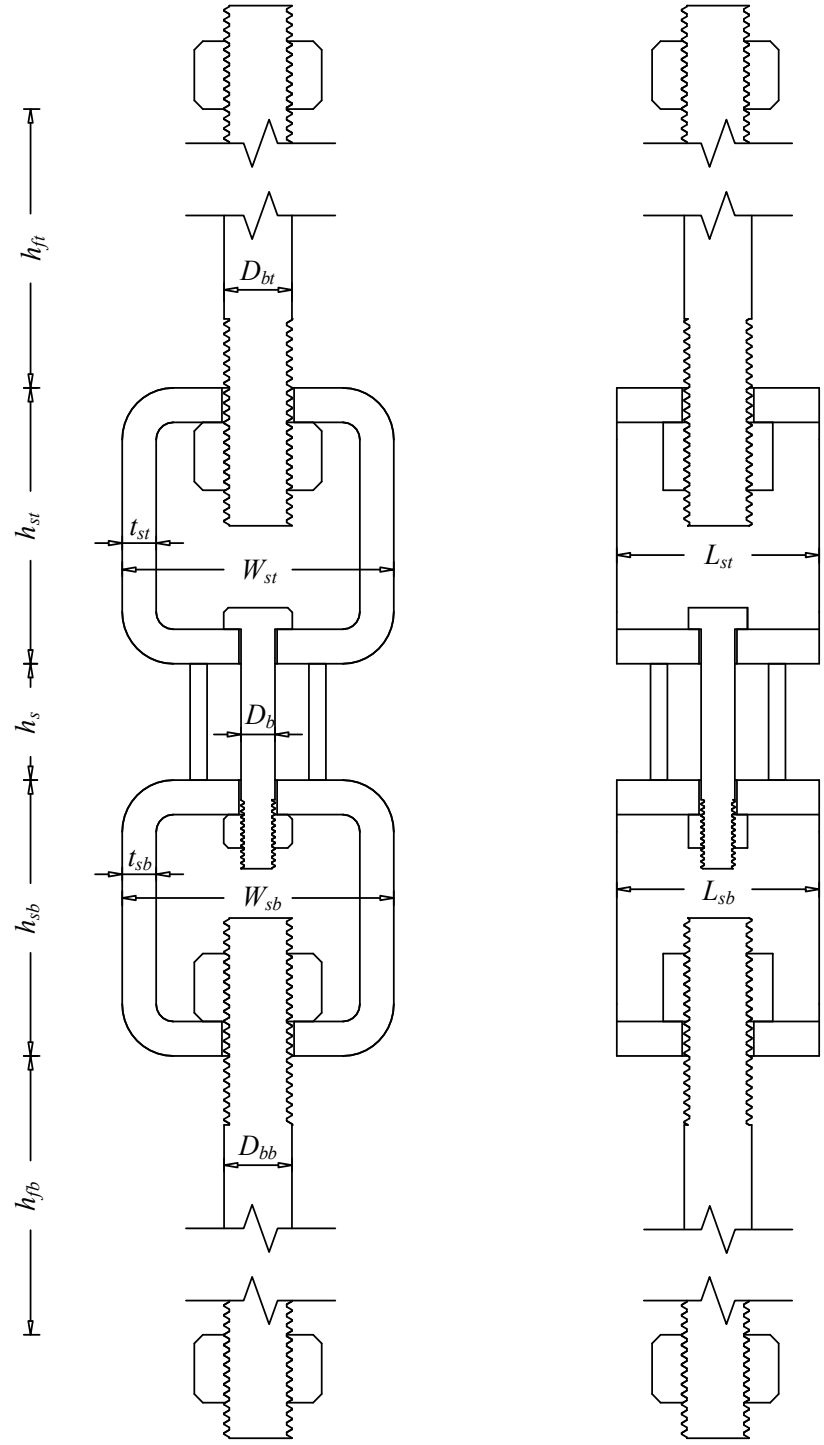

Figure 6-3 Dimensions of the test specimen

Symbol	Description	Value (in)
h_{ft}	Distance from the top fixed end to the top HSS.	19.44
h_{fb}	Distance from the bottom fixed end to the bottom HSS.	17.75
h_s	Height of spacer piece.	1.69
D_{bt}	Diameter of the top vertical bar.	1
D_{bb}	Diameter of the bottom vertical bar.	1
D_b	Diameter of bolt.	½
h_{st}	Height of the top HSS.	4
h_{sb}	Height of the bottom HSS.	4
W_{st}	Width of the top HSS.	4
W_{sb}	Width of the bottom HSS.	4
L_{st}	Length of the top HSS.	3
L_{sb}	Length of the bottom HSS.	3
t_{st}	Thickness of the top HSS.	½
t_{sb}	Thickness of the bottom HSS.	½

Table 6-2 Dimensions of the test specimen

6.3 HEATING PROGRAM

The following is an example of a heating program that was sent to the furnace control unit through an application called CN9-SW-GRAFIX.

Prog 1, Program # 1

Program settings

Power fail recovery - Reset

Ramp Rate units - Hours

Program start point - From process value

Program details

Seg 001 - Ramp(Target setpoint 100, rate 600, holdback 0) EOP

Seg 002 - Ramp(Target setpoint 200, rate 600, holdback 0) EOP

Seg 003 - Ramp(Target setpoint 300, rate 400, holdback 0) EOP

Seg 004 - Ramp(Target setpoint 400, rate 300, holdback 0) EOP

Seg 005 - Ramp(Target setpoint 500, rate 240, holdback 0) EOP

Seg 006 - Ramp(Target setpoint 600, rate 200, holdback 0) EOP

Seg 007 - Ramp(Target setpoint 700, rate 171, holdback 0) EOP

Seg 008 - Ramp(Target setpoint 800, rate 150, holdback 0) EOP

Seg 009 - Ramp(Target setpoint 900, rate 120, holdback 0) EOP

Seg 010 - Step (Target setpoint 16) EOP

Seg 011 - Soak (3000 Sec.) EOP

The program is written in segments. Each segment can reach a target set point through a Ramp, Step or a Soak procedure. The Ramp procedure reaches the target set point by increasing the temperature in the furnace linearly according to a specified rate. The Step procedure attempts a direct drop or increase in temperature in order to achieve the required target set point; however, this is not practically followed by the heating elements since some time is needed to increase the temperature and there is no way of cooling the inside of the furnace. The Soak procedure maintains a certain temperature for a specified period of time.

The actual temperature in the furnace did not adhere to the written heating program one hundred percent, but its deviation from it was not very severe except for a single case when a standard fire curve was adapted.

Figure 6-4 shows the used CN9-SW-GRAFIX application with a graphical representation of a heat program and a control window that shows the current temperature inside the furnace and the target set point the furnace will try to reach next.

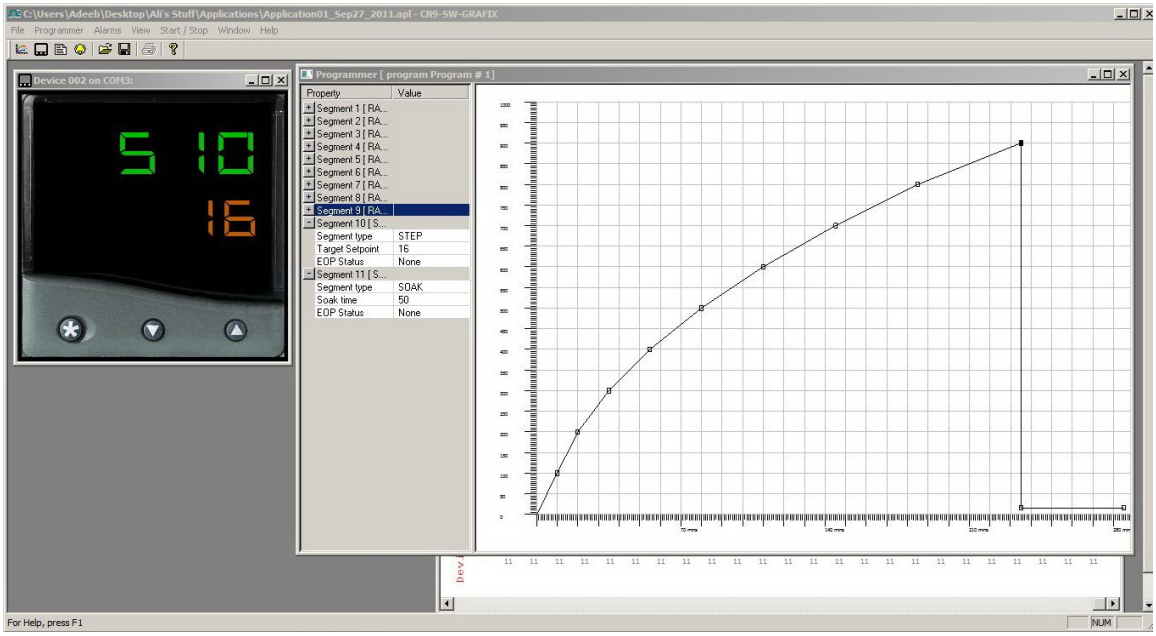

Figure 6-4 CN9-SW-GRAFIX application

6.4 APPLICATION SETTINGS

The CN9-SW-GRAFIX application communicated with a CN9600 controller box, shown in Figure 6-5, through a USB connection. The CN9600 controller received the program (heat instructions) from the computer application and it also received a measure of the current temperature inside the furnace through a connected thermocouple. Then it would monitor the progress of the stored program and try to adjust the heat in the furnace accordingly. In order to control this process safely, other parameters have been also set through the CN9-SW-GRAFIX application. The following is a full description of these parameters.

Figure 6-5 CN9600 controller box

Security Settings

Application

New Application = None
Close Application = None
Change window size or position = None
View Toolbar = None
Open application = None
Export Application = None
Save application = None
Save As application = None
Printing = None
Window options = None
Manage Device Template = None

Communications

Start Communications = None
Stop Communications = None
Restart Communications = None
Chart Communications = None
Instrument Communications = None
Restart Alarm = None

Charting

New chart = None
Close chart = None
Change window size or position = None
Export chart = None
Properties = None
Zoom = None
Show key = None
Add note = None
Add trace = None
Show notes = None

Instrument

New Instrument = None
Close Instrument = None
Change window size or position = None
Export Instrument = None
Properties = None
SP1 & Run Mode = None
Edit programs = None
Clone Instrument = None

Programmer
New program = None
Close programmer = None
Change window size or position = None
Export program = None
Delete program = None
View Program = None
Properties = None
Add segment = None
Insert segment = None
Delete segment = None
Fetch Program From Instrument = None
Send Program To Instrument = None

Alarms
Add Alarm = None
Edit Alarm = None
Dismiss Alarm = None

Alarm Settings

Instrument Settings

Instrument - Device 002 on COM3:

Device details
Opc Server = OEM.ModbusServer

Initial setup
Process units = DegC
Sensor type = K
Display resolution = 1

Setpoint 1
Setpoint value = 16
Tune mode = OFF
Proportional cycle time mode = Variable
Proportional cycle time value = 20
Proportional band = 10
Integral time = 5
Derivative time = 25
Derivative approach control = 1.5
Derivative sensitivity = 0.5
Setpoint manual power = OFF
Power level = 0
Power limit = 100

Offset = 0
Set point lock = OFF
Minimum scale value = 0
Maximum scale value = 1200

Setpoint 2
Setpoint mode = None
Setpoint Secondary mode = None
Proportional cycle time mode = OnOff
Proportional cycle time value = 0
Setpoint value = 0
Proportional band = 2
Power limit = 100
Reset setpoint latch = No

Setpoint 3
Setpoint mode = None
Setpoint Secondary mode = None
Setpoint value = 0
Hysteresis Band = 2
Reset setpoint latch = No

Analog scaling
Displayed range high scale = 1000
Displayed range low scale = 0
Input range high scale = 50
Input range low scale = 10

Programmer
Program number = 1
Program Mode = OFF

Calibration adjustment
Zero offset adjustment = 0
Span offset adjustment. = 0

Output configuration
Setpoint 1 burnout output state = Upscale
Setpoint 2 burnout output state = Upscale
Setpoint 3 burnout output state = Upscale
Setpoint 1 output mode = Reversed
Setpoint 2 output mode = Direct
Setpoint 3 output mode = Direct
Setpoint 1 indicator state = Non Inverted
Setpoint 2 indicator state = Non Inverted

Diagnosis and settings

Display averaging = 6
Auto tune settings (CT1) = 255.48
Auto tune settings (CT2) = 43.04
Auto tune settings (CT3) = 584.24
Auto tune settings (CT4) = 0
Auto tune settings (CTA) = 0
Auto tune settings (CTB) = 267.28
Auto tune settings (OS1) = 0.8
Auto tune settings (OS2) = 358.7
Auto tune settings (US) = 0.1
SoftwareVersion = Programmable PID Version 3 (953)
Level lock = None
Program auto exit = Auto
Display communications activity = OFF

Communications settings

MODBUS address = 2
Baud rate = 9600

Note: communication ports and MODBUS address could vary, especially if there is a failure in the system.

CHAPTER 7

FINITE ELEMENT MODEL DETAILS

The following is a more in-depth look at the finite element model used in this research.

7.1 UNITS

Unit System	*U.S. Customary (in, lbm, lbf, s, V, A) Degrees rad/s Fahrenheit*
Angle	Degrees
Rotational Velocity	rad/s
Temperature	Fahrenheit

Table 7-1 Units

7.2 MODEL (A4)

7.2.1 Geometry

Object Name	*Bolt*	*Nut*	*GripTop*	*GripBot*
State	Meshed			
Graphics Properties				
Visible	Yes			
Definition				
Suppressed	No			
Assignment	Steel Bolts		Multiple Materials	
Coordinate System	Default Coordinate System			
Bounding Box				
Length X	0.875 in		4. in	
Length Y	1.0104 in		3. in	
Length Z	3.785 in	0.4844 in	22.937 in	21.25 in
Properties				
Volume	0.8452 in³	0.24316 in³	34.462 in³	33.136 in³
Mass	0.2397 lbm	6.896e-002 lbm	9.7733 lbm	9.3974 lbm
Centroid X	-2.9951e-006 in	-1.6062e-004 in	-7.6478e-007 in	-7.9576e-007 in
Centroid Y	8.3092e-007 in	7.6871e-004 in	3.0486e-016 in	-5.4341e-017 in
Centroid Z	2.2663 in	0.54247 in	9.9287 in	-5.0657 in

Moment of Inertia Ip1	0.32153 lbm·in²	5.8967e-003 lbm·in²	455.77 lbm·in²	366.22 lbm·in²
Moment of Inertia Ip2	0.32152 lbm·in²	5.9006e-003 lbm·in²	462.7 lbm·in²	373.14 lbm·in²
Moment of Inertia Ip3	1.1585e-002 lbm·in²	9.1108e-003 lbm·in²	15.819 lbm·in²	15.773 lbm·in²

Table 7-2 Body groups

7.2.2 Connections

Object Name	***Frictional - Bolt To Nut***
State	Fully Defined
Scope	
Scoping Method	Geometry Selection
Contact	1 Face
Target	1 Face
Contact Bodies	Bolt
Target Bodies	Nut
Definition	
Type	Frictional
Friction Coefficient	0.15
Scope Mode	Automatic
Behavior	Asymmetric
Suppressed	No
Advanced	
Formulation	Pure Penalty
Detection Method	Program Controlled
Interface Treatment	Add Offset, No Ramping
Offset	0. in
Normal Stiffness	Manual
Normal Stiffness Factor	5.
Update Stiffness	Each Iteration
Stabilization Damping Factor	0.
Pinball Region	Program Controlled
Time Step Controls	None

Table 7-3 Contact regions

7.2.3 Mesh

Object Name	*Mesh*
State	Solved
Defaults	
Physics Preference	Mechanical
Relevance	0
Sizing	
Use Advanced Size Function	Off
Relevance Center	Coarse
Element Size	Default
Initial Size Seed	Part
Smoothing	Medium
Transition	Fast
Span Angle Center	Coarse
Minimum Edge Length	6.8644e-003 in
Inflation	
Use Automatic Inflation	None
Inflation Option	Smooth Transition
Transition Ratio	0.272
Maximum Layers	5
Growth Rate	1.2
Inflation Algorithm	Pre
View Advanced Options	No
Patch Conforming Options	
Triangle Surface Mesher	Program Controlled
Advanced	
Shape Checking	Standard Mechanical
Element Midside Nodes	Program Controlled
Straight Sided Elements	No
Number of Retries	Default (4)
Extra Retries For Assembly	Yes
Rigid Body Behavior	Dimensionally Reduced
Mesh Morphing	Disabled
Defeaturing	
Pinch Tolerance	Please Define
Generate Pinch on Refresh	No
Automatic Mesh Based Defeaturing	On
Defeaturing Tolerance	Default
Statistics	
Nodes	248009
Elements	74563
Mesh Metric	Element Quality
Min	4.37828714045429E-02
Max	0.999873539901736
Average	0.677106334772679

Table 7-4 Mesh

7.3 STATIC STRUCTURAL (A5)

Object Name	*Analysis Settings*
State	Fully Defined
Step Controls	
Number Of Steps	3.
Current Step Number	1.
Step End Time	1. s
Auto Time Stepping	On
Define By	Time
Initial Time Step	7.5e-002 s
Minimum Time Step	1.e-002 s
Maximum Time Step	0.5 s
Solver Controls	
Solver Type	Program Controlled
Weak Springs	Program Controlled
Large Deflection	On
Inertia Relief	Off
Restart Controls	
Generate Restart Points	Program Controlled
Retain Files After Full Solve	No
Nonlinear Controls	
Force Convergence	Program Controlled
Moment Convergence	Program Controlled
Displacement Convergence	Program Controlled
Rotation Convergence	Program Controlled
Line Search	Program Controlled
Stabilization	Off
Output Controls	
Stress	Yes
Strain	Yes
Nodal Forces	Yes
Contact Miscellaneous	No
General Miscellaneous	No
Calculate Results At	All Time Points
Max Number of Result Sets	1000.

Table 7-5 Analysis settings

Step	*Step End Time*	*Minimum Time Step*	*Carry Over Time Step*
1	1. s	1.e-002 s	
2	2. s		Off
3	3. s	1.e-003 s	

Table 7-6 Analysis settings step-specific "Step Controls"

Object Name	*Fixed Support*	*Force*	*Thermal Condition*
State	Fully Defined		
Scope			
Scoping Method	Geometry Selection		
Geometry	1 Face		64 Bodies
Definition			
Type	Fixed Support	Force	Thermal Condition
Suppressed	No		
Define By		Components	
Coordinate System		Global Coordinate System	
X Component		0. lbf (ramped)	
Y Component		0. lbf (ramped)	
Z Component		Tabular Data	
Magnitude			Tabular Data
Tabular Data			
Independent Variable			Time

Table 7-7 General loads information

Steps	*Time [s]*	*X [lbf]*	*Y [lbf]*	*Z [lbf]*
1	0.	0.	0.	0.
	1.			
2	2.	= 0.	= 0.	2000.
3	3.			= 2000.

Table 7-8 Force

Steps	*Time [s]*	*Temperature [°C]*
1	0.	22
	1.	
2	2.	
3	2.1	100
	2.2	200
	2.3	300
	2.4	380
	2.5	440
	2.7	530
	2.8	570
	3.	640

Table 7-9 Thermal condition

Object Name	*Bolt Pretension*
State	Fully Defined
Scope	
Scoping Method	Geometry Selection
Geometry	1 Body
Coordinate System	Bolt Shank Coordinate System
Definition	
Type	Bolt Pretension
Suppressed	No
Define By	Load
Preload	2500. lbf

Table 7-10 Bolt pretension

Steps	*Define By*	*Preload [lbf]*	*Adjustment [in]*
1.	Load	2500.	N/A
2.	Lock	N/A	
3.			

Table 7-11 Bolt pretension application

7.4 MATERIAL DATA

7.4.1 Steel Bolts

Density	*0.2836 lbm in^-3*
Coefficient of Thermal Expansion	6.6667e-006 F^-1
Specific Heat	0.10366 BTU lbm^-1 F^-1
Thermal Conductivity	8.0917e-004 BTU s^-1 in^-1 F^-1

Table 7-12 Constants

Temperature F	Young's Modulus psi	Poisson's Ratio	Bulk Modulus psi	Shear Modulus psi
71.6	2.9e+007	0.3	2.4167e+007	1.1154e+007
212	2.9e+007	0.3	2.4167e+007	1.1154e+007
392	2.61e+007	0.3	2.175e+007	1.0038e+007
572	2.32e+007	0.3	1.9333e+007	8.9231e+006
752	2.03e+007	0.3	1.6917e+007	7.8077e+006
932	1.74e+007	0.3	1.45e+007	6.6923e+006
1112	8.99e+006	0.3	7.4917e+006	3.4577e+006
1292	3.77e+006	0.3	3.1417e+006	1.45e+006
1472	2.61e+006	0.3	2.175e+006	1.0038e+006
1652	1.96e+006	0.3	1.6333e+006	7.5385e+005

Table 7-13 Isotropic elasticity

Stress psi	Plastic Strain in in^-1	Temperature F
92000	0	71.6
92000	0.2	71.6
92000	0	212
92000	0.2	212
92000	0	392
92000	0.2	392
92000	0	572
92000	0.2	572
92000	0	752
92000	0.2	752
71760	0	932
71760	0.2	932
43240	0	1112
43240	0.2	1112
21160	0	1292
21160	0.2	1292
10120	0	1472
10120	0.2	1472
5520	0	1652
5520	0.2	1652

Table 7-14 Multilinear isotropic hardening

7.4.2 Steel HSS

Density	*0.2836 lbm in^-3*
Coefficient of Thermal Expansion	6.6667e-006 F^-1
Specific Heat	0.10366 BTU lbm^-1 F^-1
Thermal Conductivity	8.0917e-004 BTU s^-1 in^-1 F^-1

Table 7-15 Constants

Temperature F	Young's Modulus psi	Poisson's Ratio	Bulk Modulus psi	Shear Modulus psi
71.6	2.9e+007	0.3	2.4167e+007	1.1154e+007
212	2.9e+007	0.3	2.4167e+007	1.1154e+007
392	2.61e+007	0.3	2.175e+007	1.0038e+007
572	2.32e+007	0.3	1.9333e+007	8.9231e+006
752	2.03e+007	0.3	1.6917e+007	7.8077e+006
932	1.74e+007	0.3	1.45e+007	6.6923e+006
1112	8.99e+006	0.3	7.4917e+006	3.4577e+006
1292	3.77e+006	0.3	3.1417e+006	1.45e+006
1472	2.61e+006	0.3	2.175e+006	1.0038e+006
1652	1.96e+006	0.3	1.6333e+006	7.5385e+005

Table 7-16 Isotropic elasticity

Stress psi	Plastic Strain in in^-1	Temperature F
50000	0	71.6
50000	0.2	71.6
50000	0	212
50000	0.2	212
50000	0	392
50000	0.2	392
50000	0	572
50000	0.2	572
50000	0	752
50000	0.2	752
39000	0	932
39000	0.2	932
23500	0	1112
23500	0.2	1112
11500	0	1292
11500	0.2	1292
5500	0	1472
5500	0.2	1472
3000	0	1652
3000	0.2	1652

Table 7-17 Multilinear isotropic hardening

7.4.3 Steel Bars

Density	*0.2836 lbm in^-3*
Coefficient of Thermal Expansion	6.6667e-006 F^-1
Specific Heat	0.10366 BTU lbm^-1 F^-1
Thermal Conductivity	8.0917e-004 BTU s^-1 in^-1 F^-1

Table 7-18 Constants

Temperature F	Young's Modulus psi	Poisson's Ratio	Bulk Modulus psi	Shear Modulus psi
71.6	2.9e+007	0.3	2.4167e+007	1.1154e+007
212	2.9e+007	0.3	2.4167e+007	1.1154e+007
392	2.61e+007	0.3	2.175e+007	1.0038e+007
572	2.32e+007	0.3	1.9333e+007	8.9231e+006
752	2.03e+007	0.3	1.6917e+007	7.8077e+006
932	1.74e+007	0.3	1.45e+007	6.6923e+006
1112	8.99e+006	0.3	7.4917e+006	3.4577e+006
1292	3.77e+006	0.3	3.1417e+006	1.45e+006
1472	2.61e+006	0.3	2.175e+006	1.0038e+006
1652	1.96e+006	0.3	1.6333e+006	7.5385e+005

Table 7-19 Isotropic elasticity

Stress psi	Plastic Strain in in^-1	Temperature F
36000	0	71.6
36000	0.2	71.6
36000	0	212
36000	0.2	212
36000	0	392
36000	0.2	392
36000	0	572
36000	0.2	572
36000	0	752
36000	0.2	752
28080	0	932
28080	0.2	932
16920	0	1112
16920	0.2	1112
8280	0	1292
8280	0.2	1292
3960	0	1472
3960	0.2	1472
2160	0	1652
2160	0.2	1652

Table 7-20 Multilinear isotropic hardening

7.5 RESULTS

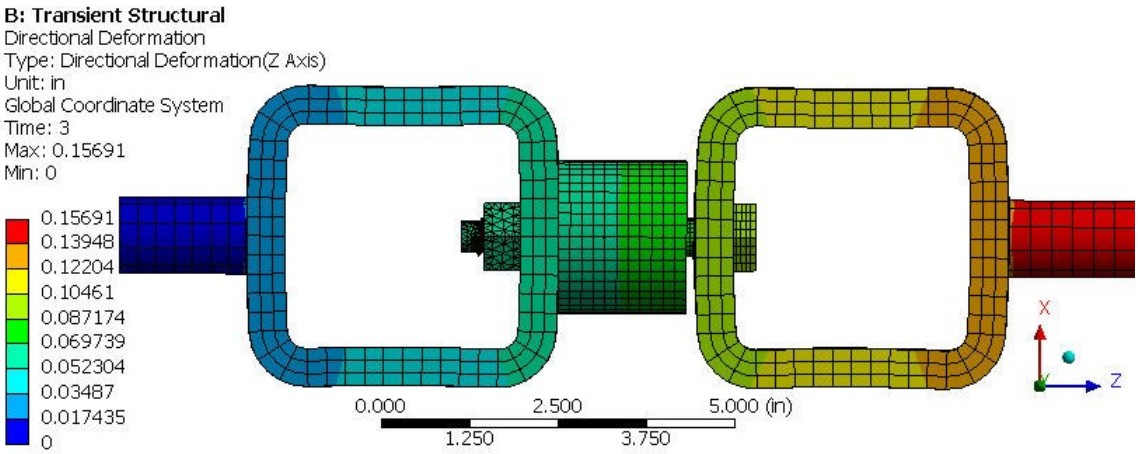

Figure 7-1 Gap between the spacer piece and the top HSS

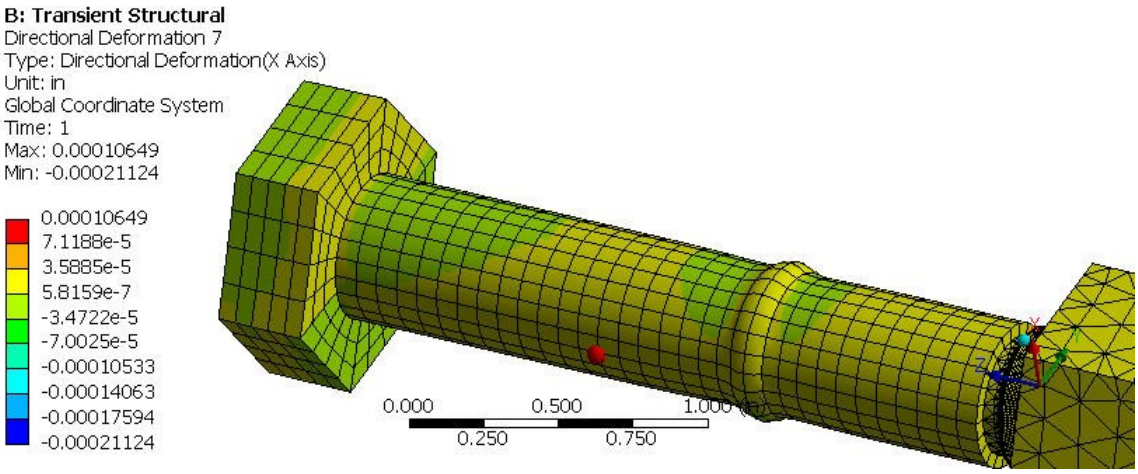

Figure 7-2 Effects of bolt pretensioning

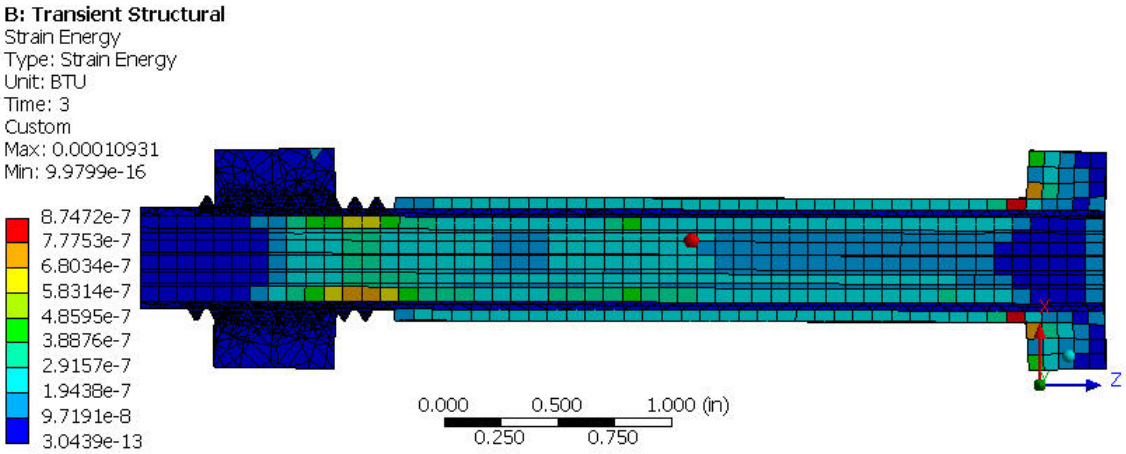

Figure 7-3 Strain Energy

REFERENCES

1. Al-Jabri, Khalifa S., *The Behaviour of Steel and Composite Beam-to-Column Connections in Fire*. University of Sheffield, December 1999.

2. Wai-Fah, Ed. Chen., *Structural Engineering Handbook*. Boca Raton: CRC Press LLC, 1999.

3. McCormac, Jack C., and Nelson, James K., *Structural Steel Design: LRFD Method*. Third Edition, Pearson Education, Inc. 2003.

4. Wastney, Clayton, *Performance of unprotected steel and composite steel frames exposed to fire*. University of Canterbury, February 2002.

5. Bose B, Sarkar S, and Bahrami M, *Finite Element Analysis of unstiffened extended end plate connections*, Structural Engineering Review, 1991.

6. Patel, K. V., and Chen, W. F., *Nonlinear Analysis of Steel Moment Connections*, J. Struct. Engng, ASCE, 110(8), 1984.

7. Atamiaz Sibai, W., and Frey, F., *Numerical Simulation of the Behaviour up to Collapse of Two Welded Unstiffened One-Side Flange Connections*, In Connections in Steel Structures: Behaviour, Strength and Design, R. Bjorhovde et al.(Ed.), Elsevier Applied Science, London, 1988, pp. 85-92.

8. Krishnamurthy, N., and Graddy, D. E., *Correlation between 2- and 3-Dimensional Finite Element Analysis of Steel Bolted End-plate Connections*, Computers and Structures, 1976.

9. Lipson, S. L., Hague, M. I., *Elasto-Plastic Analysis of Single-Angle Bolted Welded Connections using the Finite Element Method*, Computers and Structures, 1978.

10. Richard, R. M., Gillet, P. E., Kriegh, J. D., and Lewis, B. A., *The Analysis and Design of Single Plate Framing Connections*, Engrg. J., AISC, 1980.

11. Krishnamurthy, N., *Modelling and Prediction of Steel Bolted Connection Behaviour*, Computers and Structures, 1980.

12. Murray, T. M., and Kukreti, A. R., *Design of 8-Bolt Stiffened Moment End Plates,* Engrg J., AISC, 2nd Quarter, 1988, pp. 45-53.

13. Al-Jabria K.S., Seibib A., and Karrechc A., *Modelling of Unstiffened Flush End-plate Bolted Connections in Fire*, Journal of Constructional Steel Research, 2005.

14. Rahman, A. A.; Mahamid, M.; Amro A. A.; and Ghorbanpoor A.; *Analyses of the Shear-Tab Steel Connections, Part I: Unstiffened Connections*. Engineering Journal. American Institute of Steel Construction (AISC), 2007.

15. Rahman, A. A.; Mahamid, M.; and Ghorbanpoor A.; *Analyses of the Shear-Tab Steel Connections, Part II: stiffened Connections*. Engineering Journal. American Institute of Steel Construction (AISC), 2007.

16. Han L., Huo J., Wang Y. *Behavior of Steel Beam to Concrete-Filled Steel Tubular Column Connections after Exposure to Fire*. Journal of Structural Engineering. June 2007.

17. Lu W., Mäkeläinen P., Outinen J. *Finite Element Modeling of Single Lap Shear Screw Connection in Steel Sheeting in Fire*. Open Construction & Building Technology Journal. January 2008.

18. Yu H., Burgess I.W., Davison J.B., Plank R.J., *Tying capacity of web cleat connections in fire, Part 1: Test and finite element simulation*, Engineering Structures, Volume 31, Issue 3, March 2009.

19. Buchanan A.H., *Structural Design for Fire Safety*. John Wiley & Sons, England, 2001.

20. ANSYS, Inc. *ANSYS Workbench Documentation*, Version 14.0.

21. AISC, Inc. *Manual of Steel Construction*. LRFD, Third Edition.

22. El-Rimawi, J. A.; Burgess, I. W.; and Plank, R. J., *Modelling the Behaviour of Steel Frames and Sub-frames with Semi-Rigid Connections in Fire*, Research Report DCSE/93/S/02, Department of Civil and Structural Engineering, University of Sheffield, April 1993.

23. Eurocode 3, *Design of Steel Structures: General rules – Structural fire design. ENV 1993-1-2-2001*, European Committee for Standardisation, Brussels, 2001.

24. Outinen; Kaitila; and Mäkeläinen. *High-Temperature Testing of Structural Steel and Modelling of Structures at Fire Temperatures*. Helsinki University of Technology Laboratory of Steel Structures Publications, 2001.

25. Lewis, Kathryn R. *Fire Design of Steel Members*. University of Canterbury, February 2001.

26. Kaitila, Olli. *Finite Element Modelling of Cold-Formed Steel Members at High Temperatures*. Helsinki University of Technology Laboratory of Steel Structures Publications, 2002.

27. Naus DJ. *The Effect of Elevated Temperature on Concrete Materials and Structures – A Literature Review*. NUREG/CR-6900 ORNL/TM, 2005.

28. Leston-Jones, L. C., *The Influence of Semi-rigid Connections on the Performance of Steel Framed Structures in Fire*, Ph.D. Thesis, Department of Civil and Structural Engineering, University of Sheffield, 1997.

29. Rahman; Shrih; and Al-Jabri; *Computational Analysis of Flush End-Plate Bare Steel Connection under Fire Conditions.* 11th International Conference on Inspection Appraisal & Maintenance of Structures, North Cyprus, 14-17 November 2007, pp 293-302.

30. Rahman, A.; Hawileh, R.; and Mahamid, M.; *The effect of fire loading on a steel frame and connection.* Wessex Institute of Technology, High Performance Structures and Materials. WIT Press Publisher 2004, Edited by C.A Brebbia and W.P. De Wilde, 2004, pp. 307-316.

31. Lennon, T; *Structural Fire Engineering.* Institution of Civil Engineers Publishing. 2011

32. Brockenbrough, Roger L., and Frederick S. Merritt. *Structural Steel Designer's Handbook.* Third ed. New York: McGraw-Hill, 1999. Print.

33. Wang, Y. C., and I. Burgess. *Performance-based Fire Engineering of Structures.* Boca Raton: CRC, 2013. Print.

34. Hobbs, J. W., R. L. Burguete, and E. A. Patterson. "Investigation into the Effect of the Nut Thread Run-Out on the Stress Distribution in a Bolt Using the Finite Element Method." *Journal of Mechanical Design* 125.3 (2003): 527. Print.

35. Shrih A., and Rahman A. *Finite Element Analyses of Flush End-Plate Connections between Steel Beams and Columns at Elevated Temperatures*, Advances in Structural Engineering Journal, Vol. 12, No. 3, pp. 311-324, 2009.

36. Chen, J., Young, B, and Uy, B. *Behavior of High Strength Structural Steel at Elevated Temperatures*, Journal of Structural Engineering 132.12 (2006): 1948. Print.

37. Johnson, G.R., Cook W.H., *A Constitutive Model and Data for Metals Subjected to Large Strains, High Strain Rates and High Temperatures*, Proceedings of the 7th International Symposium on Ballistics, The Hague, The Netherlands, April 1983.

38. Williamson, F. *Richard Courant and the Finite Element Method: A Further Look.* Historia Mathematica 7.4 (1980): 369-78.

39. Lien, K.H., Y.J. Chiou, R.Z. Wang, and P.A. Hsiao. *Nonlinear Behavior of Steel Structures considering the Cooling Phase of a Fire.* Journal of Constructional Steel Research 65.8-9 (2009): 1776-786.

40. Mao, C.J., Y.J. Chiou, P.A. Hsiao, and M.C. Ho. *Fire Response of Steel Semi-rigid Beam–column Moment Connections.* Journal of Constructional Steel Research 65.6 (2009): 1290-303.

41. Yu, Liang, and Karl H. Frank. *Shear Behavior of A325 and A490 High-Strength Bolts in Fire and Post-Fire.* Engineering Journal (2009).

42. Pilkey, Walter D., and Peterson R. E. *Peterson's stress concentration factors.* 2nd ed. New York, Wiley, 1997.

43. Sarraj M, Burgess I, Davison J, Plank R. *Finite element modelling of steel fin plate connections in fire*. Fire Safety Journal. September 2007.

44. Talamona D, Franssen J. *A Quadrangular Shell Finite Element for Concrete and Steel Structures Subjected to Fire*. Journal of Fire Protection Engineering. November 2005.

45. Wei-Yong Wang, Guo-Qiang Li, Behavior of steel columns in a fire with partial damage to fire protection, Journal of Constructional Steel Research, Volume 65, Issue 6, June 2009, Pages 1392-1400, ISSN 0143-974X, DOI: 10.1016/j.jcsr.2009.01.004.

46. O. Mirza, B. Uy, Behaviour of headed stud shear connectors for composite steel-concrete beams at elevated temperatures, Journal of Constructional Steel Research, Volume 65, Issue 3, March 2009

47. J. Ding, Y.C. Wang, Realistic modelling of thermal and structural behaviour of unprotected concrete filled tubular columns in fire, Journal of Constructional Steel Research, Volume 64, Issue 10, October 2008, Pages 1086-1102, ISSN 0143-974X, DOI: 10.1016/j.jcsr.2007.09.014.

48. Explosion and Fire Analysis of Steel Frames Using Mixed Element Approach Hong Chen and J. Y. Richard Liew, J. Engrg. Mech. 131, 606 (2005)

49. Alexandre Landesmann, Eduardo de M. Batista, Jose L. Drummond Alves, Implementation of advanced analysis method for steel-framed structures under fire conditions, Fire Safety Journal, Volume 40, Issue 4, June 2005, Pages 339-366, ISSN 0379-7112, DOI: 10.1016/j.firesaf.2005.02.003.

50. Stability of the World Trade Center Twin Towers Structural Frame in Multiple Floor Fires A. S. Usmani, J. Engrg. Mech. 131, 654 (2005), DOI:10.1061/(ASCE)0733-9399(2005)131:6(654)

51. Liew J, Tang L, Choo Y. Advanced Analysis for Performance-based Design of Steel Structures Exposed to Fires. Journal of Structural Engineering [serial online]. December 2002;128(12):1584. Available from: Academic Search Premier, Ipswich, MA. Accessed November 15, 2009.

52. V.K.R. Kodur, M.M.S. Dwaikat, Response of steel beam-columns exposed to fire, Engineering Structures, Volume 31, Issue 2, February 2009

53. Tan K, Ting S, Huang Z. Visco-Elasto-Plastic Analysis of Steel Frames in Fire. Journal of Structural Engineering [serial online]. January 2002;128(1):105. Available from: Academic Search Premier, Ipswich, MA. Accessed November 15, 2009.

54. Toh W, Fung T, Tan K. FIRE RESISTANCE OF STEEL FRAMES USING CLASSICAL AND NUMERICAL METHODS. Journal of Structural Engineering [serial online]. July 2001;127(7):829. Available from: Academic Search Premier, Ipswich, MA. Accessed November 15, 2009.

55. Predicting the temperatures of steel members in the Cardington fire tests using the THELMA finite element model.pdf

56. Toh W, Tan K. STRENGTH AND STABILITY FRAMES IN FIRE: RANKINE APPROACH. Journal of Structural Engineering [serial online]. April 2001

57. Zhaohui H, Burgess I. THREE-DIMENSIONAL ANALYSIS OF COMPOSITE STEEL-FRAMED BUILDINGS IN FIRE. Journal of Structural Engineering [serial online]. March 2000;126(3):389. Available from: Academic Search Premier, Ipswich, MA. Accessed November 15, 2009.

58. Aldina Santiago, Luis Simoes da Silva, Paulo Vila Real, Milan Veljkovic, Numerical study of a steel sub-frame in fire, Computers & Structures, Volume 86, Issues 15-16, August 2008, Pages 1619-1632, ISSN 0045-7949, DOI: 10.1016/j.compstruc.2008.01.006.

59. Kang-Hai T, Zhan-Fei H. Structural Responses of Axially Restrained Steel Beams with Semirigid Moment Connection in Fire. Journal of Structural Engineering [serial online]. April 2005;131(4):541-551. Available from: Academic Search Premier, Ipswich, MA. Accessed November 15, 2009.

CURRICULUM VITAE

Ali Shrih

Place of birth: Aleppo, Syria

Education:

B.S., University of Aleppo-Syria, May 2001

Major: Structural Engineering

M. S., University of Wisconsin-Milwaukee, August 2007

Major: Structural Engineering

Dissertation Title: Experimental and Finite Element investigation of Tension-Loaded ASTM A325 Bolts under Simulated Fire Loading.

Teaching Experience:

University of Wisconsin-Milwaukee, 2005-2013

Dynamics, Engineering Surveying, Strength of Materials, Introduction to Structural Design and Finite Element Analysis

Publications:

Rahman; Shrih; and Al-Jabri; *Computational Analysis of Flush End-Plate Bare Steel Connection under Fire Conditions.* 11th International Conference on Inspection Appraisal & Maintenance of Structures, North Cyprus, 14-17 November 2007, pp 293-302.

Shrih A., and Rahman A. *Finite Element Analyses of Flush End-Plate Connections between Steel Beams and Columns at Elevated Temperatures*, Advances in Structural Engineering Journal, Vol. 12, No. 3, pp. 311-324, 2009.

Honors

Chancellor's Graduate Student Award, UWM (2005-2012)

Al-Bassel Award for Academic Excellence, ranked 1st in my class, Aleppo University (2001)